CHARACTERIZATION OF STIFFNESSS DEGRADATION IN HIGH PERFORMANCE, WELDED, ALUMINUM STRUCTURES

A Thesis

Presented to the Faculty of the Graduate School

of Cornell University

In Partial Fulfillment of the Requirements for the Degree of

Master of Science

by

Kevin James Muich

May 2014

ABSTRACT

The stiffness of a structure is controlled by the materials that make up the structure and the geometry in which the members are configured, if either of these change over the life of a structure the stiffness will change. Changes in the geometry of a structure are often easily detected through routine maintenance operations. But what is happening in the material is often not as easy to detect.

There are many different ways in which a material will degrade over the life of a structure. Rust is an easy example to illustrate this. As the steel member of bridge rusts it loses mass and is less able to sustain load. Often rust is mitigated through coatings, such as paint, and often other materials are used. Aluminum is a great substitute for steel because it has comparable strength and is a ductal material, and although it corrodes in other ways, it does not rust as steel rusts and it is lighter than steel.

Many different industries use aluminum for various applications. The Navy uses aluminum to create faster and more fuel efficient ships. But these ships are huge complex structures and are often difficult to model and impractical to experiment on. To avoid these prohibitions an analogous high performance, welded, aluminum structure is used to characterize stiffness degradation. In this thesis a welded aluminum bike frame is used as that substitute structure.

An experiment is developed, designed, constructed, and executed on a purchased aluminum bike frame. This experiment found that stiffness degradation does appear to occur in the bike frame.

Over 1.2 million, displacement controlled, loading cycles the stiffness appears to degrade. Obtaining 90% confidence intervals for the stiffness degradation, a lower bound of 0.0662% and an upper bound of 0.6414% were obtained. A 90% confidence interval on correlation is also obtained, which describes the confidence of stiffness depending on the number of cycles.

A material model is developed to reproduce published experimental data that was obtained using an aluminum notched beam in a 3-point bend test subjected to cyclic displacement controlled loading. This data shows stiffness degradation of 17.7% over 140,000 loading cycles. While developing a finite element model of the notched beam it was observed that the cycling of the notched beam appears to be occurring in the elastic regime. As a result, the material model is based on accumulated elastic strain. A damage multiplier is applied to the accumulated strain and a value for this multiplier is found that matches the experimental data.

The aluminum bike frame used in the experiment was then measured and modeled using finite elements. The material model developed using the notched beam experiment is applied to this finite element model. The results of the bike frame experiment were then examined using this finite element model. The multiplier needed to match the experimental result is 5000 times smaller than the expected multiplier.

The experimental evidence obtained from the bike frame can conclude that stiffness degradation does occur in high performance, welded, aluminum structures. The actual and expected multiplier values are vastly different concluding that the developed material model lacks predictive accuracy.

BIOGRAPHICAL SKETCH

Kevin received his undergraduate degree in Civil Engineering from Cornell University in January of 2012, where his coursework was targeted at developing breadth in the field, allowing movement along several different paths after graduation. After completing his undergraduate degree he decided to stay at Cornell University to pursue a graduate degree, in Structural Engineering, through working with the Computational Mechanics and Fracture Research Group under the advisory guidance of Dr. Derek Warner. While pursuing his graduate degree Kevin took coursework in the finite element method, materials science, numerical computation, and mechanics. Kevin also found guidance in machining and electronics, focusing on experiments, from various resources at Cornell University.

ACKNOWLEDGMENTS

I would first and foremost like to acknowledge Dr. Paul Hess III and the Ship Structural Reliability Program of the U.S. Office of Naval Research for financial support through grant number N00014-12-0343.

I would like to acknowledge my advisor, and friend, Dr. Derek Warner for his continuous academic and personal guidance.

I would like to acknowledge a few individuals who helped me develop and perform the experimental part of this project. Timothy Brock, Cornell University Equipment Technician, for sharing his knowledge and expertise as a machinist in helping me create the experimental setup used in this project. Timothy Bond, Manager Technician Services for Bovay CI Complex, for sharing his knowledge and expertise pertaining to experimental electronics. Matt Ulinski, Hansen Director of Instructional Labs, for helping me find space and equipment to perform my experiments and the guidance to get setup and started.

I would like to acknowledge Dr. Christopher Earls for his ability and willingness to share his own academic journey with me and for offering me guidance and support along mine.

I would like to acknowledge my friends and colleagues in the Cornell community for helping me find the emotional and academic support I needed.

I would like to acknowledge Sierra Young, a Cornell civil engineering undergraduate student for her help in acquiring the large amount of data from the bike frame experiment. Without her help performing the experiment and modeling simultaneously would not have been possible.

I would like to acknowledge Brett Davis, Sarah Clement, Heather Reed, Geoffrey Bomarito, Patty Chung, Ashley Spear, Brad Wham, Jose Cano, and Albert Cerrone for welcoming me into Cornell's informal structural engineering club with open arms and hearts and for making sure to include me on all social invitations, without them my work-life balance would not have been possible.

I would like to acknowledge Danielle Lertola, for her unwavering personal support, big heart, and the guiding light she has always been. Without her, I would be adrift.

TABLE OF CONTENTS

1.0 Introduction

1.1 Motivation and Literature Review

The initial design of a structure is done with an understanding of the ability of the material and geometry to support a desired load. If either the material or geometry changes during the service life of the structure the initial design is in danger of being inadequate. Therefore, a thorough understanding and characterization of these changes is important to ensure the structure performs as intended. Stiffness can degrade if either the material properties degrade or the geometry of the structure changes.

All structures, whether made by nature or man, are susceptible to degradation over time. Mountains turn into sand and bridges collapse. Large, as well as small, structures are vulnerable to this degradation. Anything from skyscrapers to the fan blades keeping a computer cool, a naval ship or bike frame, is in danger of degrading to a point of safety concerns or failure. The US government spends a lot of money to build and maintain the World's largest naval fleet. The Navy's main goal in maintenance is mission preparedness; a ship being worked on in port isn't able to perform its mission at sea. One battle that the Navy must constantly fight is with rust. While the salt water can corrode the hull of a ship, the salty air can get inside the ship and rust it from the inside out, see Figure 1.1.

Figure 1.1 Rusted Ship[13]

This rust can corrode critical components weakening the overall structural integrity of the entire ship, making it unsuitable for warfare or the sailors that inhabit it. Rust can remove mass from a structural member or completely sever the piece making it ineffective at carrying its intended load.

Rust is inherent to iron containing materials, such as steel. Just as any material, steel has both desirable and undesirable qualities. It is used frequently in all types of construction because it is cheap and ductile, meaning it will stretch before it breaks, but while being ductile is a great quality of steel, rust can weaken it. There are many methods to prevent a steel member from rusting, such as painting. But an even better way to avoid rust is to use a completely different metal, such as aluminum.

Aluminum is a ductile material like steel, but it doesn't rust the way steel does, and is lighter than steel. While the majority of the U.S. Navy's fleet is made of steel; aluminum is being used more frequently. Using lightweight aluminum can decrease the weight of a ship providing for greater fuel efficiency and higher ship speeds. This allows the Navy more flexibility in where they can operate and how quickly and cheaply they can get there. For example, the Navy's newer class of ships, the Littoral Combat Ship, or LCS. These ships are designed to operate closer to shore where the water is shallower. The strength and lightweight properties of aluminum make it an exceptional material for such an application by producing a lighter ship and allowing it to sit higher in the water.

Other industries are also aware of these properties of aluminum and use it as a substitute for steel. The aircraft industry uses aluminum to produce lightweight fuselages and wings. The weight reduction that aluminum provides saves airline passengers money when a ticket is purchased through the fuel savings the aluminum provides. The auto industry uses aluminum to reduce the weight of car and truck frames while maintaining the strength. These weight savings benefit the driver every time they fill up their fuel tank. These fuel savings also allow automakers to meet ever stricter government regulations on emissions and fuel efficiency. Bicycle manufacturers also use aluminum to reduce weight while maintaining strength. This weight reduction benefits the user by reducing the energy needed to move them and the bike which reduces fatigue on the rider.

While aluminum is lighter than steel and provides adequate strength is isn't a perfect material and has some draw backs. Aluminum doesn't rust like steel, but it does still corrode and

corrosion is just one example of how a material will degrade over time. Different chemical and mechanical processes take place in materials constantly. Some other material degrading processes are fracture, change in residual stress, or material modulus degradation. These processes can deteriorate a material, and in turn, a structure over time. If the elastic modulus decreases over the course of a material's life then that material will become softer, and will be less able to perform its intended job in a structure. Think about constructing a truss to support a bridge, the truss is initially designed for, and built using, steel members. Now, suppose that during a late night prank someone removes one of the steel members and replaces it with a member that is identical in geometry but is made out of rubber. The only thing that has changed is the properties of the material, including a new lower value for Young's modulus of that member. This could be disastrous for the structure.

When dealing with the behavior of a material and investigating stress, strain, force, or displacement a material model is the first step. A material model is a definition of how a material will behave when acted upon. A material model utilizes the constitutive equations of a material. These constitutive equations are used to go from a known imposed strain, on a material, to the amount of stress that strain creates in the material. When a known stress is imposed on a material the constitutive equations are used to determine the amount of strain that will be produced. A common example of a constitutive equation is that seen in a simple tensile test, stress is equal to Young's modulus times strain.

A ship is a complex structure; there are many different design and analysis considerations when thinking about any complex structure. As discussed earlier the stiffness of a structure depends

on both material and geometry. Changing either changes the stiffness of the structure. Adding or taking away a member from a truss will make it more or less stiff, respectively. Using a stronger material will increase the stiffness of a structure. Filling a hollow aluminum tube with another material would make that tube stiffer, how much stiffer depends on the material. If the material was concrete the tube would be much stiffer, but if the material was a sponge it would only be negligibly stiffer. A ship can be thought of the same way. A ship has a specific stiffness when it is designed and built, but after it is built it is filled with wiring, piping, and equipment, all of these additional components make the ship a weapon instead of a floating shell. These added components are attached to the walls, floors, and ceilings around them. A bundle of copper wires running the length of the ship caring electricity from the generators in the back to the dining area in the front could increase the stiffness of the ship. These additional components create a vast number of variables that are difficult to model.

Looking at stiffness degradation on the scale of a ship would be complicated and produce many variables that might not be helpful in answering questions about stiffness degradation in a high performance, welded, aluminum structure. Modeling and experimenting with a large complex ship would also be incredibly expensive and impractical. To characterize stiffness degradation of a high performance, welded, aluminum structure a more practical and manageable analogous structure is needed. An aluminum bike frame meets the definition of a high performance, welded, aluminum structure. Bike manufactures have been using aluminum as a material of choice for many years to develop some expensive and competitive bike frames.

Aluminum bicycle frames are a popular choice for many riders because of the high strength to weight ratio that aluminum provides. A bike designer has only two major variables to control when designing a bike: geometry and material. A material doesn't care if a structure is a giant naval vessel or a manageably sized bike and while the geometry may be different between the two, the principles are the same. An aluminum bike frame is an ideal candidate for looking at stiffness degradation of an aluminum welded frame.

Experienced riders sometimes report a weakening of their bike frames. It is easy to search the Internet for this topic and find forums with riders discussing how their bike frames have become weak or soft; this information is often disputed by other posters as merely an excuse to purchase a new bike. Tour Magazine looked into this phenomenon to try and settle the debate. The article sites a rider who claims that, "After 3 years of racing, my frame was so soft and fluttery that I could not ride hands free to put on a rain jacket."[12] The Tour Magazine report performed an experiment using 6 aluminum frames. The loading was meant to simulate a rider pedaling a bike; therefore a two way pedal stroke of 1,200 N was applied at an angle of 10 degrees for 100,000 strokes or until failure and the clamping of the frame was meant to simulate a rider, see Figure 1.2.[12] The Tour Magazine experimental results show that the frame stiffness subtly declines with a maximum of 4% degradation in stiffness, leading up to a sudden failure, see Figure 1.3.[12] The article concludes that, "During 99% of the lifespan, the variation of the frame stiffness is so little, that a cycler could not notice. When the overall displacement adds up to a few millimeters, which is shortly before the break, the rider may notice."12] The article also goes on to say that the "fluttering" that most riders experience would most likely be attributed to bearings and wheels.[12]

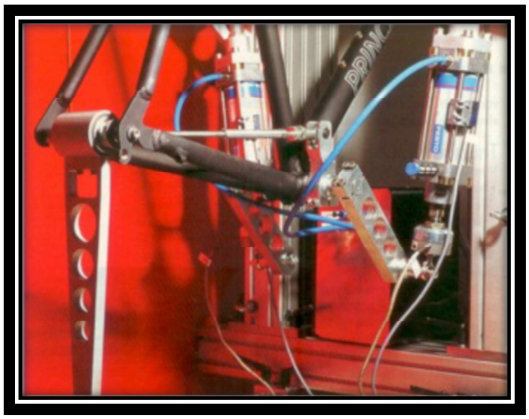

Figure 1.2 Tour Magazine Experimental Setup[12]

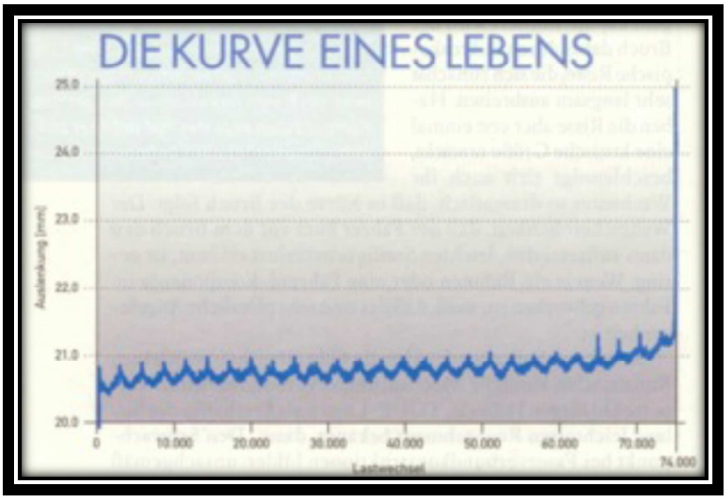

Figure 1.3 Tour Magazine Experimental Results[12]

While the stiffness degradation of aluminum bike frames appears to be minor, it does appear to be happening. Broadly, the two mechanisms that could be causing the stiffness of an aluminum bike frame, or any structure, to degrade would be a change in geometry or a change in material properties. During the typical service life of a structure, such as a bike or ship, the geometry would not be expected to change such that stiffness degradation would occur. Structures are typically designed with redundancy of critical members in mind and maintenance of the structure would ascertain such a change in geometry of the structure. This leaves a change in material properties as the most interesting reason stiffness degradation would occur. There are many plausible mechanisms on the material level that could cause stiffness degradation, this thesis will not attempt to address to what extent each mechanism is contributing to the degradation, but instead will degrade the modulus of the material as a lump sum of all of the different mechanism's effects.

In a paper by Zagrai et al. stiffness degradation appears to be occurring in a notched beam sample in a 3 point bend test.[1] This paper is discussed more in Section 3.1.2. Over an approximated 140,000 cycles it appears that stiffness degraded in the samples by about 15%. This research will be used as a foundation for the aluminum material. A material model will be developed based on this research using a finite element model.

The development of a material model requires an experimental test to determine how accurate it is and how well it can predict experimental results. This thesis will use a full scale experimental test of a fully welded aluminum bike frame to determine if stiffness is degrading, and to what extent, and to examine the material model developed.

1.2 Objectives

The overarching goal of this thesis is to investigate if stiffness, of a welded aluminum structure, will degrade as a function of cyclic loading. There are many different mechanisms that can cause stiffness to degrade, on many different scales, but to attempt to characterize stiffness degradation in a feasible thesis project; these mechanisms will be lumped into a single damage model with a damage parameter, also called a multiplier. This damage parameter will be explored using published research and then will be applied to an aluminum bike frame. An experiment will be performed to investigate the modeling results.

The objective of this work can be summarized in three points:

- Develop a damage model with a single adjustment parameter to match published research using a finite element model.
- Apply this damage model to a finite element model of a bike frame to investigate the amount of stiffness degradation that would be expected using the predicted damage model adjustment parameter above.
- Either confirm or refute the results of the bike frame finite element model by performing a full scale experiment directly characterizing stiffness degradation in a bike frame. If the results are refuted, determine what the adjustment parameter would need to be to match the bike frame experimental results.

2.0 Bike Experiment

2.1 Overview

The only way to know for sure the extent to which stiffness degradation occurs in a high performance, welded, aluminum structure is to test such a structure. This section discusses the design, development, execution, and results of such an experiment. A fully welded aluminum bike frame is used to investigate if stiffness degrades as a function of the number of load cycles.

An experiment based on an ASTM standard, with slight deviations, was designed to determine if stiffness degradation occurs in a bike frame, and if so, to what extent. This test was performed on an aluminum bike frame acquired from an online bike shop.

Later in this thesis a material model is developed based on published experimental results; this material model is then applied to a finite element model of a bike frame. This experiment was used to examine the results of this finite element model. While the results of the experiment do not concur with the results from the modeling this experiment stands on its own as evidence of stiffness degradation occurring in a high performance, welded, aluminum structure.

2.2 Experiment

2.1.1 Method

The experiment performed on the bike frame was a displacement controlled, cyclic test. The experiment setup is based on ASTM Standard F2711 with a few exceptions. The overall intent of the Standard was maintained in the design philosophy of the experiment. The Standard was used as the starting point for this work but was departed from to meet the intended objectives of this thesis. A main difference is that the Standard calls for both compression and tension loading but only compression was done to ensure that all stiffness degradation observed occurred in the bike and not in the experimental setup. An Instron 8502 testing machine at Cornell University was used to perform the test. The measurements were acquired by external instrumentation; this was done to provide better accuracy.

2.1.1.1 Horizontal Fatigue Test per Standard F2711

Finding a standard test to investigate the stiffness degradation of an aluminum bike frame was unsuccessful, but other standard tests for bike frames existed. The Horizontal Fatigue Test in accordance with ASTM F2711-08(2012) Standard Test Methods for Bicycle Frames was used.[2] The Standard expects that a bike will be able to withstand, by not developing a catastrophic failure after, a minimum number of cycles to be considered a safe bike. While the intent of the standard is focused on safety it was decided upon because the setup was feasible for the available machinery, it was cost efficient, and easily modified to address the desired questions. This section is intended to discuss the Horizontal Fatigue Test as stated in the standard; the exceptions to the standard are discussed later.

The overall setup of this test restrains the bike at the rear dropouts and applies a cyclic load to the front dropouts along the axis created by the front and rear dropouts, see Figure 2.1.[2]

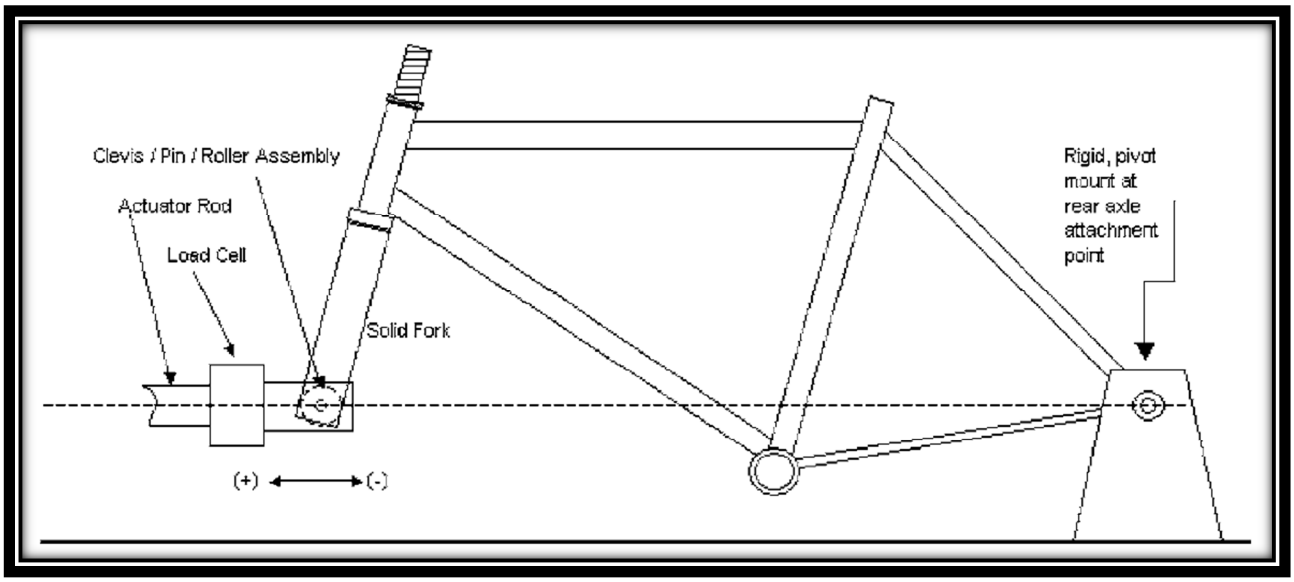

Figure 2.1 Horizontal Fatigue Test[2]

There are a few items made explicit in the standard that should be noted when looking at Figure 2.1:

1) The rigid mount holding the rear axle in place. As stated in standard F2711, "A fixture is required to restrain the frame at the rear dropouts, while allowing free rotation about the axle."[2]
2) The experimental test fork. As stated in standard F2711, "The test forks shall be designed to mount in a manner similar to the OEM [original equipment from manufacturer] fork, or in a manner using typical bicycle assembly procedures. The test forks, when mounted, shall be the same length, L, as the longest fork designed for use

with the frame and have a rake of 45 ± 6 mm. The fork shall be attached to the bicycle frame head tube using typical bicycle assembly practices."[2]

3) The front fork is noted as having a clevis, pin, or roller assembly when attached to the loading actuator. As stated in standard F2711, "The fork assembly shall be restrained at the dropouts in such a way that allows translation along the X-axis, and rotation about the Y-axis."[2] Requirements pertaining to deflection of the front fork are required per the standard. These requirements were addressed in the design of the front fork but not actually tested. See Section 2.2.1.1.1, ASTM Exceptions.
4) The actuator providing the force should not inhibit the test. As stated in standard F2711, "An actuator mounted load cell or equivalent apparatus that is capable of providing a reversible load of constant amplitude shall be attached to the front dropouts or front axle, without constricting the rotational freedom of the fork assembly. This apparatus shall allow cyclic load application to the front dropouts in a longitudinal direction along the bicycle centerline."[2]
5) There is a horizontal line created by the center of the front and rear axle. As stated in standard F2711, "The front and rear dropouts are to be equal in height when the frame and fork assembly is fixtured."[2]

Calibration of the test equipment is specified in standard F2711.[2] See Section 2.2.1.1,1 ASTM Exceptions, for more.

The magnitude and minimum number of cycles is determined based on the intended use of the bike; ASTM F2043-09 Standard Classification for Bicycle Usage addresses this discussion. The

bike being used for this project is classified as a Condition 1 Bike. As stated in standard F2043 a Condition 1 bike is that which is intended to be used, "[O]n a regular paved surface or smooth unpaved surfaces where the tires may unintentionally lose ground contact."[3] Knowing which Condition bike is being used the loading magnitude and number of cycles is then specified by another standard. For the instance of a Condition 1 bike the loading is specified in ASTM F2802-09 Standard Specification for Condition 1 Bicycle Frames. Standard F2802 specifies a minimum of 100,000 cycles with a cyclic load of 600 N tensile and 600 N compressive forces is required.[4] Converting Newtons to lbs, 600 N is 134.89 lbs.

The standard also specifies the frequency at which the experiment should be performed. The cyclic load is not to exceed 1Hz and is to be concluded after the specified minimum number of cycles or when fracture occurs.[2]

2.1.1.1.1 ASTM Exceptions

The Horizontal Fatigue Test discussed in Section 2.2.1.1 was used as a starting point for the design of the test that would be used to investigate if stiffness degradation occurs in an aluminum welded bike frame. Recall that the intent of the standard discussed in Section 2.2.1.1 is that of safety for the end user. This thesis is unconcerned with safety of the bike for the consumer and is instead more interested in how the aluminum frame performs, specifically concerning stiffness, as a function of the number of cycles the bike experiences. With this in mind it is important to discuss the deviations from the ASTM standard. There are several important

differences between the test as stated in Standard F2711 and the test used in this thesis, most of these differences can be seen in Figure 2.2.

Figure 2.2 Actual Experimental Setup Used

While looking at Figure 2.2 the following notes the differences from the ASTM Standard:

1) The most obvious difference is in the orientation of the bike frame. While the standard calls for the bike frame to be horizontal this project used the bike frame in a vertical orientation. This was done because of the access to the Instron 8502 used for this experiment and pictured in Figure 2.2. The loading direction still follows the same load path as discussed in the standard, recall from Figure 2.1 that an imaginary line is made between the front and rear axles, and the load is to be applied along this line. Using the setup vertical instead of horizontal does not violate this.
2) No roller assemblies or bearings are used. Instead, direct metal to metal contact is made through which rotation is allowed. The metal of the bike is directly in contact with the metal of either the Front Fork or the rear dropout support base, also known as the Axle Holding System. This was done to ensure that all stiffness that is being lost would be lost from the bike frame instead of the testing apparatus.
3) The Front Fork was not tested for deflection. Deflection was, however, considered in the design of the Front Fork. According to simple hand calculations the deflection in the Front Fork was negligible relative to the allowed deflection and no further investigation was performed.
4) Calibration of the measuring equipment was not done explicitly with the standard in mind. The calibration of the measuring equipment is discussed in Section 2.2.1.
5) Since the bike is being tested in a vertical manner without the use of any type of bearings it was only possible to test the bike frame in compression. Tension would have pulled the actuator away from the bike, not actually transferring the load into the bike, therefore only compression loading was used. To test the bike frame in tension would require a

more complex setup and, in turn, would create more opportunity for stiffness degradation of the setup to artificially influence the measurements.

6) The number of cycles directed in the standard was used only as a guideline as to the minimum number of cycles the bike might be able to sustain, but was not observed as a stopping point for the test because of the intent of the experiment.

2.1.1.2 The Bike

The bike used for this test is called an Ascent 52 Single-Speed Bike Frame, according to the catalog website.[5] According to the specifications provided this bike is made of Aluminum Alloy 6061.[5] The temper and age hardening properties of the material are not available. While researching this bike frame on the Internet it became clear that this bike frame is a generic model sold by various bike stores and no other detailed information on the manufacturing of the bike frame could be found. According to ASM Material Data Sheet website AA 6061 has a modulus of elasticity of 10,000 ksi and a Poisson's Ratio of 0.33.[6] The geometry of the bike can be seen in Figure 2.3.

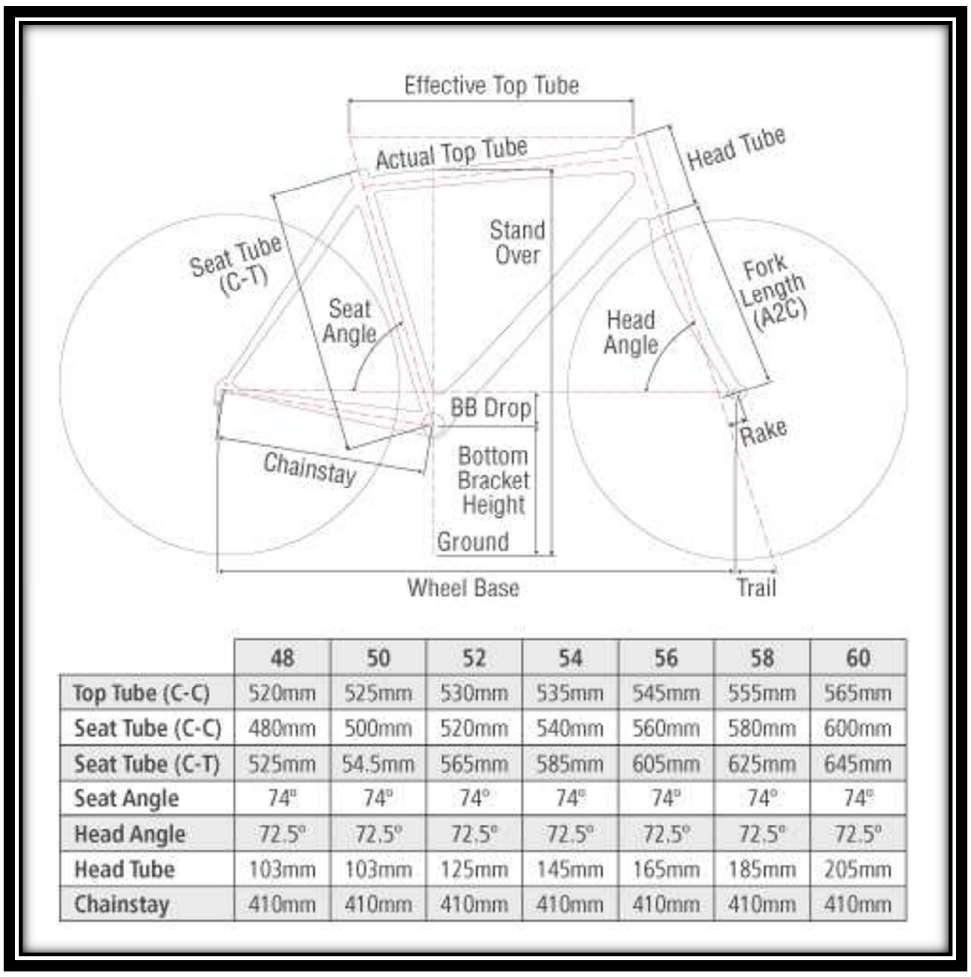

	48	50	52	54	56	58	60
Top Tube (C-C)	520mm	525mm	530mm	535mm	545mm	555mm	565mm
Seat Tube (C-C)	480mm	500mm	520mm	540mm	560mm	580mm	600mm
Seat Tube (C-T)	525mm	54.5mm	565mm	585mm	605mm	625mm	645mm
Seat Angle	74°	74°	74°	74°	74°	74°	74°
Head Angle	72.5°	72.5°	72.5°	72.5°	72.5°	72.5°	72.5°
Head Tube	103mm	103mm	125mm	145mm	165mm	185mm	205mm
Chainstay	410mm	410mm	410mm	410mm	410mm	410mm	410mm

Figure 2.3 Bike Frame Geometry[5]

2.1.1.3 Experimental Setup

The bike frame being tested needed to be affixed into the Instron testing apparatus, to do this several different parts were designed and made. The experimental setup was in line with ASTM Standard F2711 with the exceptions noted in Section 2.2.1.1.1. The members noted as being made of steel in the following are made from ASTM A36 Mild/Low Carbon Steel. This steel was purchased through Cornell University Laboratory of Atomic and Solid State Physics, or

LASSP, department. According to an Internet search the mechanical properties for A36 steel are: modulus of elasticity of 29000 ksi and Poisson's Ratio of 0.260.[19]

2.2.1.3.1 Axle Holding System

The Axle Holding System was designed to provide vertical and lateral support for the bike while allowing for free rotation, see Figure 2.4 and 2.5. The system uses no bearings and provides only metal to metal contact, which is the metal of the bike in contact with the metal of the Axle Holding System. No grease was used to lubricate this metal to metal contact. The reason no bearings or grease was used and only metal to metal contact was allowed was to ensure that all observed stiffness degradation was coming from the bike frame itself and not the experimental setup, to this end steel was also used as the material of choice for both the Axle Holding System and the Front Fork. Note that the Axle Holding System is as few pieces as possible. Machining the Axle Holding System out of a single piece of steel was looked at as an option but turned out to not be feasible. Note that the cylinder was machined to receive the rear dropouts of the bike; this is a single piece of steel. All other connections are welded. The material sizes were chosen based on extremely conservative hand calculations for axial, shear, and flexural loading.

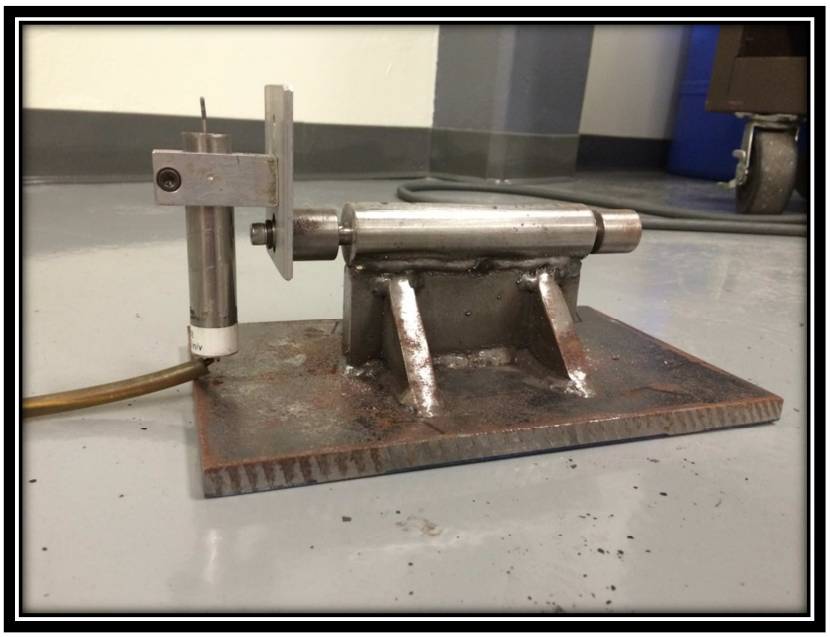

Figure 2.4 Front View of Axle Holding System

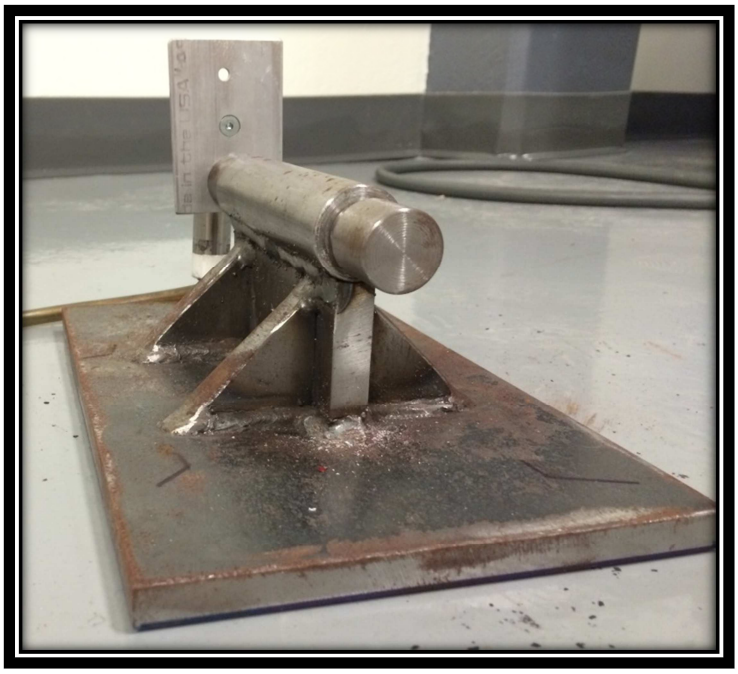

Figure 2.5 Isoperimetric View of Axle Holding System

The axle holding system is made of a combination of several different pieces each performing a different task. The cylindrical axle piece is used to provide support to the bike frame in much

the same way a wheel does for the end user, see Figure 2.6. The vertical support piece transfers the load from the cylindrical axle piece to the base of the system, see Figure 2.7. The angled side pieces provide support in the lateral direction, see Figure 2.8. While there should be negligible lateral forces because the load is directly over the axle holding system and the bike frame is allowed to rotate in the axle holder system, a conservative design called for these pieces. The flat base supports the entire system and allows all of the applied load to be transferred into the Instron base of the loading frame, see Figure 2.9.

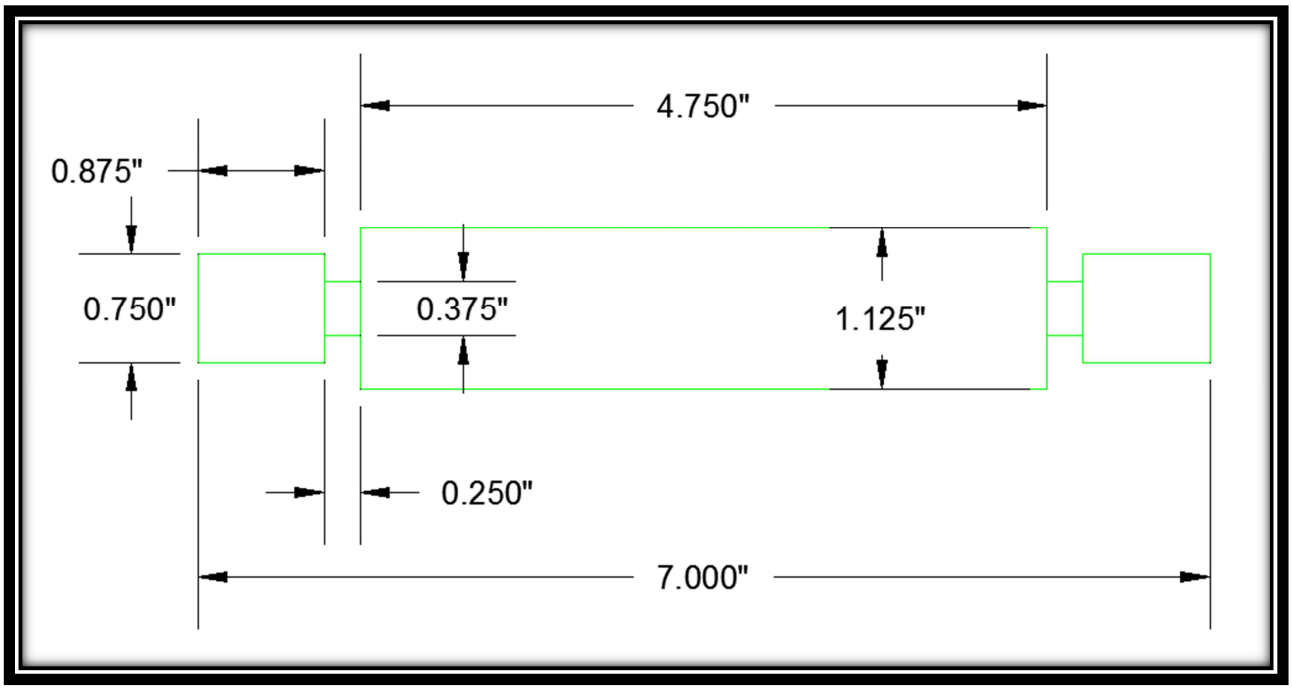

Figure 2.6 Axle Holding System - Cylindrical Axle Piece Dimensions

The cylindrical axle piece, see Figure 2.6, of the Axle Holding System is the only piece that has contact with the bike. This piece is designed to mimic the same support that the actual wheel of a bike provides. This piece is machined from a single piece of steel. The rear dropouts slide into the 0.25” slots on both sides of this cylindrical axle piece. The thicker pieces on the outsides of

these slots are used to resist any lateral movement the rear dropouts will produce as a product of the bike being loaded. This lateral motion is produced because as the bike is loaded these rear dropouts will tend to slide outward and would otherwise only be resisted by friction. These portions act just as nuts would on an end user system, except these pieces will not loosen.

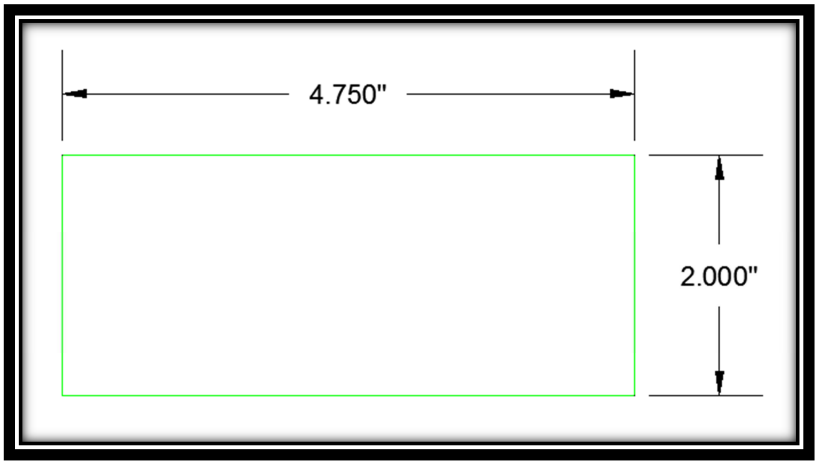

Figure 2.7 Axle Holding System – Vertical Support Piece Dimensions

The vertical support piece, see Figure 2.7, transfers load from the cylindrical axle piece to the base. This vertical support piece is welded to both the cylindrical axle piece and the flat base. Before it is welded together the three pieces are put in direct contact with each other. The weld is then performed. This creates a system of solid steel contact. The cylindrical axle piece is essentially sitting directly on top of this vertical support piece and therefore the load is mostly transferred through metal to metal contact and not necessarily relying on the welds. The welds provide stability to the pieces allowing the Axle Holding System to be moved around during the setup of the experiment. But since the experiment is all done in compression the bulk of the load is being transferred through metal to metal contact and the welds are used to provide stability support.

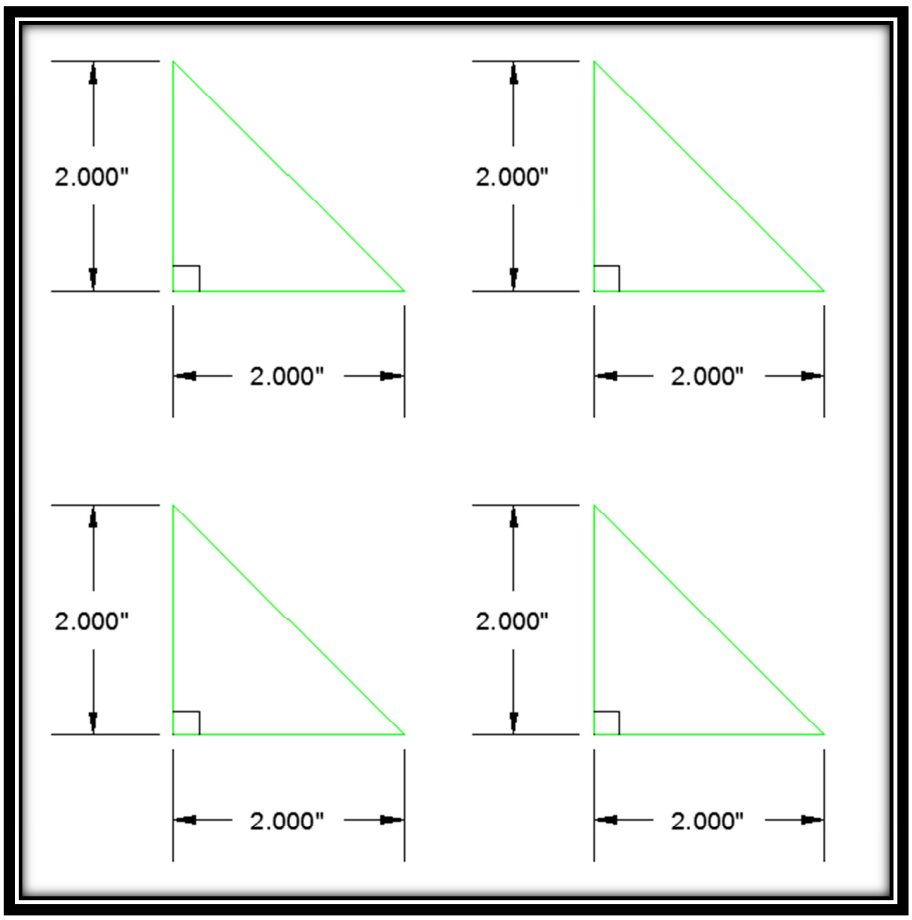

Figure 2.8 Axle Holding System – Angled Side Pieces Dimensions

The angled side pieces, see Figure 2.8, are welded to the sides of the vertical support piece and the flat base. These angled side pieces connect the vertical support piece to the base. These pieces are meant to provide lateral support. This lateral force is expected to be negligible because all of the load is applied vertically through the bike into the Axle Holding System and the bike is allowed to rotate within the cylindrical axle piece. But since this rotation depends on metal to metal contact which will produce a certain amount of friction and thereby resist the rotation of the bike frame. This rotation will produce slight lateral movement in the form of a

moment about the center of the cylindrical axle piece. From hand calculations these angled side pieces seem to be not necessary but were used to ensure a conservative system.

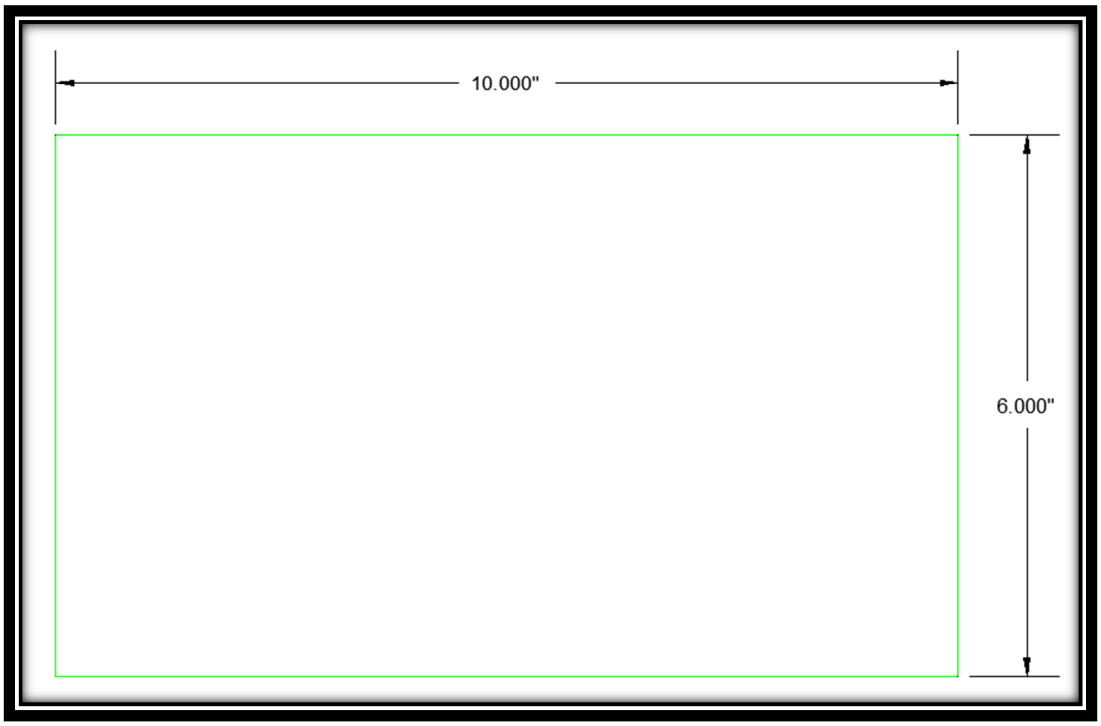

Figure 2.9 Axle Holding System –Flat Base Dimensions

The flat base is simply a rectangular piece of steel, see Figure 2.9. This provides a base for which to attach all of the other pieces of the Axle Holding System for transportation of a single unit and a way to securely clamp the system to the Instron support base. The load is transmitted from the bike to the cylindrical axle portion, to the vertical support piece, to the flat base, and finally to the Instron loading frame, while the angled side pieces and the welds provide lateral support and stability.

2.2.1.3.2 Front Fork

The Front Fork has the same design focus in mind; try to ensure all the stiffness that is observed as degrading happens in the bike and not in the experimental setup. For this reason the Front Fork is mostly one piece. The Front Fork is designed to insert into the bike as a manufactured fork would. Most other connections are welded.

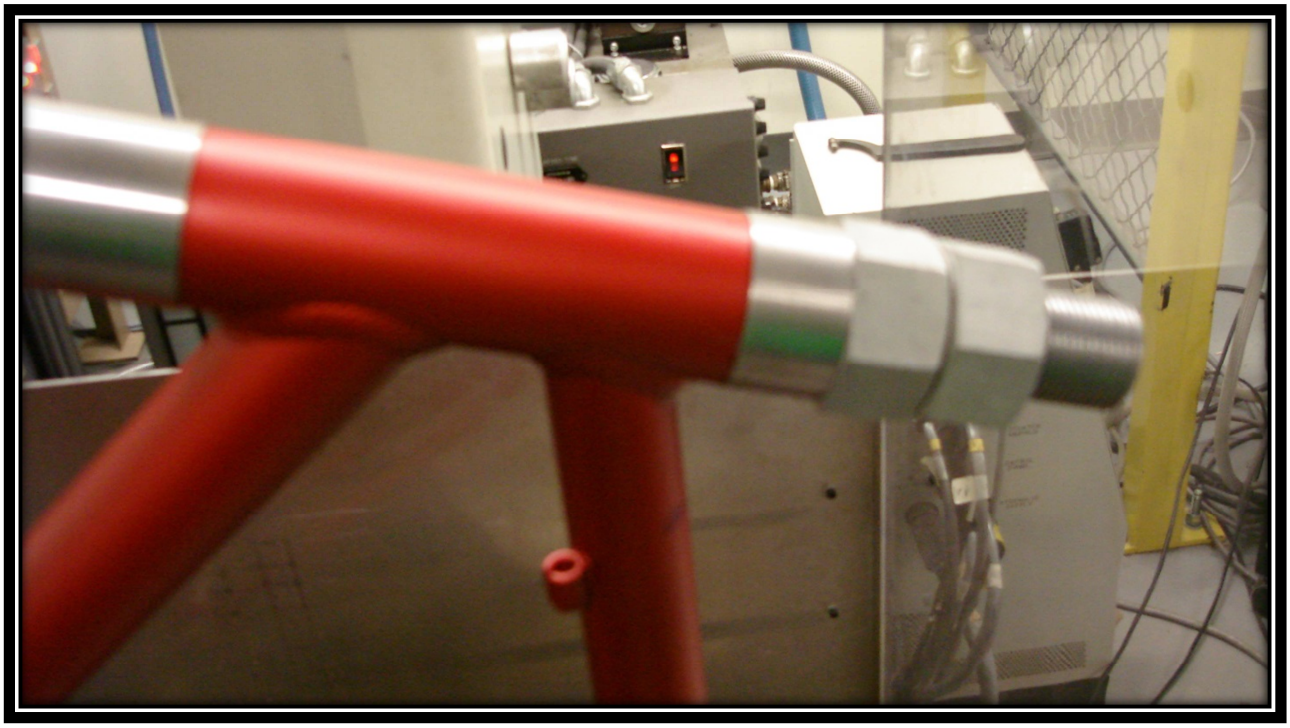

Figure 2.10 Front Fork Connection to Head Tube

The Front Fork is inserted through the bottom of the bike and attached with one spacer and two nuts, see Figure 2.10. The spacer is meant to provide a more uniform surface over which the force of the nut is distributed into the bike. See Figure 2.10 and 2.11.

Figure 2.11 Front Fork

Taking a closer look at the components of the Front Fork, it is easy to see two different systems in Figure 2.11 which are connected via a cylindrical solid piece of steel. The system on the left, the loading side, receiving the load from the Instron machine and the system on the right, the attaching side, is securing the fork to the bike.

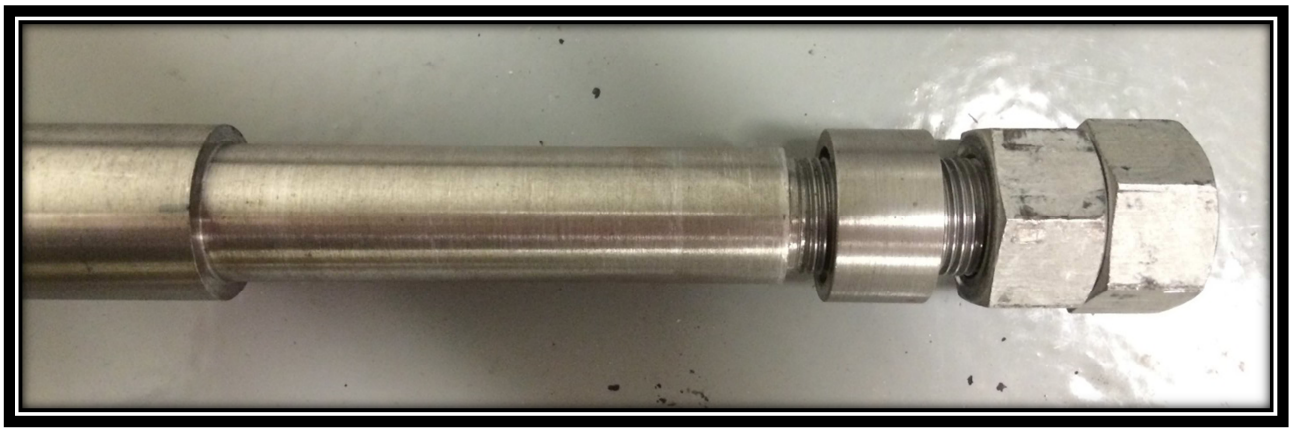

Figure 2.12 Front Fork – Attaching Side

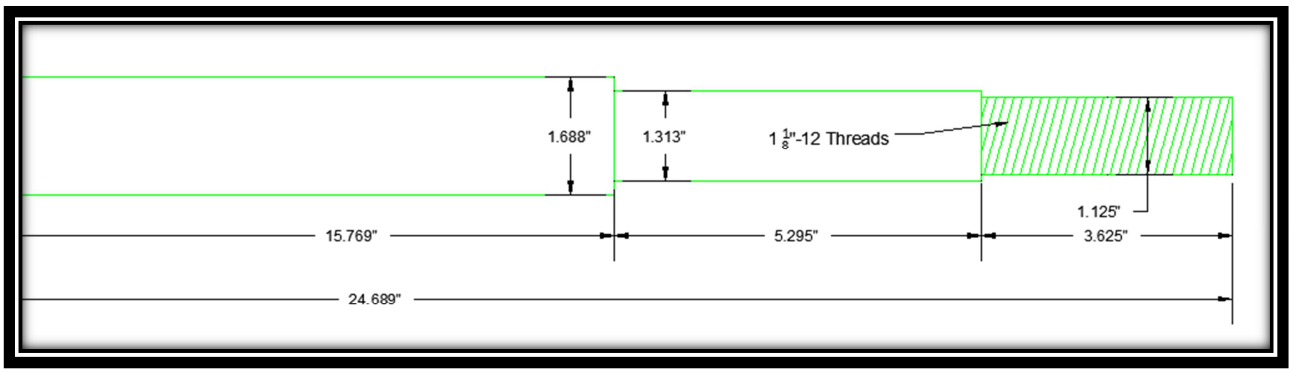

Figure 2.13 Front Fork – Attaching Side Dimensions

Looking at Figure 2.12 and starting from the right and moving to the left with a description. The right most object are the two tightening nuts. These nuts are meant to secure the fork onto the bike. These nuts were torqued to 130 lb-ft once the Front Fork was inserted into the bike, the spacer was moved into place, and the Front Fork was aligned with the loading actuator. The nut on the left can be thought of as the nut that is actually holding the Front Fork in the bike. The nut on the right is used to prevent the nut on the left from loosening, when the nut on the left tries to loosen it will do so into the nut on the right and will be stopped from loosening any further.

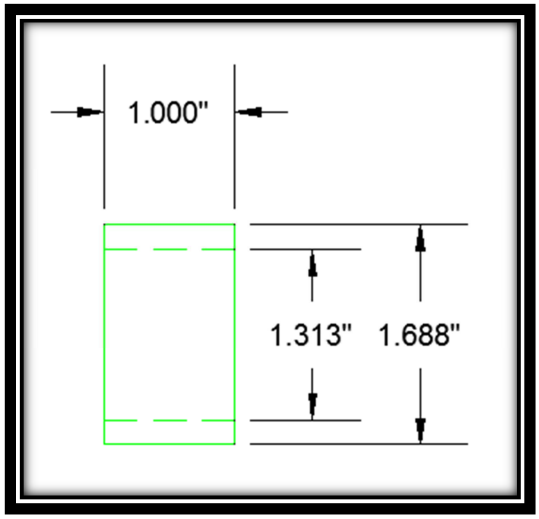

Figure 2.14 Front Fork – Spacer Dimensions

On the left of the two nuts is a spacer, see Figure 2.14. The purpose of this spacer is to apply the force, from tightening the nuts, evenly onto the head tube of the bike. This spacer acts just as a washer does but is thicker to prevent warping or distortion of the spacer as would be more easily done in a simple washer. This spacer is also machined more precisely allowing for better contact with the head tube.

To the left of the spacer there is a part of the fork that is machined down from the overall diameter of the fork, notice that this part does not have threads, see Figure 2.13. This thread-less part of the fork is where the inside of the head tube will be supported. The Front Fork will slide up, and into, the head tube. The bottom of the head tube will be supported by the shoulder to the left of this thread-less section, where it meets the larger diameter of the Front Fork. The top of the head tube will be supported by the spacer.

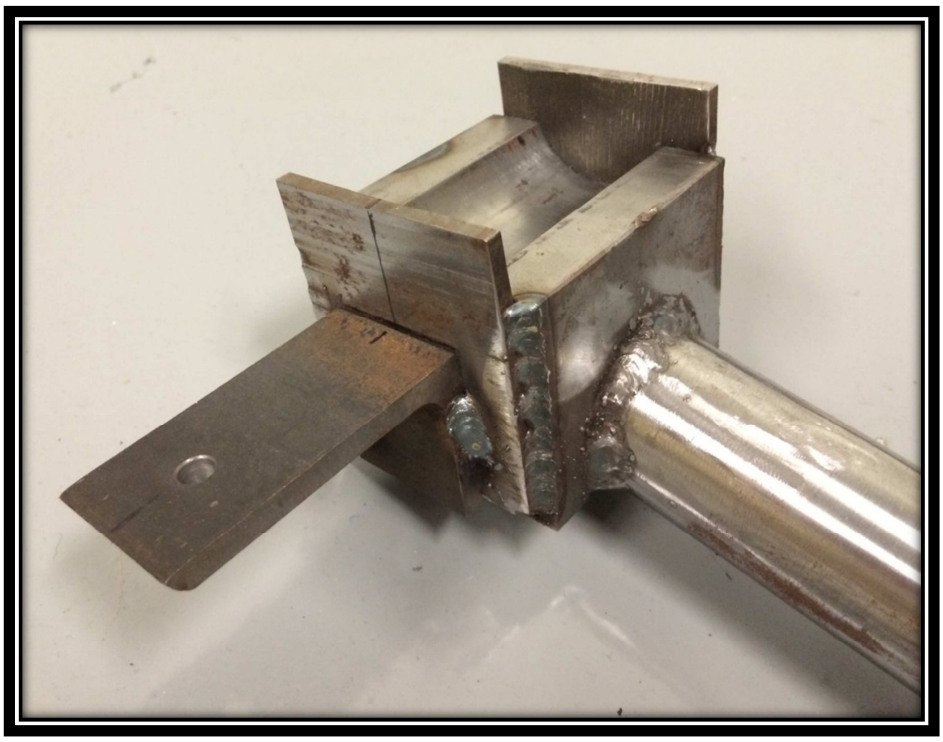

Figure 2.15 Front Fork – Loading Side

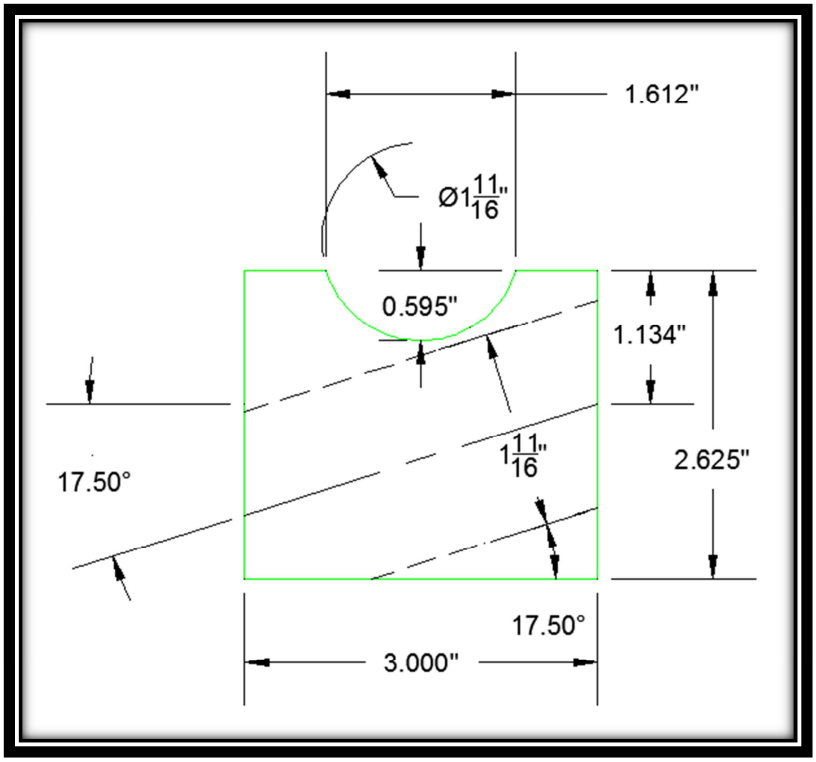

Figure 2.16 Front Fork – Actuator Reciving Block Dimensions

The far left, or the loading side, of the fork is where the load is transferred from the Instron into the bike, see Figure 2.15 and 2.16. There are three main pieces of this loading side. Starting from the left and moving right in Figure 2.15 the pieces can be seen are the displacement measurement rod bracket, a lateral support side, the actuator receiving block, and another lateral support side.

The measurement rod bracket holds an extension rod that is used to extend the overall length of the displacement measurement device. This rod is a steel rod that has threads on both sides, one side inserts into the measurement rod bracket and attaches with nuts and washers and the other end is attached to the displacement measurement device. This device will track the motion of the actuator receiving block and is discussed more in Section 2.2.1.4.1, Displacement Measurements.

The lateral supports on the sides of this block are to keep the actuator from moving side to side and falling out of the actuator receiving block. These sides are not completely necessary and are mostly used for setup and tear down of the experiment. Since the entire load being imposed on the bike is in compression, the actuator is maintained in place because there is not a horizontal force acting on it, causing it to move from side to side. However, when the experiment is being setup and torn down the bike is able to move more easily from side to side. While the experiment is actually running though this actuator cylinder does not move side to side and does not contact these lateral support sides.

The actuator receiving block, see Figure 2.16, is the block with a half cylinder machined into it. This actuator receiving block makes up the majority of the system that transfers load from the Instron into the bike frame. The half cylinder machined into this actuator receiving block will receive a matching half cylinder that is part of the Actuator Extension Assembly. These two half cylinders are made of steel and are machined to a smooth finish, which reduces the friction between the two creating a joint that allows for relatively free rotation.

These two systems combine to create the Front Fork. The block receiving the load slips onto the main part of the fork, with minimal clearance, and is then welded together. This creates a system that is essentially a single piece of steel. The welds connecting the actuator receiving block and the main fork are mostly to keep it from slipping on the main body of the front fork. Since the experiment is done only in compression the actuator is pushing on steel and is minimally relying on welds during the cyclic process.

2.2.1.3.3 Front Axle Loader

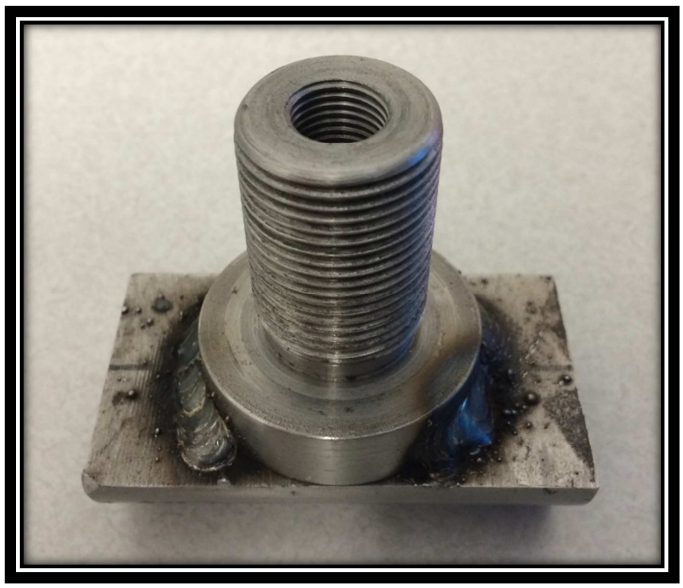

Figure 2.17 Front Axle Loader Front View

Figure 2.18 Front Axle Loader Side View

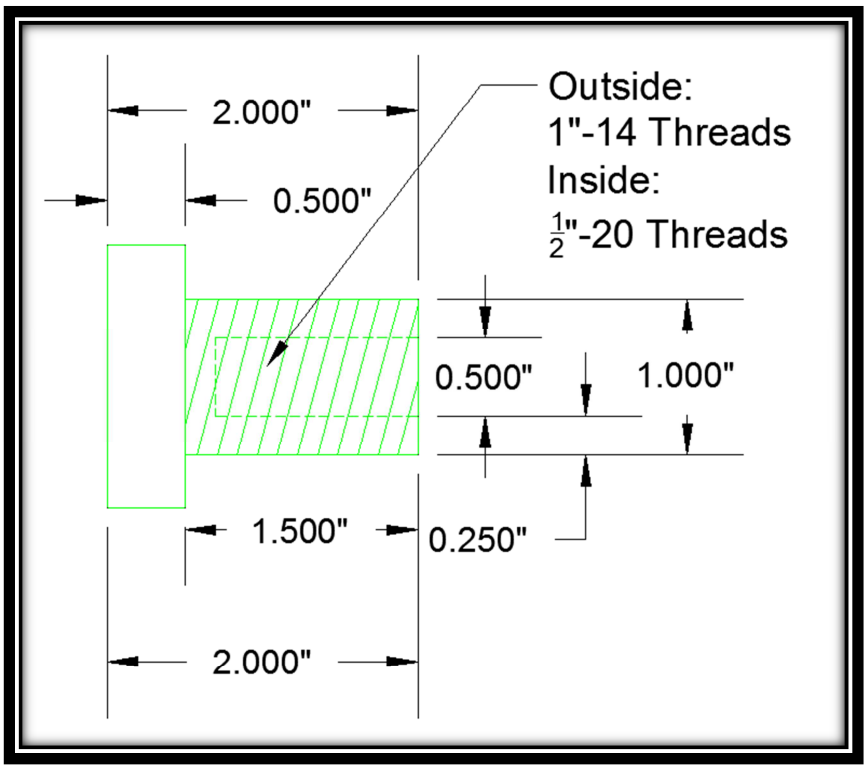

Figure 2.19 Front Axle Loader Dimensions

The Front Axle Loader, see Figures 2.17, 2.18, and 2.19, consists of a thick walled cylinder threaded on the inside and outside, allowing for connection to different load cells, and a smooth half cylinder welded together. This smooth half cylinder is meant to match the same half cylinder machined into the actuator receiving block on the Front Fork. This cylindrical joint is to allow rotation while the bike is being loaded. The threads are used to attach the front axle loader to the actuator extension assembly.

2.2.1.3.4 Actuator Extension Assembly

The actuator of a uniaxial tension testing machine, like the Instron being used is the part of the machine that is moving. During experiments the actuator is seldom in contact with the test

specimen; instead extension assemblies are fabricated to work with the exact experiment being done at the time. Recall that the main focus in designing this experiment is to make sure all observed stiffness degradation is happening in the bike frame and not in the test setup. To do this the test is done in compression only and no bearings or grease of any kind is used. The standard called for the bike to be able to rotate at the front fork. The solution to optimize over all of these parameters was to create matching half cylinders with smooth surfaces to minimize friction and allow rotation as much as possible.

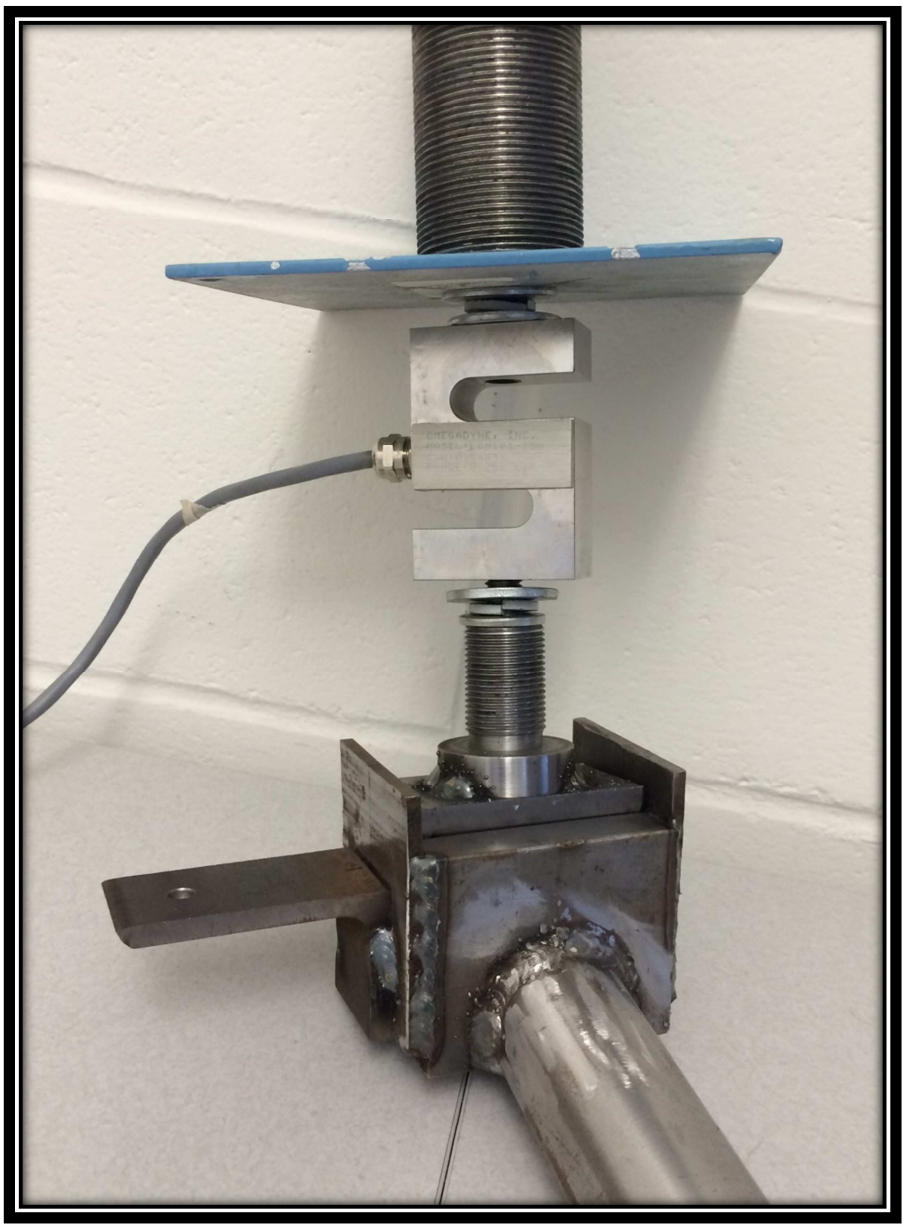

Figure 2.20 Actuator Extension Assembly

Figure 2.21 Instron Actuator Head

The actuator extension assembly, see Figure 2.20, has three main components: 1) Front Axle Loader, 2) Load Cell, and 3) Large Threaded Cylinder.

Starting from the top of Figure 2.20 the first major part encountered is the Large Threaded Cylinder; this piece is used to screw into the Instron actuator head, see Figure 2.21. Below the Large Threaded Cylinder is a blue square plate, this blue square plate is used as a giant washer. This plate is big enough to safely span the hole receiving the Large Threaded Cylinder in the actuator head. The reason this blue square plate is needed is because the Large Threaded Cylinder was loose in the actuator head, this looseness allowed for the actuator assembly to move side to side relatively easy, while there was plenty of thread to thread contact to allow for a good axial connection, side to side motion needed to be further restricted.

Moving down there is a washer, a lock washer, and another washer. These three washers are surrounding a piece of all thread that is used to connect the load cell and the Large Threaded Cylinder. When this assembly is tighten the blue plate causes the Large Threaded Cylinder to be pulled on inside the actuator head, this tension restricts the side to side movement of the actuator extension assembly. The lock washer is used to minimize loosening of the all-thread from the load cell and the Large Threaded Cylinder. The other washers provide more bearing area for the pieces they contact.

Below this set of three washers is the load cell. The load cell is described in Section 2.2.1.4.2, Force Measurements.

Below the load cell is another set of three washers and all-thread, this all-thread connects the load cell and the Front Axle Loader. The washer system provides the same support and resistance to loosening as the system connecting the load cell and the Large Threaded Cylinder, described above.

2.2.1.3.5 Entire Experiment Setup

All of these components come together to create the experimental setup. The Axle Holding System is clamped to the base of the Instron, such that the center, both ways, is directly lined up under the center of the actuator, see Figure 2.23. The Actuator Extension Assembly is assembled and threaded into the Instron actuator head, see Figure 2.22.

Figure 2.22 Entire Experimental Setup – Actuator Extension Assembly

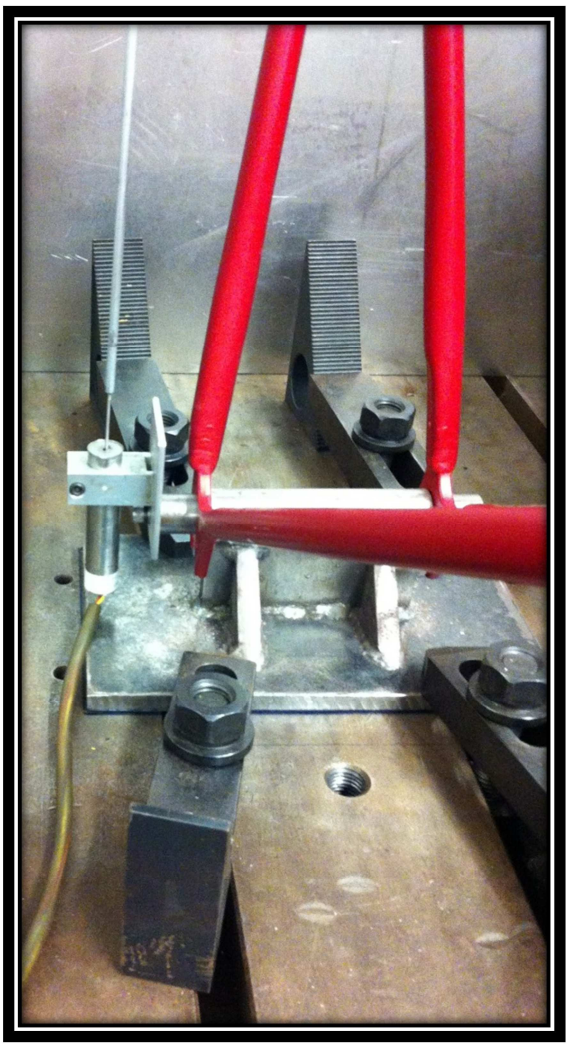

Figure 2.23 Entire Experimental Setup – Axle Holding System

The experimental setup is assembled in the following order:

1) The Axle Holder System is lined up directly under the Actuator Head using a plumb bob and is then held in place using a clamping system that is native to the Instron.
2) The Actuator Extension Assembly is threaded into the actuator head and is tightened using a large crescent wrench; it is tightened until all lock washers have been crushed, the blue square plate puts sufficient tension on the large threaded cylinder, and all side to side

allowed movement is eliminated. The actuator extension assembly should be relatively stiff when trying to move it side to side.

3) While the bike frame is on the floor, before it is moved to the Instron, the Front Fork is inserted into the bike frame, the spacer is put in place, and both nuts are tightened into place, each nut is tightened snuggly, but not to the designated torque of 130 lb-ft until the bike frame is moved to the Instron and all alignment adjustments have taken place.
4) With the bike frame still on the floor, the measurement rod is inserted into the front fork angle, nuts are put on the rod, and the rod is tightened into place.
5) The bike frame, Front Fork, and measurement rod are then picked up and put into place via the rear dropouts placed into their designated slots in the Axle Holding System. The measurement rod is attached to the displacement measurement device attached to the side of the Axle Holding System.
6) The Front Fork and the Front Axle Loader are adjusted to allow them to line up properly. Lining these up is done visually. Once these are lined-up the Front Fork nuts are then tightened to the 130 ft-lb torque.

The experimental setup is now complete and ready to begin testing.

2.2.1.4 Measurement System

The experiment was controlled by the Instron, but the recorded measurements were acquired by external measuring devices. Both the position and the force were measured externally from the Instron using the equipment discussed below. Measurements were taken in several different

ways, but only one set of data is viable and presented in this thesis. All data acquisition methods are discussed but only one set of results are presented.

Both displacement and force are measured using equipment external to the Instron. This was done because the accuracy of the Instron measurement systems did not appear to be stable or accurate enough at such small loads. This is because the Instron being used is capable of much larger forces, 50,000 lbs, than were being used, 140 lbs. This means that the experiment was being done in the noise range of the Instron's measurement instruments, therefore the instrumentation could not be trusted. It was decided to still use the Instron along with external instrumentation because it wasn't as important to have the experiment provide the exact displacements that were desired as it was to accurately measure both the displacements and the forces that actually existed and were exerted on the bike frame.

The measuring system was made up of three major components: 1) external power supply, 2) measuring devices, and 3) voltmeter.

Figure 2.24 External Instrumentation – Power Supply

Both the displacement and force measuring devices used the same power supply, see Figure 2.24. A basic understanding can be obtained by thinking about these devices working on a difference of voltage. Essentially a voltage is applied to these devices via the external power supply, as movement occurs a change in voltage takes place and is calibrated into either force or displacement, depending on the measuring device. This change of voltage is then read using a voltmeter and translated into force or displacement utilizing the appropriate calibration factors. This change in voltage is produced internally to the specific measuring device. The measuring device can be thought of as a black box. A specific voltage is applied to one end of both measuring devices, as force or displacement changes a different voltage is output by each device, by measuring this output voltage and applying a calibration factor the force or displacement can be discerned.

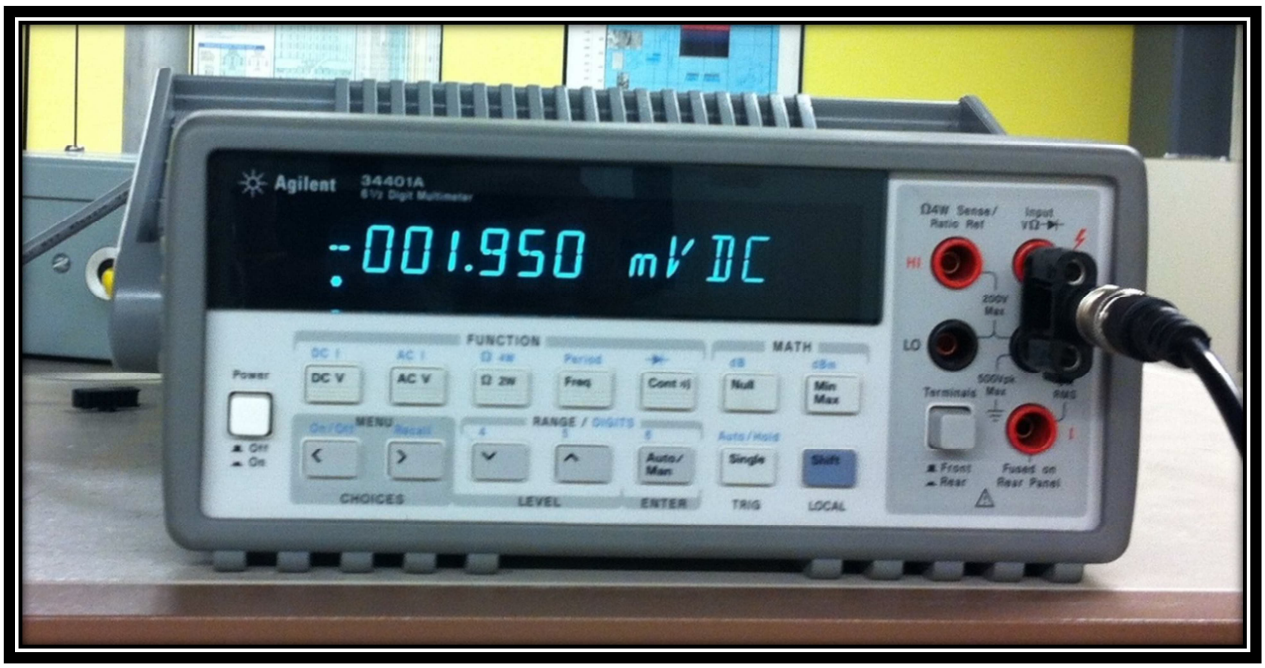

Figure 2.25 External Instrumentation – Voltmeter

Both the displacement and force measuring devices were read in the same way, using the same voltmeter, see Figure 2.25. A switch was installed to allow for easy access to both measurements. But both measurements could not be read at the exact same time. A voltage would be read and then converted into a displacement or force using an Excel spreadsheet and then recorded. These recorded measurements were then used to calculate stiffness.

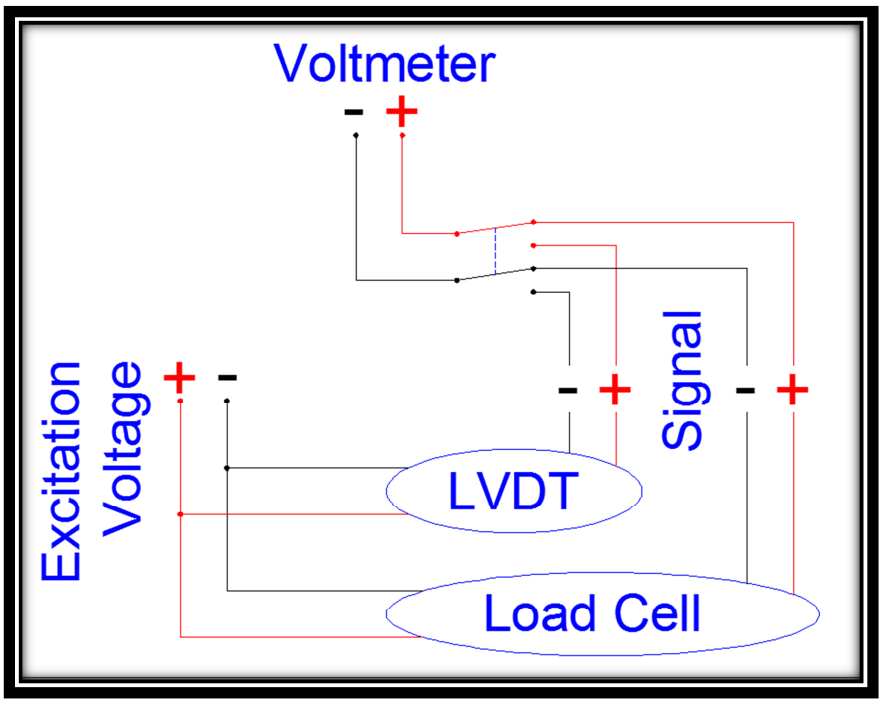

Figure 2.26 External Instrumentation – Wiring Diagram

Figure 2.26 shows the wiring diagram of the instrumentation. Excitation was provided to the measuring devices using the external power source. As the bike frame was displaced the displacement measuring device output a voltage associated with this displacement, the load cell output a voltage associated with the reaction force the bike frame experienced. Which voltage the voltmeter was reading was controlled by the switch depicted. This switch allowed for easy and quick access to each measuring device voltage but did not allow recording of both voltages at the same time.

When measurements were being read the voltage of the current position was read and the switch was moved to the other position, the voltage was read, and then the switch was switched back, if the original voltage was the same as the first reading the voltage readings were accepted and

recorded. This was done to ensure that the measurements went together and coincided with each other.

2.2.1.4.1 Displacement Measurements

The displacement measuring device is essentially what is known as a Linear Variable Differential Transformer or LVDT. While the displacement measuring device used in this thesis is not exactly the same because of the way power is supplied for all intents and purposes it is an LVDT. Essentially, as the center pole, see Figure 2.27, of the device is moved up and down a differential voltage is created in the transformer windings on the inside of the device, this differential voltage is measured and converted into a displacement.

2.2.1.4.1.1 Device Description

Figure 2.27 Displacement Measuring Device

The displacements were acquired using an LVDT style displacement device with an external power source. This device was acquired from the Department of Civil and Environmental Engineering at Cornell University. No device name, model name, or model number is denoted on the device. The device was calibrated and used using the English unit of inches.

2.2.1.4.1.2 Device Calibration

The calibration of the displacement measuring device was done using a device as seen in Figure 2.28. This device uses a dial micrometer which has the shaft of the center pole attached to it, readings were taken at different locations on this dial micrometer and a linear equation of voltage, as a function displacement was acquired, see Figure 2.30. The slope of this line is the conversion factor.

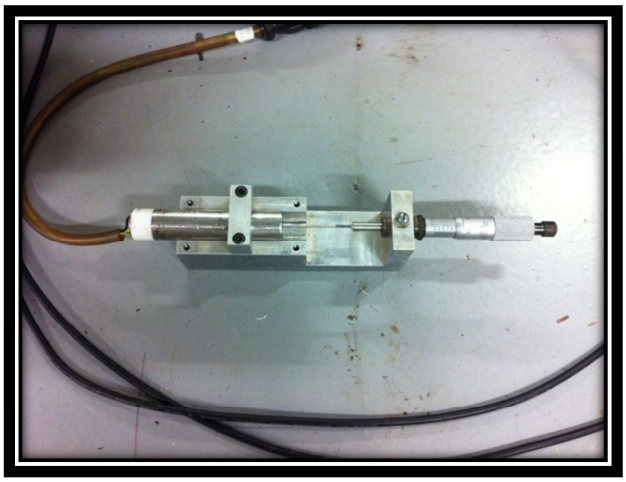

Figure 2.28 Displacement Device – Calibration Unit

Figure 2.29 Displacement Device – Calibration Unit Micrometer

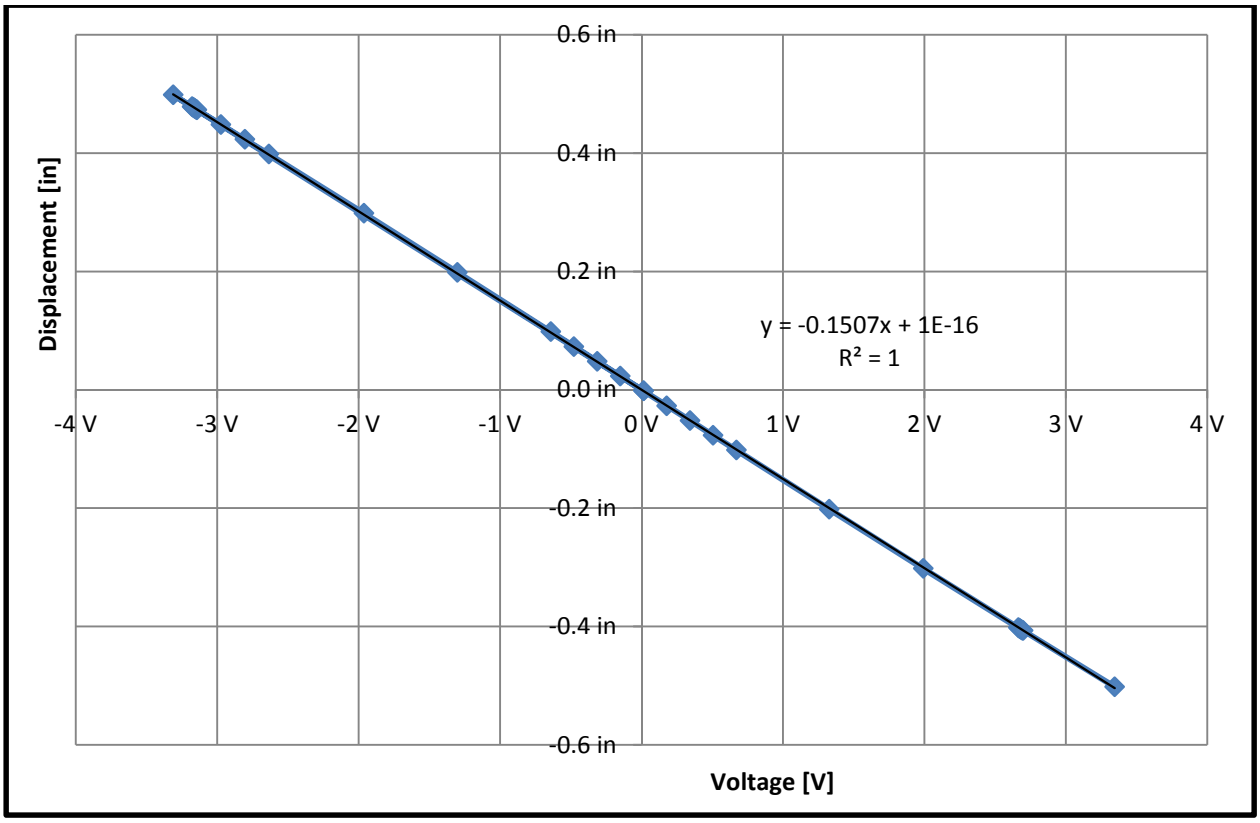

Figure 2.30 Displacement Measuring Device Calibration Data

2.2.1.4.2 Force Measurements

The force measurements were done using a standard load cell. A load cell is essentially a block of metal with a strain gauge attached to it. A load cell works much the same way a uniaxial tension test does. As load is applied, the force increases, the stress on the metal block increases, and the strain increases proportional to the stress multiplied by an elastic modulus. This is a familiar equation of stress equal strain multiplied by Young's modulus. The strain gauge outputs a differential voltage which is measured and converted into a force.

2.2.1.4.2.1 Device Description

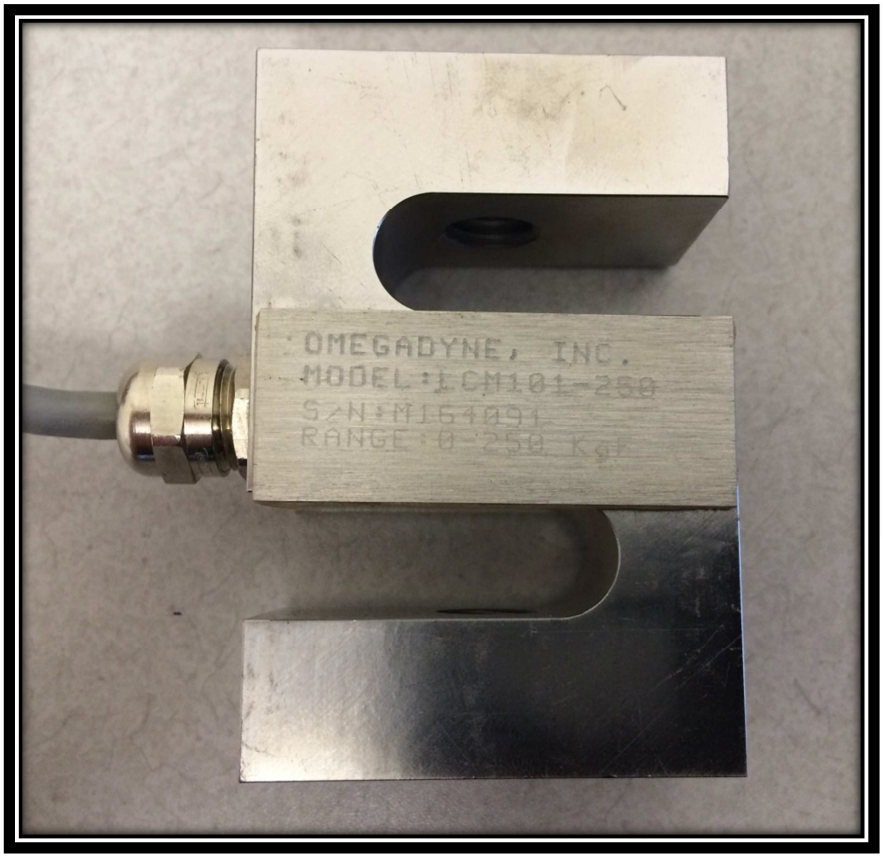

Figure 2.31 Load Cell Used

The load cell being used was acquired from the Department of Civil and Environmental Engineering at Cornell University. The load cell is a product of Omegadyne Inc. with a model number of LCM101-250 and a serial number of M164091 and has a stated range of 0 – 250 KgF. While the range is stated in metric units the device was calibrated and used using English units of pounds.

2.2.1.4.2.2 Device Calibration

This load cell was calibrated by weighing, in pounds, different metal objects lying around the lab using a 6 kg scale. These differing objects were then placed on top of the load cell, see Figure 2.32, and a voltage reading was acquired. A linear equation relating voltage as a function of force was acquired, see Figure 2.34. The obtained equation is used to convert voltages to force measurements.

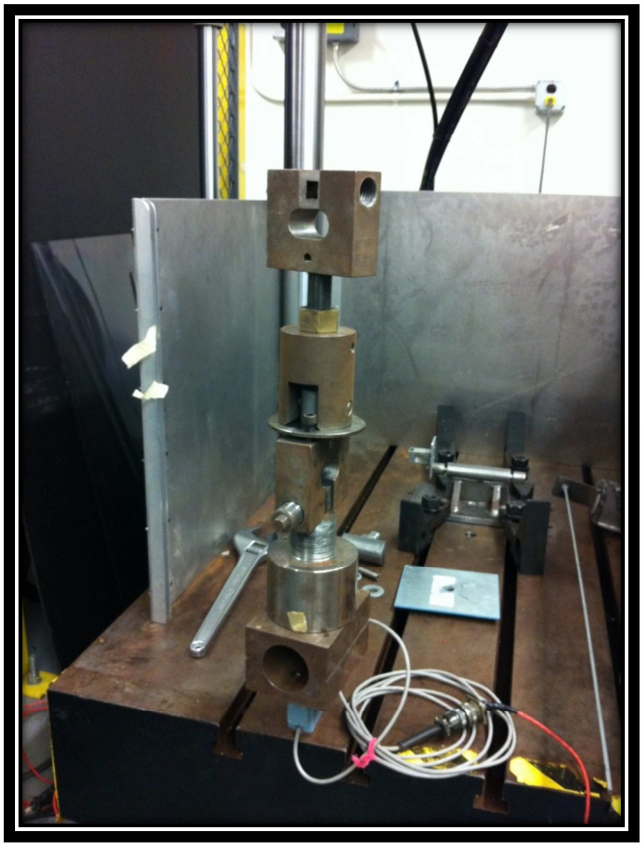

Figure 2.32 Load Cell Calibration

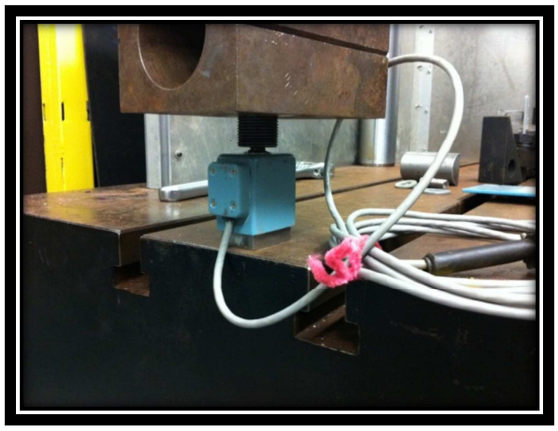

Figure 2.33 Load Cell Calibration – Close-up

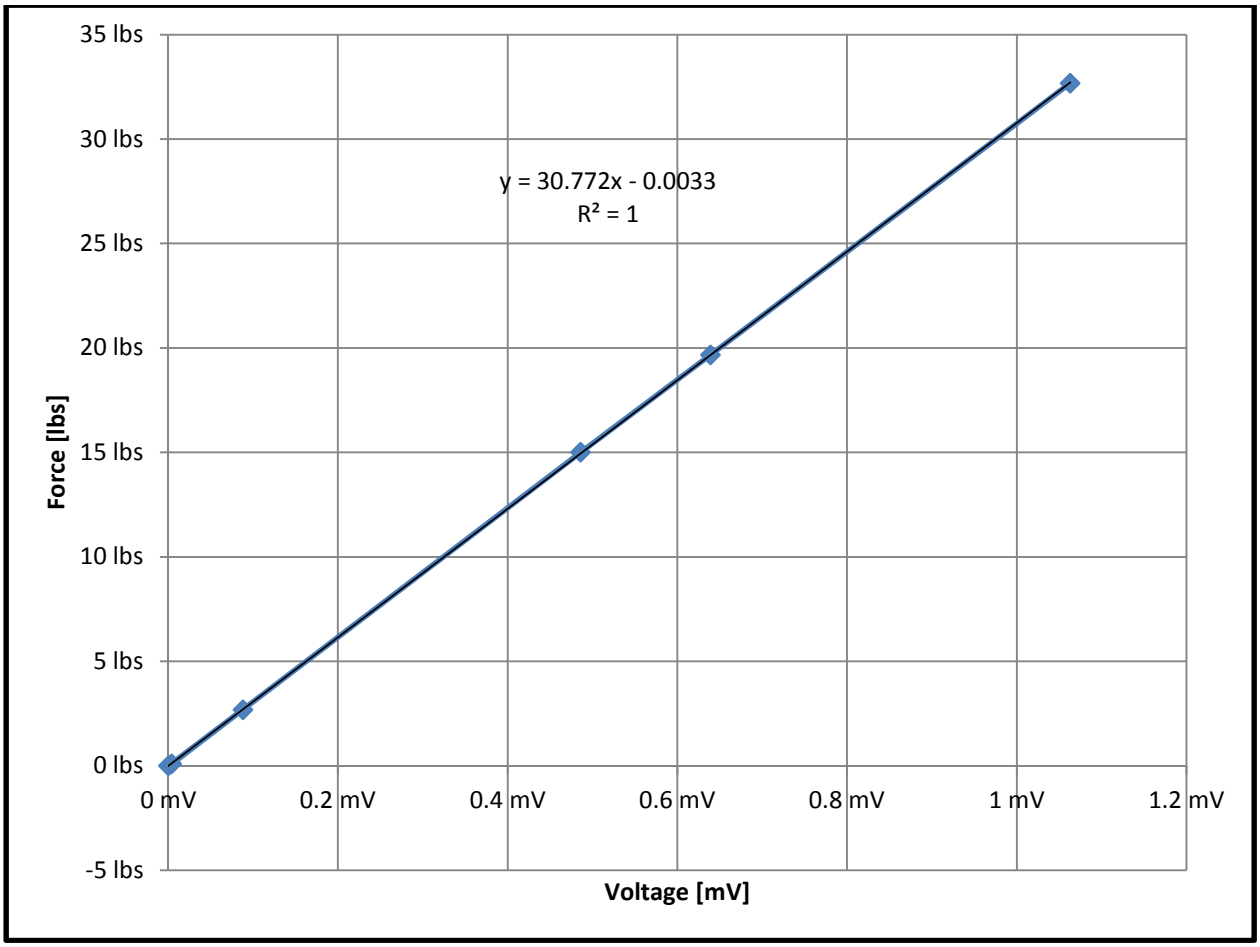

Figure 2.34 Load Cell Calibration Data

2.2.1.4.3 How Measurements Were Acquired

Once the experiment was setup and running measurements were taken of force and displacement. Force was measured directly using the load cell discussed above, which was directly attached to the actuator via the Actuator Extension Assembly. Displacement is measured using the device discussed above, while the displacement measuring device is held stationary on the Axle Holding System, it is measuring the displacement of the Front Fork at the same location that load is being measured, via the extension rod.

Accuracy and precision were the main objectives when obtaining measurements. In this experiment, just like any experiment, there is a chance for human or machine error, electrical noise, and vibrations. All of these different facets could cause a reading to be inaccurate. In an attempt to avoid as much error as possible measurements were documented using three different methods, which are discussed below. Unfortunately, only one of these methods produced viable data. While only this viable set of data is presented in the results all three methods are discussed below for completeness.

2.2.1.4.3.1 While Held

The Instron used a sine wave of displacements to perform this displacement controlled test. The actuator was moved to a starting point, from this starting point the Instron would increase displacement until the maximum displacement was achieved, it would then decrease displacement until the minimum displacement was achieved, and finally it would increase displacement until the starting point was achieved. This created a full loading cycle. The Instron had a capability of running for a set number of full cycles; therefore it would always start and stop at the same midpoint location.

The While Held method was done such that measurements were recorded at this midpoint. The Instron was set to run for a given number of cycles and then stopped after those cycles were completed. After stopping the Instron actively tried to hold the location of the displacement, because of this significant vibration was present, this showed up in the voltmeter readings by

fluctuating numbers in the last decimal places. Effort was made in trying to get numbers for force and displacement that coincided with the same point in time, but it was clear that a certain amount of error would be produced by this vibration.

2.2.1.4.3.2 While Off – 20 Min After Held

After the measurements in Section 2.2.1.4.3.1 were obtained the machine was turned off by the test operator. After the machine was turned off the displacement drifted because the Instron no longer had the ability to actively maintain the displacement. Being that the actuator is a hydraulic cylinder it was able to passively maintain the displacement because hydraulic fluid was not allowed to be discharged from the cylinder due to all valves being closed. This passive system was able to maintain the displacement in a range that was approximately a quarter of the entire displacement range, that is, the minimum displacement subtracted from the maximum displacement. The displacement seemed to level off and become constant around 15 minutes, by waiting 20 minutes stable displacement and force measurements were acquired. Force and displacement measurements were taken as described above and effort went into trying to get numbers for force and displacement that went together at the exact same moment in time. This method was used to avoid the fluctuation caused by the vibration of the Instron's running mechanical parts, such as the heavy duty hydraulic pump.

2.2.1.4.3.3 Multiple Points

After the measurements in Section 2.2.1.4.3.2 were obtained the Instron was turned back on and the displacement was put to the starting point, the midpoint displacement or the starting displacement, and both force and displacement measurements were taken. The displacement was then increased six more times until the peak of the cycle was obtained, at each of these increments force and displacement was obtained. A line was fit to this data and the slope of this line was said to be the stiffness at that many cycles.

As you can see from the results in Section 2.3 this method only has data starting at about 200,000 cycles, this is because this method was an afterthought and only implemented after problems, with unknown solutions, were observed in the other two measuring methods. The other two methods, the While Held method and the While Off – 20 Min After Held method, had significant issues. The major issue that called for their abandonment was that they did not match each other. No cycles occurred between the two measurements and yet they did not give the same stiffness readings. The Multiple Points method was implemented because several data points would be used to obtain a single value of stiffness, instead of using a single data point as in the other two methods. Also, the Multiple Points method did not rely as heavily on the value of the displacement. Several readings were taken and a line was fit to the data, the absolute value of the displacement became less important compared to the relative value of the displacement. It was essentially like recalibrating the displacement measuring device every time stiffness was recorded.

Test Number =			21	363404 Cycles	To zero Intercept=		-0.00532753
Test Number	Instron Controller Displacement [in]	Displacement Voltage [V]	Corrected Displacement [in]	Displacement [in]	Force Voltage [mV]	Force [lbs]	Stiffness [lbs/in]
1	4.123 in	0.60821 V	0.09166 in	0.08633 in	1.992 mV	63.49 lbs	735.49 lbs/in
2	4.110 in	0.69579 V	0.10486 in	0.09953 in	2.295 mV	72.82 lbs	731.64 lbs/in
3	4.096 in	0.78705 V	0.11861 in	0.11328 in	2.634 mV	83.25 lbs	734.90 lbs/in
4	4.083 in	0.87249 V	0.13148 in	0.12616 in	2.939 mV	92.64 lbs	734.29 lbs/in
5	4.070 in	0.95978 V	0.14464 in	0.13931 in	3.254 mV	102.33 lbs	734.53 lbs/in
6	4.056 in	1.05376 V	0.15880 in	0.15347 in	3.590 mV	112.67 lbs	734.12 lbs/in
7	4.043 in	1.14087 V	0.17193 in	0.16660 in	3.902 mV	122.27 lbs	733.90 lbs/in
	Uncorrected		Corrected				
	Slope=	734.1219599	Slope=	734.1219599			
	Intercept=	-3.91105853	Intercept=	0.000000000			
	R-Value=	0.999967476	R-Value=	0.999967476			

Figure 2.35 Multiple Points Method – Stiffness Reading Example Data

Figure 2.35 is a sample taken from the spreadsheet used to record data acquired using the Multiple Points method. The columns in purple are the columns of input data. Each of the 7 points that is acquired is on its own row. The columns are described as follows:

1) "Test Number": This denotes which of the several points are being observed.
2) "Instron Controller Displacement [in]": This is the location of the actuator head, this location is controlled by the hydraulics of the Instron, this is a set point value that can be entered into the machine and the Instron will move the actuator head to this location. This value is relative and only says something about displacement when compared to another value in this column.
3) "Displacement Voltage [V]": This is the voltage as read on the voltmeter corresponding to the displacement measuring device.

4) “Corrected Displacement [in]”: This is the corrected displacement. It is corrected using a linear fit to all 7 data points that are collected; see the discussion for the “Uncorrected” column below.
5) “Displacement [in]”: This is the displacement value that is obtained from applying a conversion factor to the recorded voltage corresponding to displacement.
6) “Force Voltage [mV]”: This is the voltage as read on the voltmeter corresponding to the load cell.
7) “Force [lbs]”: This is the value of the reaction force produced by the bike frame resisting the applied displacement. This value is obtained by applying a conversion factor to the voltage associated with the force.
8) “Stiffness [lbs/in]”: This is the stiffness. This value is obtained by dividing the value in the force column by the value in the displacement column.
9) ‘Uncorrected”: This block of information is based on a linear regression fit of the data in the “Displacement [in]” column and the “Force [lbs]” columns. This data is obtained to correct the displacement values. Therefore, the values in the “Corrected Displacement [in]” column are obtained by applying this information as a correction factor to the values in the “Displacement [in]” column.
10) “Corrected”: This block of information is based on a linear regression fit of the data in the Corrected Displacement and Force columns. By looking at the Intercept it is easy to see that this data has been corrected. The slope value in the red box is the final value of stiffness at this number of cycles.

The process of obtaining these values starts by inputting the actuator set point value in the "Instron Controller Displacement [in]" column. The Instron then moves the actuator to that position, once the voltage values are stable the voltage corresponding to the displacement is read, the switch is moved to read the voltage associated with the force, and then the switch is switched back and the voltage associated with the displacement is read again, if this voltage is the same as the first time then both voltages, for displacement and force, are recorded in their respective columns.

2.2.2 Instron

Figure 2.36 Instron –Front View

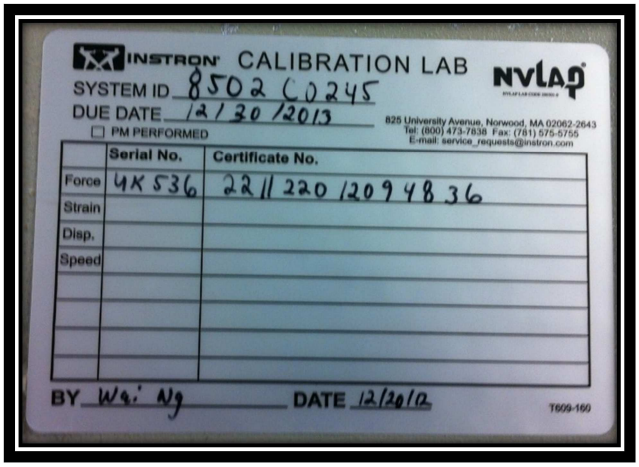

Figure 2.37 Instron – Label View

The Instron used was a model 8502, see Figure 2.36, it is a 50 kip machine. The Instron machine is the property of Cornell University Mechanical Engineering Department. The experiment is displacement controlled and the Instron controlled this displacement, a sine waveform was used for this applied displacement, very little else was used on the machine.

2.3 Results

The multiple points method of data collection seemed to be the most useful because of the way it recalibrated the displacement measurement each time. By finding the slope of a line through several measurements multiple data points were relied on instead of a single measurement. The method also was able to move away from the noise range of the load cell by measuring larger values, that is, from the midpoint displacement to the maximum displacement.

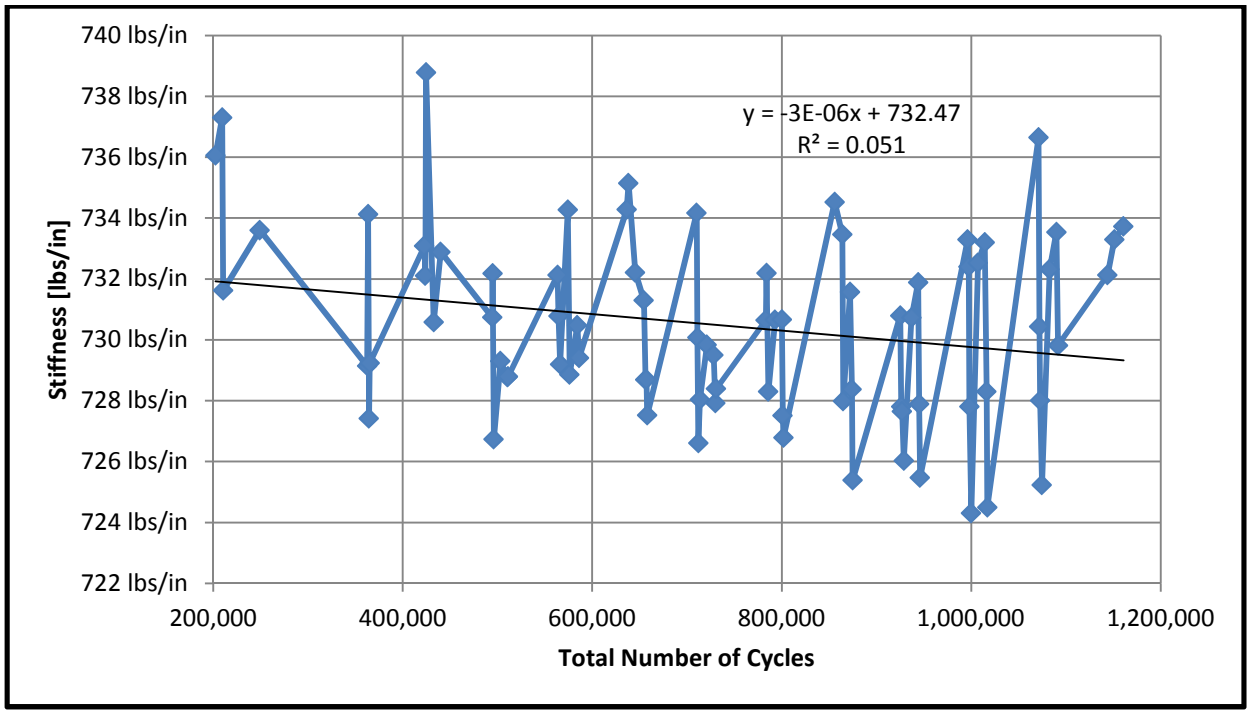

Figure 2.38 Multiple Point Method Results

Figure 2.38 shows the data acquired using the multiple points method. A simple linear fit, which is a mathematical model, is applied to the data and a decreasing linear relationship appears to be present, but it is important to determine if this trend is statistically significant.

The simple linear fit used is a mathematical model, and in all mathematical models assumptions are inherent. It is important to discuss these assumptions and if they are upheld or not. Assumptions tell the user of the model what the bounds of the model are. Staying within the bounds increases the significance of the results. The farther the user strays from these bounds the more uncertain the results become.

The assumptions of linear regression are as follows[18]:

- Linearity of the relationship between dependent and independent variables.
- Independence of the errors.
- Homoscedasticity, or constant variance, of the errors.
- Normality of the error distribution.

For this set of data these assumptions can be tested by looking at two different plots:

- Plot of the residuals versus predicted values. To satisfy assumptions the points in this plot should be symmetrically distributed around a horizontal line and maintain a constant thickness throughout, where the thickness is the distance from the top point to the bottom point.
- Histogram of the residuals. To satisfy assumptions the histogram should follow a normal distribution.

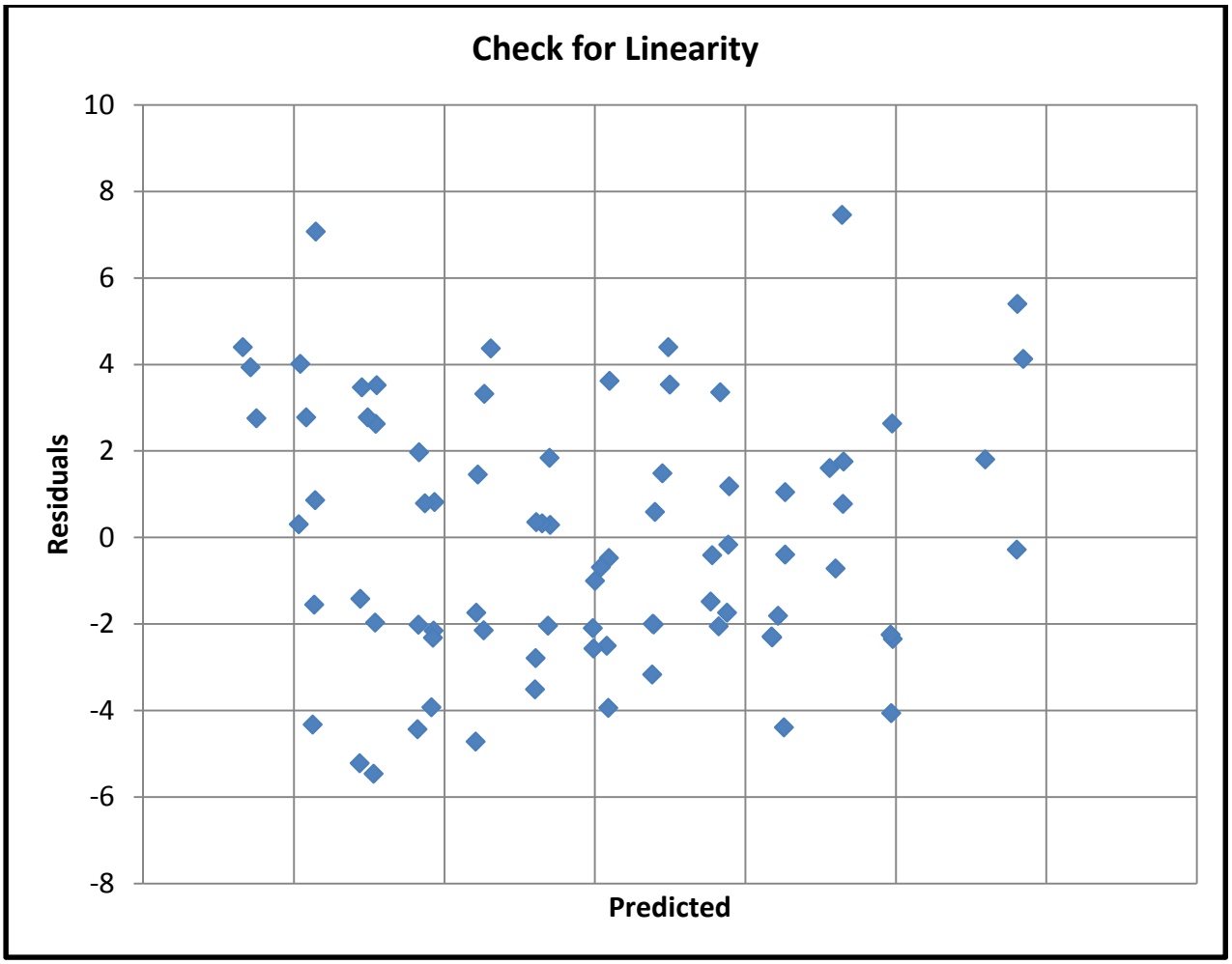

Figure 2.39 Linear Regression – Plot of Residual Errors Versus Predicted Values

Figure 2.39 is a plot of the residuals versus the predicted values. These points appear to be symmetric about a horizontal line at zero, which satisfies the assumptions. Notice that the thickness of the points is remaining relatively constant when moving left to right in the plot. This satisfies the assumptions.

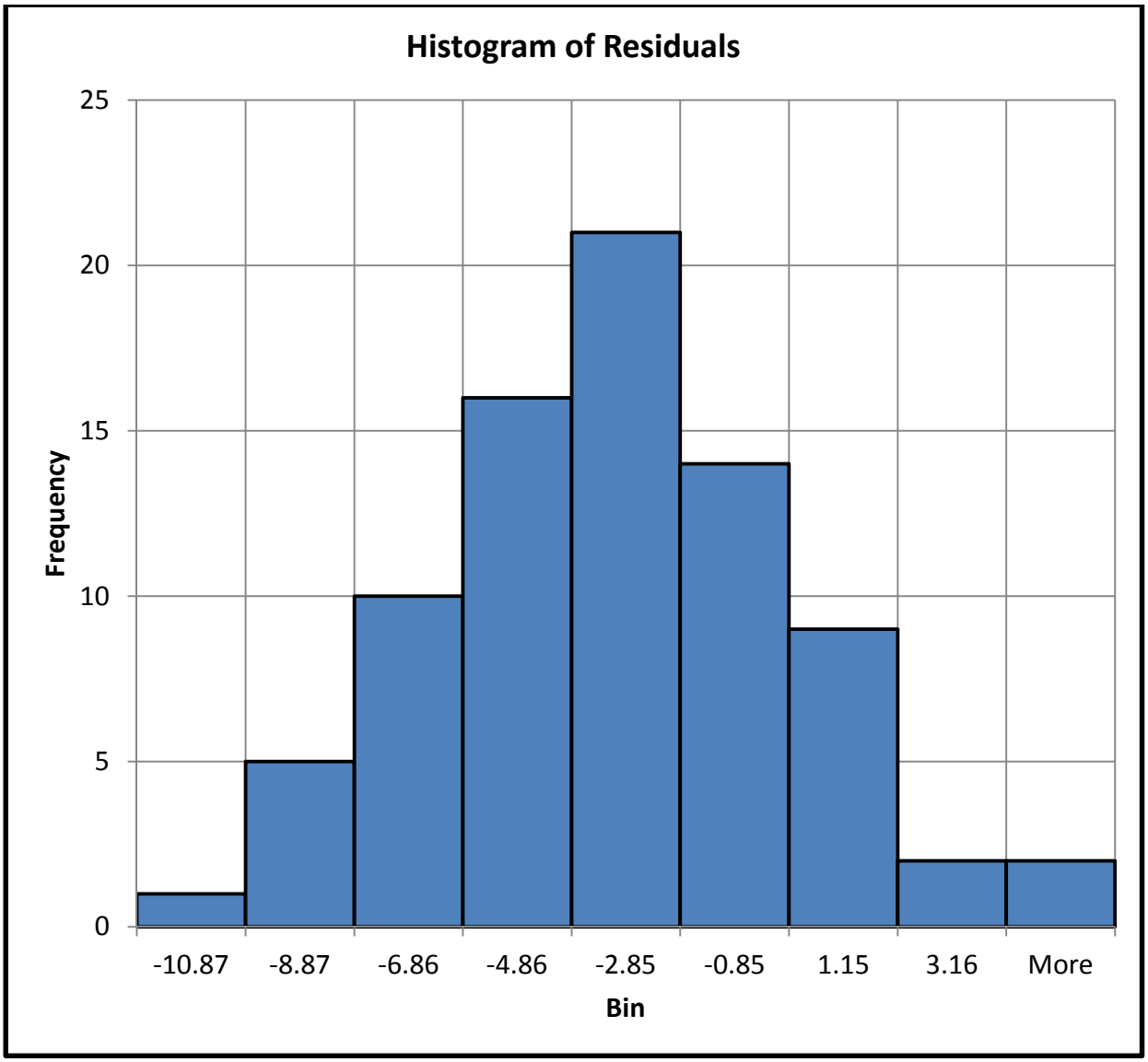

Figure 2.40 Linear Regression – Histogram of Residuals

Figure 2.40 is a histogram of the residuals. Notice that the residuals seem to follow a normal distribution, satisfying the assumptions.

S_x	S_y	S_{xx}	S_{xy}	S_{yy}	n
59091820	58437.74182	4.86924E+13	43151258362	42687845.42	80

95%					
df	P-value	S_e^2	S_B^2	S_a^2	t*
78	0.025	8.815803342	1.74765E-12	1.063713729	1.990847069
		Slope, B	Intercept, a		
					Degradation
	95%	-7.374E-08	734.524	95% Upper Bound	0.6975 %
		-5.337E-06	730.417	95% Lower Bound	0.0097 %

90%					
df	P-value	S_e^2	S_B^2	S_a^2	t*
78	0.05	8.815803342	1.74765E-12	1.063713729	1.664624645
		Slope, B	Intercept, a		
					Degradation
	90%	-5.050E-07	734.187	90% Upper Bound	0.6414 %
		-4.906E-06	730.753	90% Lower Bound	0.0662 %

Figure 2.41 Linear Regression – Confidence Intervals

Confidence intervals can be found for both the slope and the intercept of the data displayed in Figure 2.39. The slope is the interesting value because it indicates the amount of stiffness degradation; the intercept is only describing the initial value of stiffness. As seen in Figure 2.41 for a 90% confidence interval the slope of the line falls between:

$$-5.05 \times 10^{-7} \frac{lb}{in\,(Number\ of\ Cycles)}\ and\ -4.91 \times 10^{-6} \frac{lb}{in\,(Number\ of\ Cycles)}.$$

These values translate into an upper bound of 0.6414% and a lower bound of 0.0662% for stiffness degradation.

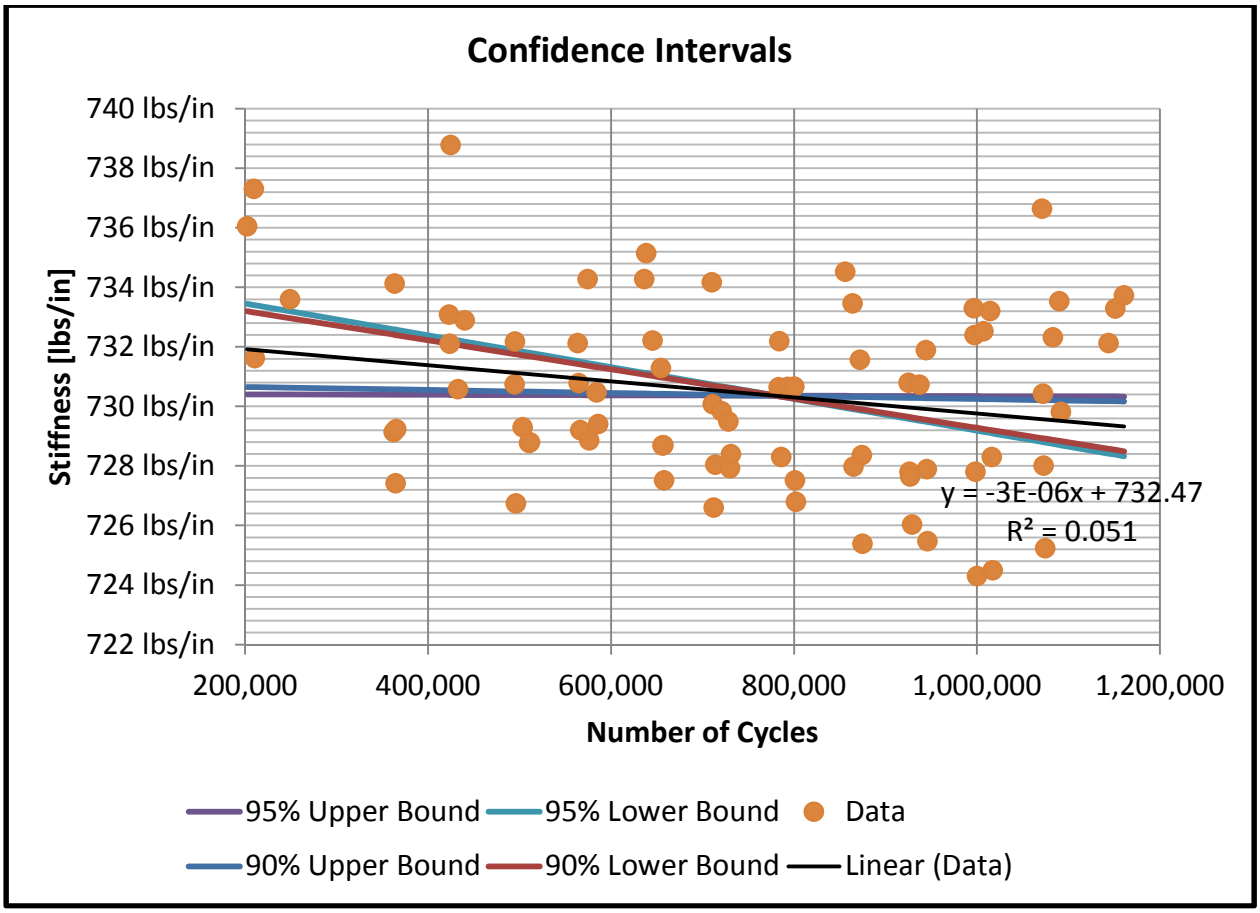

Figure 2.42 Linear Regression – Confidence Intervals Plot

Figure 2.42 shows the data obtained in the experiment and the lower and upper bounds of the different confidence intervals.

While the confidence intervals of the linear regression fit give information about the intercept and, more importantly in the case of this thesis, the slope, it is not the only important piece of information. The correlation describes how stiffness depends on the number of cycles. If the correlation is equal to one or negative one, then all the points in that data set fall on the same line, if the correlation is zero, then the points don't really make any kind of line and can be thought of more as a cloud of points with no real trend.

95%					
Correlation	Z'	Var	Z'	r	Bound
-0.2258	-0.2297	1.9600	-0.4531	-0.4244	95% Upper Bound
	-0.2297	1.9600	-0.0064	-0.0064	95% Lower Bound

90%					
Correlation	Z'	Var	Z'	r	Bound
-0.2258	-0.2297	1.6449	-0.4172	-0.3945	90% Upper Bound
	-0.2297	1.6449	-0.0423	-0.0422	90% Lower Bound

Figure 2.43 Correlation – Confidence Intervals

The 95% and 90% inclusive confidence intervals, along with the Fisher Transformation information, are provided in Figure 2.43. The confidence interval on correlation describes the confidence of describing how dependent stiffness is on the number of cycles. The 90% confidence on correlation produces a lower bound of -0.0422 and an upper bound of -0.3945.

3.0 Modeling

3.1 Material Model

3.1.1 Overview

A material model is a useful starting point when examining the behavior of a material. When combined with a finite element model it can be used in an iterative fashion to determine what would happen if certain aspects of the model are tweaked or changed. This combination of tools creates a cost effective way to ask "what if" questions about materials.

A damaged based material model is developed to determine if the degradation of the material modulus would cause structural stiffness degradation. This material model is being developed to match published experimental data of stiffness degradation during a notched three point bend test. Once developed it was implemented in the Bike FEM, which is discussed later. The results of the Bike FEM do not concur with those of the experiment done on the bike frame. The material model was used to determine how much the modulus would need to degrade, through the use of a damage multiplier, to match the results of the experiment.

3.1.2 Paper with Experiment

A paper written by Andrei Zagrai utilizing ultrasonic testing to detect damage within a structure forms the foundation of the material model development.[1][8] This paper mostly investigates the

technology used to find damage at the micro-scale, which is not of interest in this thesis. However, as part of the investigation and application of the discussed technology this paper experiments with aluminum and stainless steel notched beam specimen in 3-point bending which shows stiffness degradation as a function of cyclic loading which became the basis of the damage model used in this project.

3.1.2.1 Experimental Details

The aluminum specimens used were cut from aluminum alloy 2024-T4 bars, the size of the tested specimens were 305 mm x 25.4 mm x 6.35 mm rectangular bars.[1] A groove of 1.27 mm[1] was machined in the specimen to localize damage initiation and accumulation.[8] Although it is not clearly stated in the paper where the grooves are machined it is assumed that they are in the center of the specimen, see Figure 3.1. According to ASM Material Data Sheet website the modulus of elasticity for AA 2024-T4 is 73.1 GPa, Poisson's ratio is 0.33, and the tensile yield strength is 324 MPa.[7]

[1] There is a typo pertaining to this number in the Zagrai paper titled Micro- and Macroscale Damage Detection Using the Nonlinear Acoustic Vibro-Modulation Technique. This paper says the groove is 0.127 mm and 0.05" which is actually 1.27 mm. The Zagrai paper titled Micro/meso scale fatigue damage accumulation monitoring using nonlinear acoustic vibro-modulation measurements, confirms the 0.05".

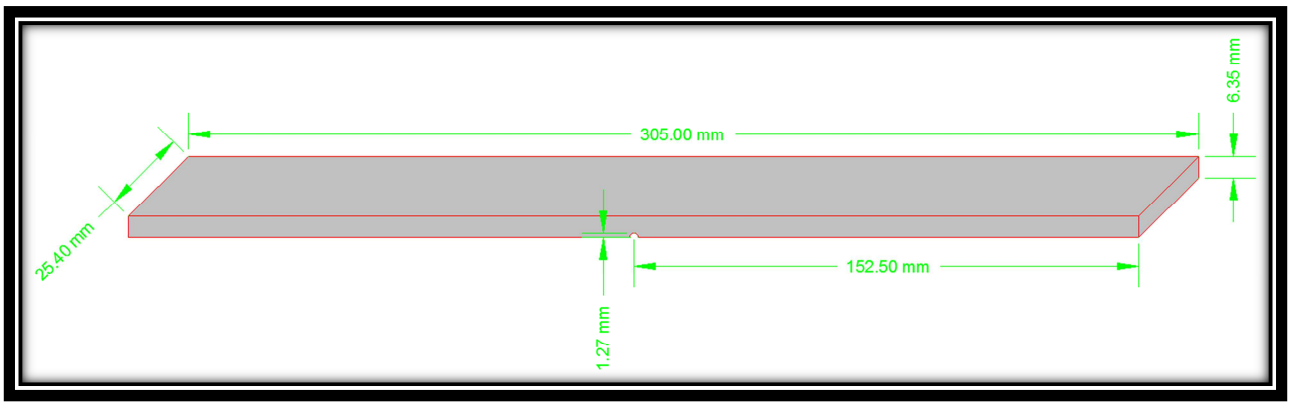

Figure 3.1 Notched Beam – Dimensions

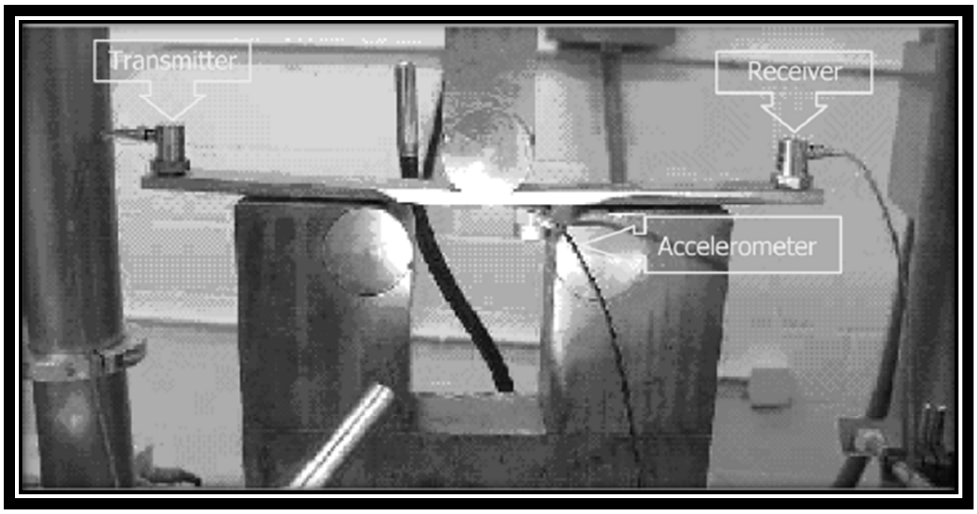

Figure 3.2 Notched Beam – Experimental Setup[1]

Figure 3.2 shows a photograph taken from the paper showing the experimental setup. While details about the setup such as exactly how the beam was loaded, where the notch was placed, and where the supports are located, are lacking in the text, this photograph gives a large amount of insight into how the experiment was setup.

The 3-point bend test used in this experiment is displacement controlled. From the paper it appears that the specimen is displaced 1.35 mm and then cycled between 1.35 mm and 1.5 mm, therefore the cyclic displacement amplitude is 0.15 mm.

3.1.2.2 Data to Match

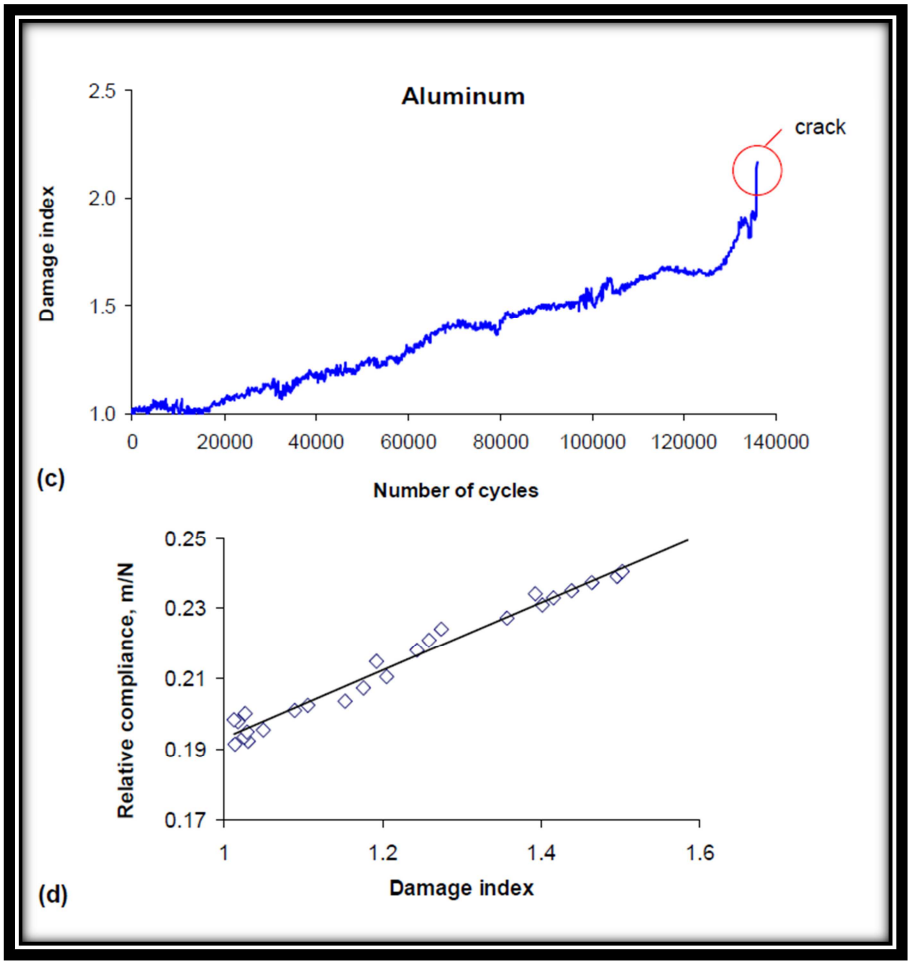

Figure 3.3 Notched Beam – Results to Match[8]

Figure 3.3 from the published paper reports the change in relative compliance with the number of cycles.[8] It should be noted that the units for relative compliance appear to be incorrect. The

term relative compliance is not discussed in the paper, through emailing the first author, who was not directly involved with the experimental portion of the paper, the definition of relative compliance is 0.36 divided by the average force over one loading cycle in kilo Newtons.[15]

By looking at the percentage change in the relative compliance versus the number of cycles one can obtain the percentage change in stiffness versus the number of cycles. This percentage can then be used as the target value for the finite element model and the damage model development. In other words, a goal is needed when developing the damage model; the following develops that goal from the two graphs in Figure 3.3.

Definitions:

$RC = Relative\ Compliance$

$DI = Damage\ Index$

Equations from Figure 3.3:

$$RC = 0.09667(DI) + 0.09533 \quad \text{Equation 3.1}$$

$$DI = 2.5 \times 10^{-6}(Cycles) + 1 \quad \text{Equation 3.2}$$

The above equations create a starting point and are described as follows:

- Equation 3.1: This equation of RC is obtained from the bottom graph of Figure 3.3 by using two points on the fitted line and creating an equation from these two points using a simple algebraic equation of a line.

- Equation 3.2: This equation of DI, damage index, is obtained from the top graph of Figure 3.3. The data in this graph was fitted visually using a ruler and two points were obtained on this line. An equation of DI was developed using the equation of a line.

Equation 3.3 is obtained by substituting Equation 3.2 into Equation 3.1. Algebraically reducing Equation 3.3 arrives at Equation 3.4.

$$RC = 0.09667(2.5 \times 10^{-6}(Cycles) + 1) + 0.09533 \quad \text{Equation 3.3}$$

$$RC = 2.41675 \times 10^{-7}(Cycles) + 0.192 \quad \text{Equation 3.4}$$

Solving Equation 3.4 for the minimum and maximum values available for relative compliance the following are obtained:

$$At\ 0\ cycles\ RC = 0.192 \quad \text{Equation 3.5}$$

$$At\ 140{,}000\ cycles\ RC = 0.226 \quad \text{Equation 3.6}$$

These values of relative compliance are the values at the beginning and the end of the experiment and are used to determine the percentage decrease of stiffness. Equation 3.7 is obtained by using these values and a simple percent decrease equation.

$$\frac{0.226\ -0.192}{0.192} \times 100\% = 17.7\ \%\ Decrease \quad \text{Equation 3.7}$$

3.1.3 FEM Model

A two dimensional FEM, or finite element model, of this experimental specimen was developed. This model utilized symmetry and truncated at the support locations, that is everything outside of the supports was disregarded, for computational efficiency. See Figure 3.4 for a visual of the FEM model. This model was used to find the support locations and determine the parameters of the damage model that matched the results of the published paper.

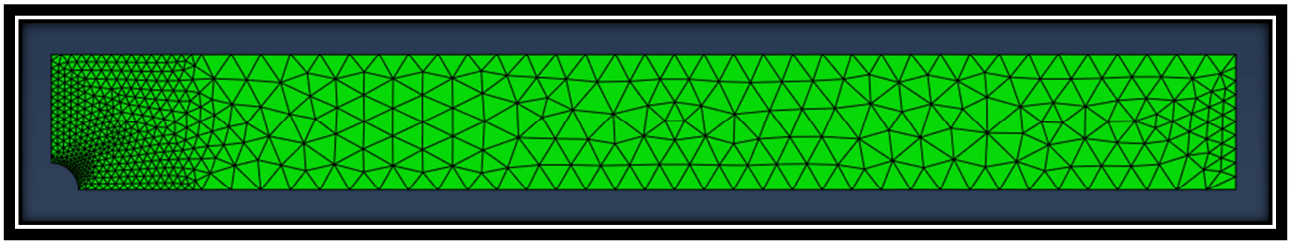

Figure 3.4 Two-Dimensional FEM Model of Notched Beam

3.1.3.1 Boundary Conditions

There is only one type of displacement boundary condition used in this model, the roller. But it is used in two different locations. Looking at Figure 3.4 there is a roller that provides vertical support at the far right side of the notched beam. This roller supports the lower right corner, at a single node, in the vertical direction only, and allows translation in the horizontal direction and rotation in all directions. The second location that utilizes a roller is on the far left. The plane created by the symmetry discussed in the next section creates a line of nodes from the middle of the arc of the notch to the loading node, at the upper left corner; all nodes on this line have a roller providing support in the horizontal direction. This roller boundary condition fixes these nodes in the horizontal direction and allows translation in the vertical direction and rotation in all directions.

To lower the computational cost of running the model symmetry of the problem was used. The symmetry used was to split the model across an imaginary plane made by the center of the notch and the point of loading. The right half of the model was used as can be seen in Figure 3.4. A roller was used for vertical support on the bottom right node. Rollers were also used for horizontal support along the left most edge to create the symmetry.

3.1.3.2 Element Type

The elements used were Abaqus CPE6M elements. These are continuum, plane strain, 6 node modified elements with hourglass control.[9] The modified refers to an aspect that allows for better use in contact problems, which is not applicable to their use here.[10] These are the only second-order plane strain elements available in Abaqus/Explicit.[10] These are triangular elements with three integration points per element, and utilize quadratic shape functions.

3.1.4 Convergence Testing

Computational modeling is different from experimental modeling in that certain assumptions need to be made because it is trying to model reality. Reality exists in the world; computational modeling takes the problem being examined out of the world and puts it into a computer. Just as when drawing a free body diagram of a structure assumptions are made about the supports as in if they are pins, fixed, or rollers. These assumptions idealize the real physical world and simplify it into a model with fewer variables. When designing an experiment or looking at the

results of a performed experiment assumptions are made, but during the actual experiment no assumptions exist, just the physics of the problem. Often the assumptions designed into an experiment are not sufficient for simplifying and idealizing the problems that are to be addressed and as a result there are more variables active than the experimenter would desire. For example, the assumption that the temperature and humidity of the room in which the experiment is taking place might have a negligible impact on the results, perhaps the experimenter would like to be sure and not make this assumption but the cost of controlling these two variables might be prohibitive, therefore acceptance of this assumption would be an acceptable one. This is an acceptable assumption to make because the impact is deemed negligible; therefore spending the money to control for these variables would not gain the experimenter much value.

In computational modeling money is analogous to the number of computations a computer is asked to perform, the more complex a model is the more computations that are needed to be performed. Computational modeling needs to make many assumptions because of the nature of taking a problem out of the physical world and putting it into a language a computer can understand. Assumptions and idealizations arise from this process, what is gained from these assumptions is fewer computations needing to be performed, shortening the runtime of a simulation to something that is feasible to work with.

Convergence testing is a way of looking at these assumptions and determining what level of resolution is needed to adequately model the problem. It is a way of optimizing between the accuracy of these assumptions, or the resolution of the problem, and the computational resources necessary to perform the calculations. While it might be great to have infinite resolution, it is

probably not computationally feasible; figuring out what resolution is acceptable to provide the best results is done through convergence testing.

3.1.4.1 Support Location Convergence

The paper does not specify the location of the supports. From Figure 3.2, and the general definition of a 3-point bend test it was inferred that the specimen was placed such that the longest dimension was perpendicular to the loading and the supports, and that the beam was being bent about its weak axis. The FEM model described in Section 3.1.3 was used to figure out where the support locations should be located by running several simulations iterating through different support locations until the output of the simulation matched that of the experimental data in the paper, seen in Figure 3.5.[8]

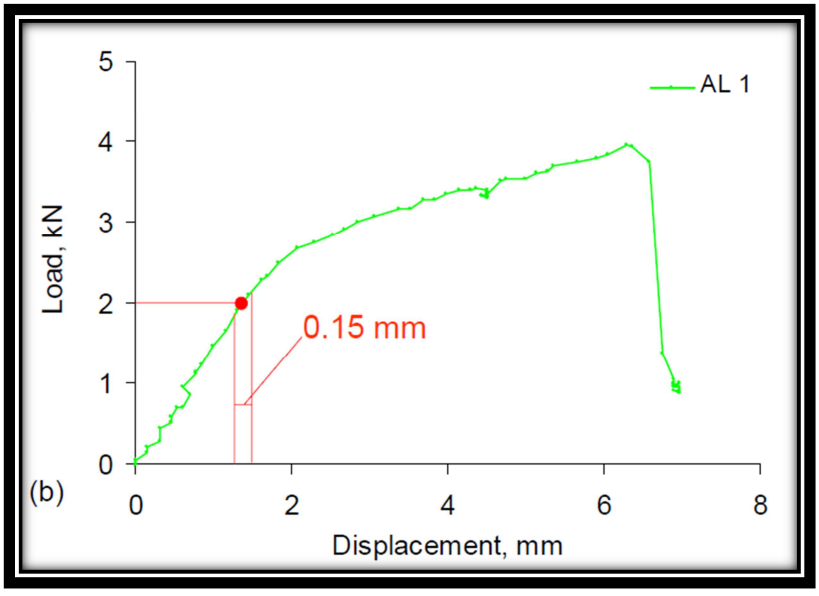

Figure 3.5 Published Graph Used to Find Support Locations[1][8]

This method of finding the support locations was possible because knowledge of the material properties, the geometry of the specimen, the boundary conditions, and where loading was located, was all available. This left the only unknown to be the support locations. The data was matched in the elastic region of the data shown in Figure 3.5. The specific point on the graph of Figure 3.5 that was used as a target value was 1.0 mm, which corresponded to a reaction force of 1500 N. This means that the notched beam was displaced, at the upper left hand loading node, 1.0 mm and the reaction force was observed. The location of the support was moved until the reaction force was 1500 N.

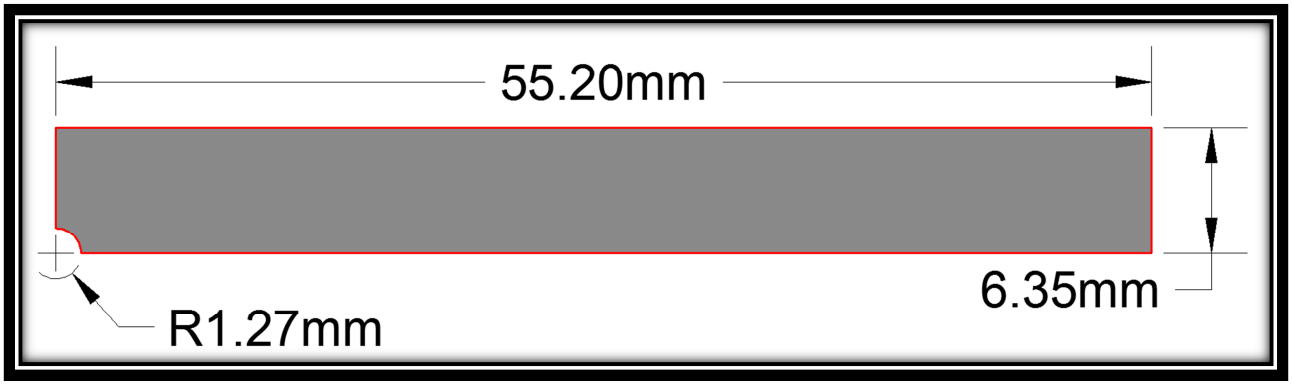

Figure 3.6 Two Dimensional Notched Beam with Symmetry Applied – Dimensions

It was found that the support distance was 55.2 mm from the center of the notch. Therefore, the overall length of the beam is 55.2 mm at its longest point. Recall that a two dimensional half section of the beam is being used and that material outside of the supports is truncated, this means that from the far left side of the beam, the plane created by the middle of the arc forming the notch and the loading node, and the far right of the beam, where the vertical support roller is located, is a total of 55.2 mm, see Figure 3.6 for a visual.

3.1.4.2 Mesh Convergence

After the support location was found this model was used to figure out how many elements should be used, and the placement of these elements. Particular attention was paid to the notch because it was assumed that damage would develop and accumulate around the notch and capturing this feature was desired.

3.1.4.3 Displacement Rate Convergence

An explicit solver was used because of the development of the damage. There would be elements whose stiffness would come close to zero and inverting the stiffness matrix would become problematic. Therefore, the use of small increments in the explicit solver to solve the problem was desired. To be able to run each simulation more quickly a way of speeding up the simulation was needed. Artificially increasing the displacement rate seemed to be the best solution. To be sure that this speed up was not impacting the results of the simulations this convergence test was done on the displacement rate.

The displacement rate that is discussed in this section can more easily be thought of as the inverse of the displacement rate. That is, a displacement rate of 1.0 meter/sec is the displacement rate as actually applied. That means that the notched beam is displaced 1.0 meters every second. A value less than 1.0 meter/sec means the displacement rate is faster than 1.0 meter/sec and therefore the simulation will complete more quickly. The values discussed in this section are the actual values used in Abaqus.

Figure 3.7 shows a frequency analysis of the notched beam FEM model. The first mode has a frequency of 1242 cycles/sec. A rule of thumb for a starting displacement rate is 10 times the period, therefore 10/1242 = 0.008 meter/sec is a good starting point for looking for an acceptable displacement rate.

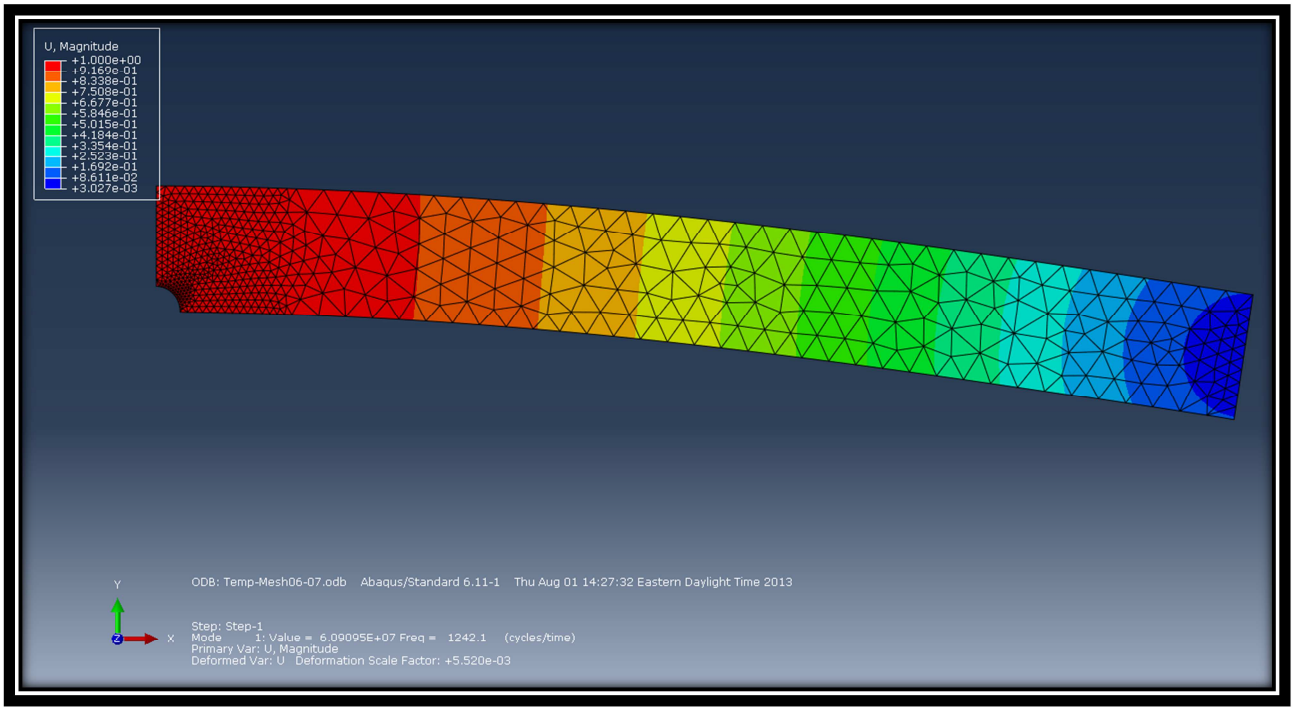

Figure 3.7 Notched Beam – Frequency Analysis

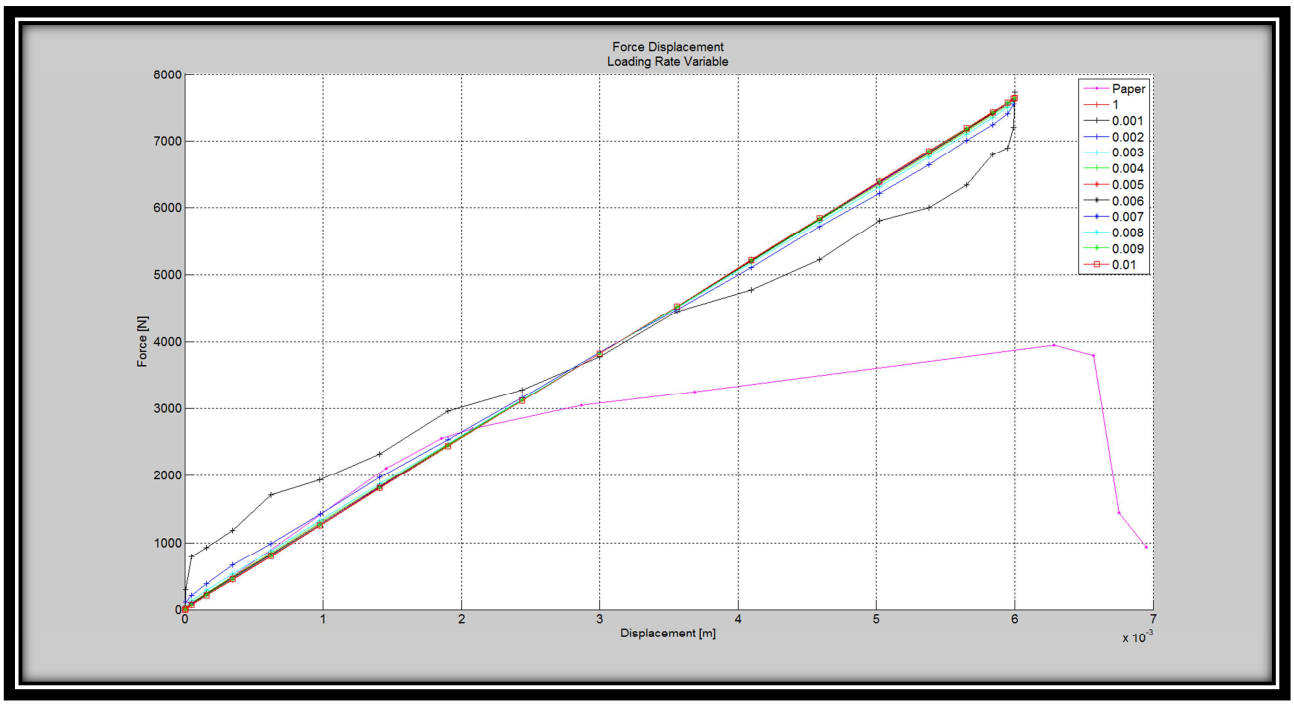

Figure 3.8 Notched Beam – Various Displacement Rates

Figure 3.8 shows the different displacement rates and how they affect force versus displacement. The units for the displacement rate in the legend are meter/sec. Force versus displacement is of interest because the ultimate desire is stiffness of the structure, which is the force divided by the displacement, essentially the slope of the force versus displacement line. Looking at Figure 3.8 it is easy to see that 0.001 meter/sec as a displacement rate is too small because of how distorted the results are compared to the others, but it also looks like it might be okay to use a displacement rate smaller than 0.008 meter/sec as provided by the rule of thumb.

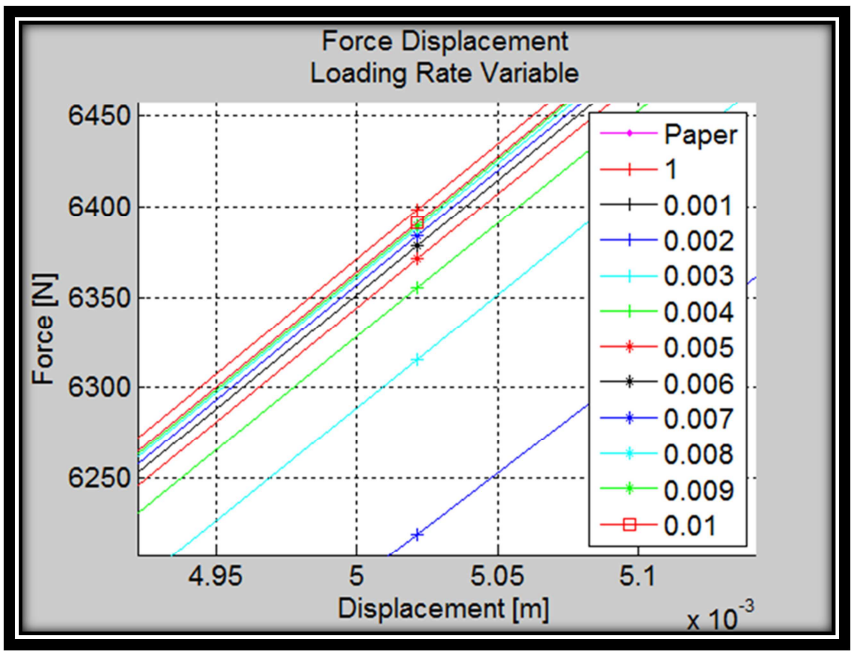

Figure 3.9 Notched Beam – Various Displacement rates, Zoomed

Disp	@0.005m	@0.0054m
0.001	9.224%	12.410%
0.002	2.804%	3.071%
0.003	1.296%	1.343%
0.004	0.677%	0.743%
0.005	0.428%	0.473%
0.006	0.312%	0.325%
0.007	0.229%	0.235%
0.008	0.169%	0.180%
0.009	0.135%	0.141%
0.01	0.112%	0.114%

Figure 3.10 Various Displacement rates Results

Figure 3.9 zooms in on the relevant data from Figure 3.8. These curves do not prove a convergence point as much as convey how the different displacement rates impact the results. Assuming that a displacement rate of 1.0 meter/sec is the standard, because no speed up is applied, by which to compare all of the other displacement rates Figure 3.10 is obtained. This Figure looks at two different displacements where the deviation is the most significant. Essentially the data points create a vertical line at any given point, by looking at the forces at each of these data points and comparing them to the force using the displacement rate of 1.0 meter/sec.

There is not a predetermined percentage that creates a limit when doing convergence testing. Remember that convergence testing is all about optimizing between a desired resolution and the computational cost of that resolution. If a given increase in resolution creates a small increase in

accuracy, for a large amount of computational cost, then that increase in resolution is not valuable. If that same given increase in resolution creates a large increase in accuracy, for a small amount of computational cost, then that increase in resolution is valuable. This is difficult to define because the terms a little, a lot, small, or large are subjective. These definitions will vary from model to model and from modeler to modeler, and as with all of the nuances associated with engineering one's ability to determine these definitions grows with experience.

As for this specific case, a displacement rate of 0.003 meter/sec was decided on. Notice that it is only about 1.3% off from the standard of the displacement rate of 1.0 meter/sec. This allows for a significant speed up while reducing the deviation from the standard results.

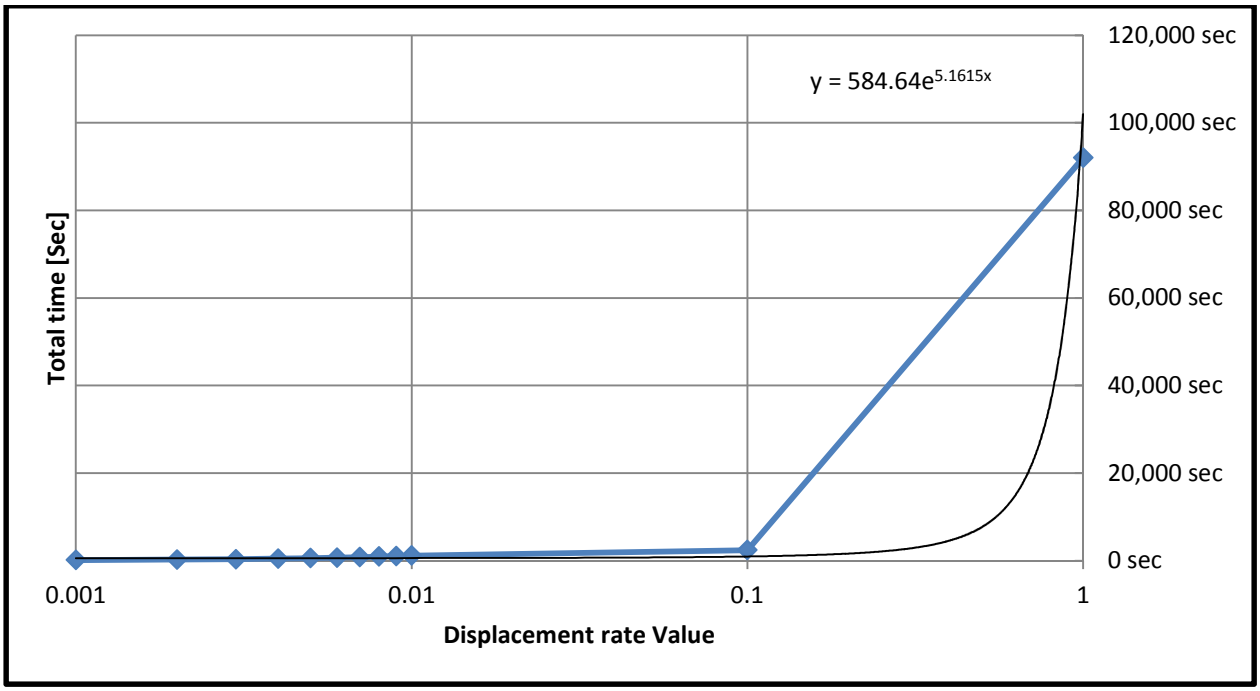

Figure 3.11 Displacement rate Simulation Runtime – Chart

	Simulation Run Time					Speed Up	
Run	Days	Hours	Min	Sec	Total in Sec	Percent Reduction From Previous	Percent Reduction From First
1	1	8	16	35	92,003 sec		
0.1	0	3	11	26	2,414 sec	97 %	97.3762 %
0.01	0	0	19	32	1,172 sec	51 %	98.7261 %
0.009	0	0	17	52	1,072 sec	9 %	98.8348 %
0.008	0	0	15	51	951 sec	11 %	98.9663 %
0.007	0	0	13	42	822 sec	14 %	99.1066 %
0.006	0	0	11	52	712 sec	13 %	99.2261 %
0.005	0	0	10	2	602 sec	15 %	99.3457 %
0.004	0	0	8	2	482 sec	20 %	99.4761 %
0.003	0	0	6	1	361 sec	25 %	99.6076 %
0.002	0	0	4	12	252 sec	30 %	99.7261 %
0.001	0	0	2	31	151 sec	40 %	99.8359 %

Figure 3.12 Displacement rate Simulation Runtime – Data

Figures 3.11 and 3.12 investigate the amount of time a simulation takes to run given a specific displacement rate. The columns on the right of Figure 3.12 look at the percentage reduction of time to run the simulation. The right most column is the percentage reduction from the first, meaning that it compares the time it takes to run a simulation with a given displacement rate with the standard displacement rate of 1.0 meter/sec. The column to the left of that looks at how much of a speed up, or percent reduction in time to run the simulation, compared to the previous. Basically, it is the incremental gain in speed by lowering the displacement rate. Based on this it can be seen how the displacement rate of 0.003 meter/sec compares to the other displacement rates around it.

3.1.5 Development of the VUMAT

Abaqus uses a VUMAT to allow the user to create a user defined material model. By using a VUMAT the user has the ability to alter constitutive equations in any manner desired. For the purpose of this project the constitutive equations were altered by the addition of the damage parameter. This damage parameter reduces the stiffness of the material.

3.1.5.1 Elastic Strain Based Model Motivation

This section develops an elastic strain based damage model. As discussed later the notched beam appears to cycle in the elastic regime, not allowing for plastic strain to accumulate. This is the basic motivation for using elastic strain.

Recall that the notched beam experiment is displacement controlled. The loading cycle is as follows:

1) The notched beam is initially loaded to a displacement of 1.35 mm.
2) The loading cycle begins by continued loading to the maximum displacement of 1.5 mm. This can be thought of as the first half of the cycle, or the loading half-cycle.
3) The loading cycle completes by unloading to the original displacement of 1.35 mm. This can be thought of as the second half of the cycle, or the unloading half-cycle.

This loading from 1.35 mm to 1.5 mm is considered the loading cycle. See Figure 3.13 for a visual of the loading cycle as displayed by Abaqus. Note that in Figure 3.13 the vertical axis is in meters; the FEM was setup in units of meters and Newtons.

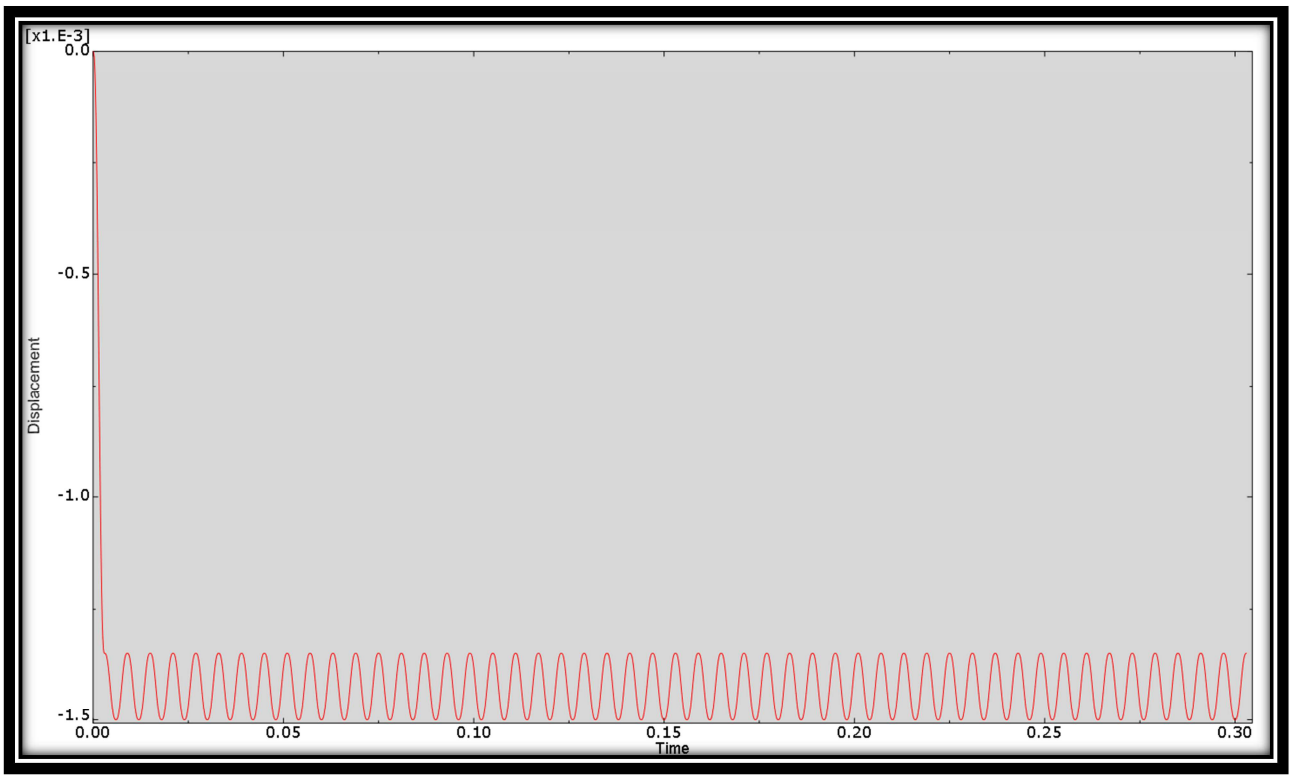

Figure 3.13 Cycled Displacement Loading Applied to the Notched Beam

Figures 3.14 and 3.15 display results from implementing two different material models in the FEM model described in Section 3.1.3. Figure 3.14 uses an elastic material model only and Figure 3.15 incorporates a plastic material model. Both of these figures show the results, force as a function of displacement, from a full loading of 6.0 mm; 6.0 mm is considered full loading from the evidence of failure in the static loading results seen in Figure 3.5. Notice how the simulation matches the paper data in the elastic regime as discussed in Section 3.1.4.1, for both Figures 3.14 and 3.15.

Figure 3.16 shows the FEM model utilizing a plastic material model and being cycled, just as in the experiment. The specimen in this simulation is subjected to an initial loading and then 50

full cycles of loading, as described above. Notice how the line characterizing the cycles remains unchanged, that is, when the notched beam is loaded and unloaded, it follows the same load path for each cycle. Figure 3.17 is a zoomed in version of Figure 3.16. If there is any variation it is slight and does not show up here. For this to be the case the cyclic loading would need to be in the elastic regime of the notched beam.

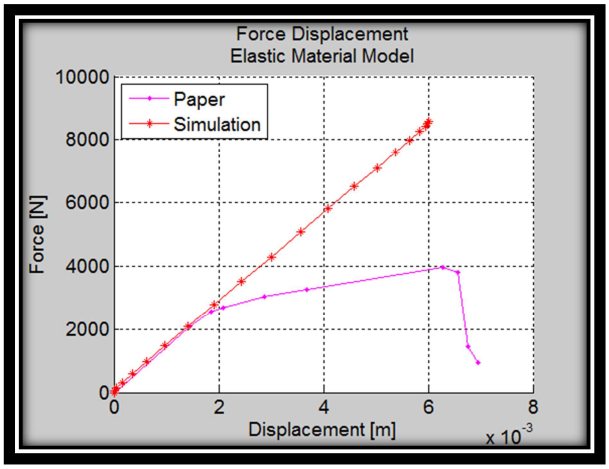

Figure 3.14 Notched Beam FEM Full Loading – Elastic Material Model

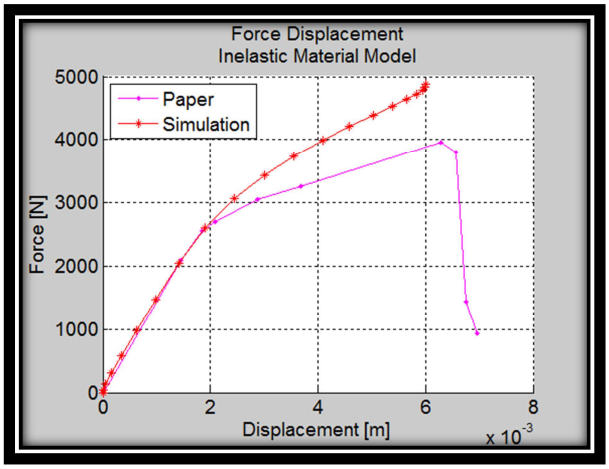

Figure 3.15 Notched Beam FEM Full Loading – Plastic Material Model

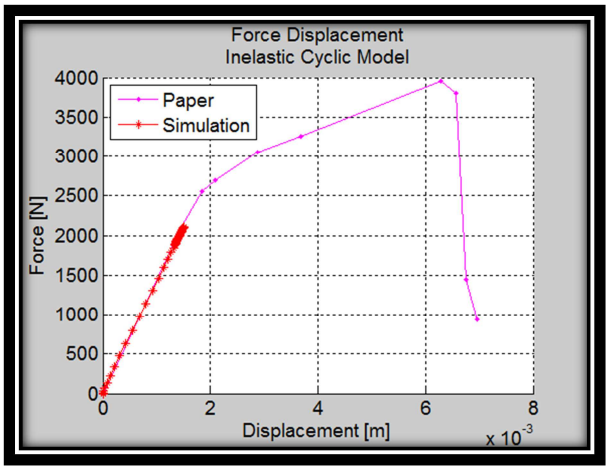

Figure 3.16 Notched Beam FEM Cycled Loading – Plastic Material Model

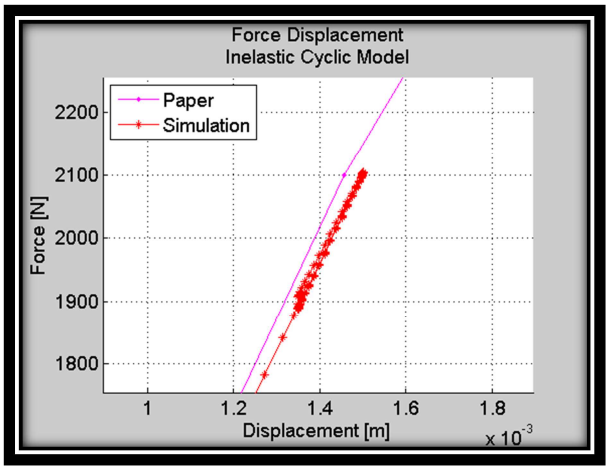

Figure 3.17 Notched Beam FEM Cycled Loading – Plastic Material Model Zoomed In

It is not completely clear from this whether the notched beam is yielding or not. While these figures seem to indicate that the specimen is not yielding, it is only looking at the entire specimen; perhaps material is yielding in small amounts and would not be enough to show up on these figures.

Looking further into these results the Von Mises Stress and the equivalent plastic strain were investigated. Figures 3.18 and 3.19 shows Von Mises Stress and Figures 3.20 and 3.21 show the equivalent plastic strain, all figures show contours overlaid on the FEM model used to obtain the data in Figures 3.13 through 3.16 above. Figures 3.18 and 3.20 are taken from the beginning of the simulation, this is after the first loading half-cycle, of cycle number one, has been completed, and therefore the Figures are showing the specimen when the maximum load is experienced. Figures 3.19 and 3.21 are taken from the end of the simulation, this is after the last loading half-cycle, of cycle number 50, has been completed, and therefore the Figures are showing the specimen when the maximum load is experienced. Figure 3.19 shows that the amount of yielded material doesn't increase, recall that the yield strength is 324 MPa, the displayed numbers are in Pa, Pascals. Figure 3.21 shows that the amount of plastic strain has not increased from the beginning to the end of the simulation, after 50 cycles have been completed.

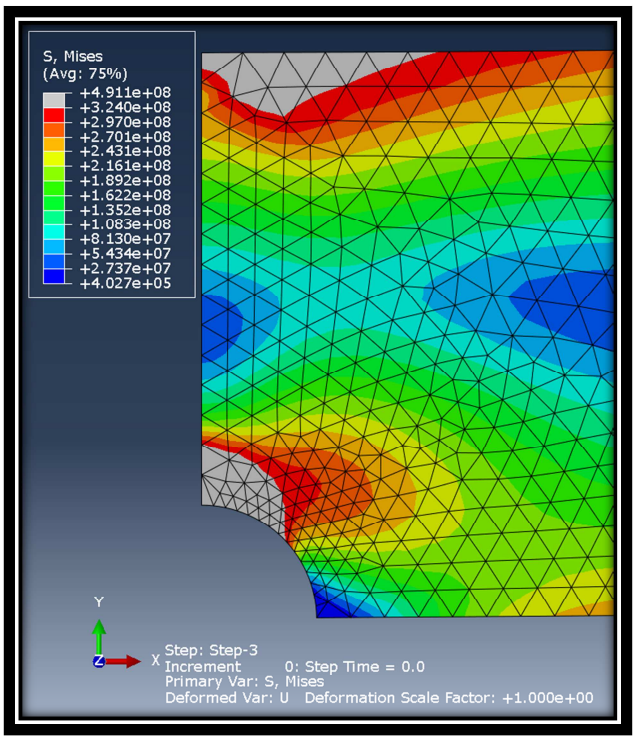

Figure 3.18 Max Load of First Cycle – Von Mises Stress

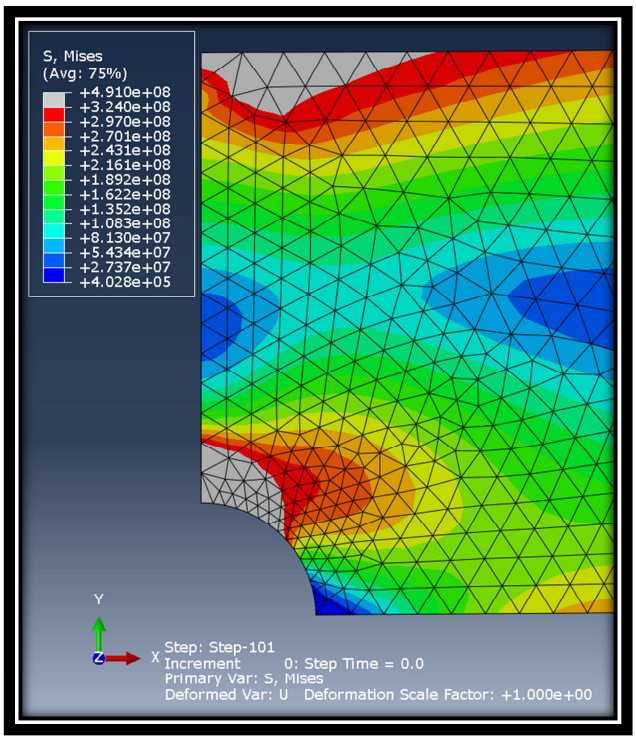

Figure 3.19 Max Load of Last Cycle – Von Mises Stress

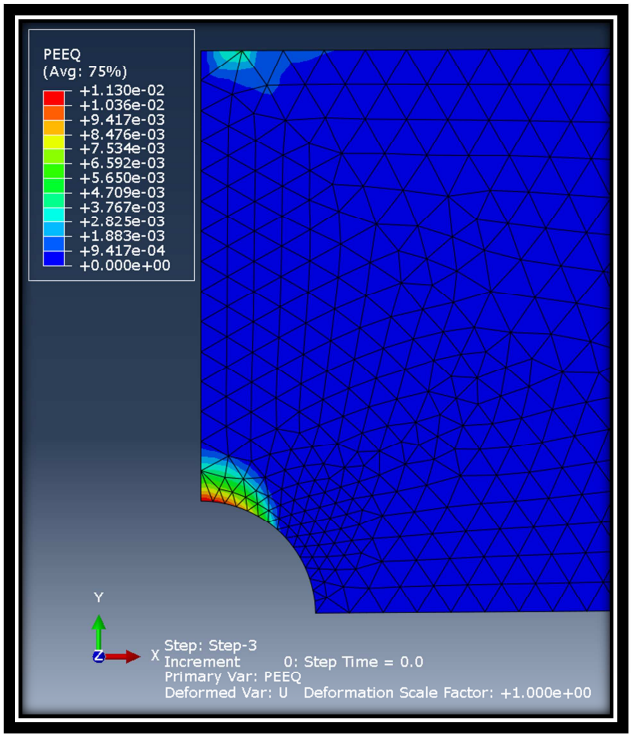

Figure 3.20 Max Load of First Cycle – Equivalent Plastic Strain

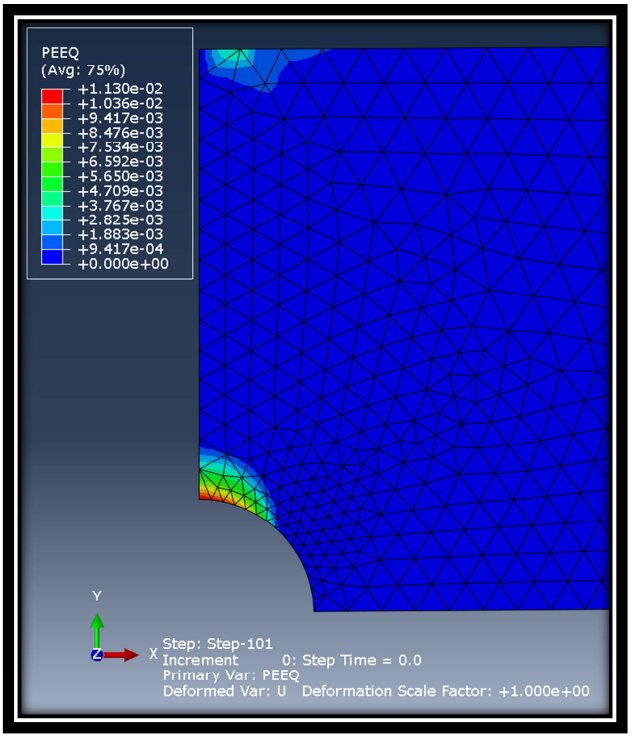

Figure 3.21 Max Load of Last Cycle – Equivalent Plastic Strain

The notched beam slightly plastically deforms in the initial loading up to the maximum loading it is not unloaded such that plasticity is activated again. This can be seen when examining Figures 3.20 and 3.21 notice how all of the equivalent plastic strain is accumulated in the initial loading and the loading half-cycle, therefore, before the specimen even begins to be cycled all of the plastic strain that will exist in the model has already accumulated. For a reference, during purely elastic loading the maximum Von Mises stress occurs just above the notch and has a value of 611 MPa.

The specimen yields due to the initial loading and the loading-half cycle, this plastic deformation changes the yield point in the material that has yielded. As the material yields it becomes stronger, hence the movement of the yield point. This can be easily observed when bending a paperclip. When a paper clip is bent the material at the bend plastically deforms to relax the amount of stress on that material, this material that plastically deforms becomes stronger, through microscopic processes, and resists bending when the paper clip is bent in the opposite direction. This process is occurring in the notched beam, with the exception of being bent in the opposite direction. When the notched beam is loaded it yields and becomes stronger, that material will not yield again until a stress higher than that which it has already experienced is imposed, but that doesn't happen with the cyclic loading because of how small the loading is. Therefore when the notched beam is being cycled the loading and unloading happens in the elastic regime. All of the elastic strain that it experiences in the loading half-cycle is recovered in the unloading half-cycle.

Yet the specimen in the paper fails after about 140,000 cycles. This means that damage is accumulating, but it isn't accumulating in the plastic regime, it is being accumulated as a function of accumulated elastic strain. Knowing that all of the strain is elastic and not plastic a damage model can be developed based on accumulated elastic strain.

The damage model is an accumulated elastic strain based damage model. Essentially as the elastic strain accumulates, the damage increase, and therefore the stiffness decreases. The following equations illustrate the damage model:

$\underline{Equivalent\ Elastic\ Strain\ Increment}$:

$$e_{inc} = \sqrt{\frac{2}{3}\Delta\varepsilon : \Delta\varepsilon}$$

$where:\ \Delta\varepsilon\ is\ the\ elastic\ strain\ increment$

$\underline{Total\ Equivalent\ Strain}$:

$$e_{total} = \sum_{0}^{current} e_{inc}$$

$\underline{Accumulated\ Damage}$:

$$D_{acc} = \alpha(e_{total})$$

$where:\ \alpha = a\ user\ defined\ multipler\ value$

$\underline{Constiutive\ Equations\ with\ Damage\ Parameter\ Applied}$:

$$\begin{bmatrix}\sigma_{11}\\ \sigma_{22}\\ \sigma_{33}\\ \sigma_{12}\end{bmatrix} = (1 - D_{total})\begin{bmatrix}2\mu+\lambda & \lambda & \lambda & 0\\ \lambda & 2\mu+\lambda & \lambda & 0\\ \lambda & \lambda & 2\mu+\lambda & 0\\ 0 & 0 & 0 & 2\mu\end{bmatrix}\begin{bmatrix}\varepsilon_{11}\\ \varepsilon_{22}\\ \varepsilon_{33}\\ \varepsilon_{12}\end{bmatrix}$$

3.1.5.2 Element Deletion

To ensure that the damage parameter of an element does not go greater than 1.0 a cap is inserted in the VUMAT. This cap simply asks the question if the damage parameter of the element is greater than 0.99, if it is greater, then it will be set to 0.99. This value of 0.99 is used because it was the largest number, closest to 1.0, that was found to be stable and allowed the simulation to run to completion.

3.1.6 Results

The data obtained from this model was done by running simulations with different multiplier values, alpha in the equations above. Multiplier values of 0.1 – 10 were used. What was obtained from the simulation was the force and displacement from the single loading node at the end of each loading cycle. The stiffness was calculated by dividing the force by the displacement. A line was fit to this data using a simple linear regression fit. The information obtained from this fit created an equation of the line fitting these points. This equation was then used to extrapolate to determine what the stiffness would be at 0 and 140,000 cycles. These values were used to calculate a percentage decrease. This percentage decrease and the associated multiplier value were then used to find Figure 3.29.

Plots of force as a function of displacement can be seen in Figures 3.22, 3.24 and 3.26. Plots of stiffness as a function of the number of cycles can be seen in Figures 3.23, 3.25 and 3.27. Figures 3.22 through 3.27 are a sampling of the data, plots from each simulation used to create Figure 3.29 can be seen in Appendix A.

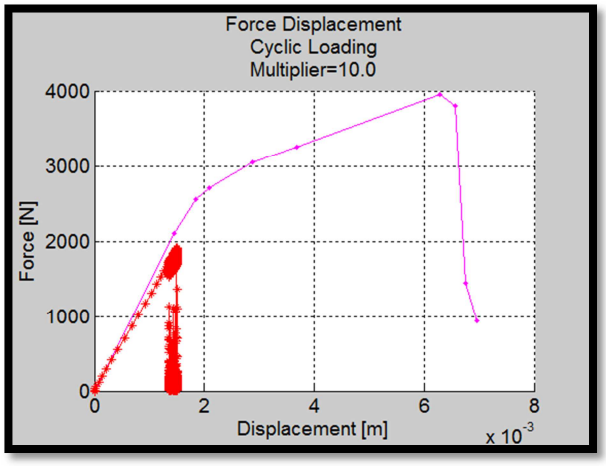

Figure 3.22 Multiplier Value of 10.0 – Force as a Function of Displacement

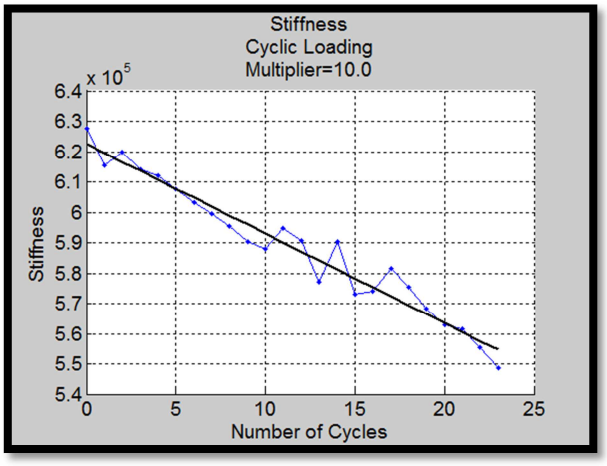

Figure 3.23 Multiplier Value of 10.0 – Stiffness as a Function of number of Cycles (Data truncated after failure)

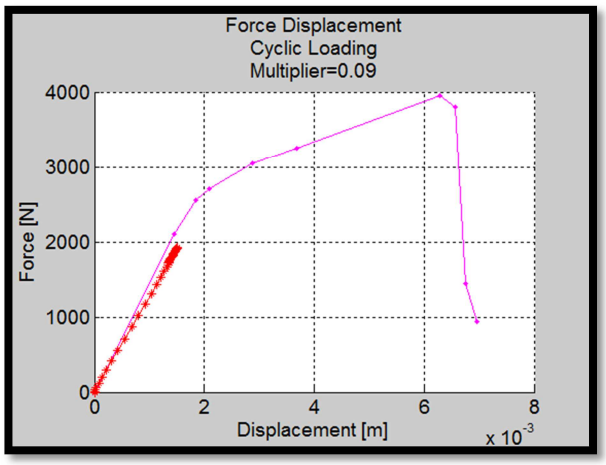

Figure 3.24 Multiplier Value of 0.9 – Force as a Function of Displacement

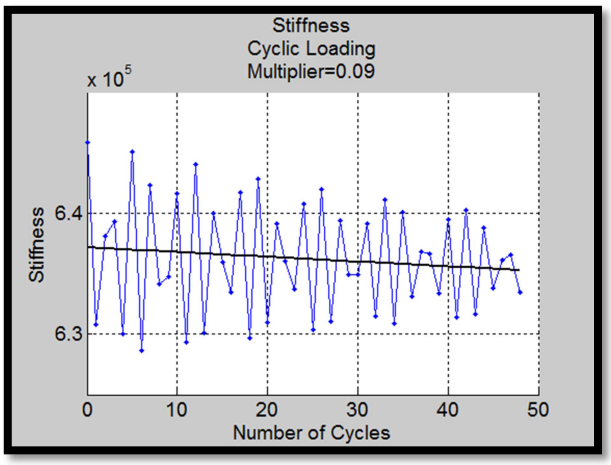

Figure 3.25 Multiplier Value of 0.09 – Stiffness as a Function of number of Cycles

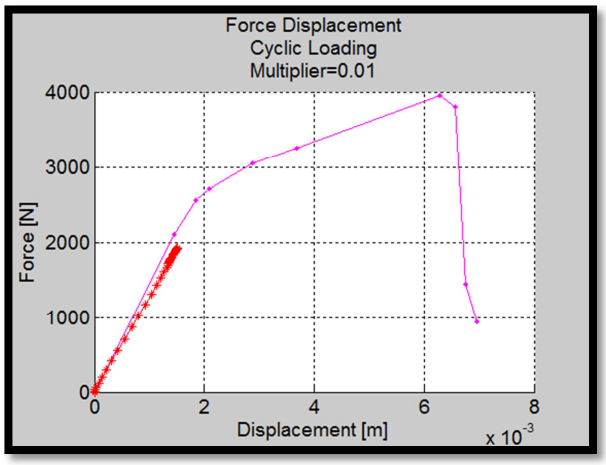

Figure 3.26 Multiplier Value of 0.01 – Force as a Function of Displacement

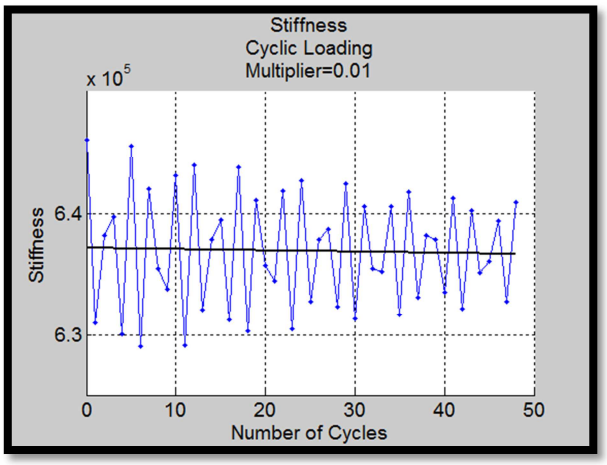

Figure 3.27 Multiplier Value of 0.01 – Stiffness as a Function of number of Cycles

Note in Figure 3.22 how the plot begins to become disordered compared to the other multiplier value plots. This occurs when the notched beam fails. In the corresponding Figure 3.23 the number of cycles is less than the others. This point of failure was identified and then all data beyond this point of failure was truncated before fitting a line to the data. Failure in the specimen occurred for multiplier values of 6 and greater.

Multiplier	Slope	Y-Intercept	R-Squared	Percent Decrease @140,000 cycles
0.1	-39.3180	6.37E+05	0.0144	863.9728 %
0.2	-67.9195	6.37E+05	0.0447	1492.6920 %
0.3	-94.8497	6.37E+05	0.0810	2084.9522 %
0.4	-123.9898	6.37E+05	0.1594	2725.9720 %
0.5	-148.2456	6.37E+05	0.1776	3260.2403 %
0.6	-172.7970	6.36E+05	0.3110	3801.3227 %
0.7	-199.2519	6.36E+05	0.3539	4384.4094 %
0.8	-227.6742	6.36E+05	0.3704	5010.8171 %
0.9	-256.9472	6.36E+05	0.4214	5656.0276 %
1	-285.2223	6.36E+05	0.4970	6279.6245 %
2	-580.8435	6.35E+05	0.9213	12811.3549 %
3	-858.5512	6.33E+05	0.9468	18981.3890 %
4	-1156.7563	6.32E+05	0.9666	25634.4369 %
5	-1584.6650	6.32E+05	0.9442	35079.7031 %
6	-1589.2155	6.28E+05	0.9099	35452.4475 %
7	-2152.0859	6.28E+05	0.9758	47964.3513 %
8	-2548.7990	6.29E+05	0.9896	56745.0992 %
9	-2887.5797	6.27E+05	0.9599	64437.6343 %
10	-2948.7995	6.22E+05	0.9530	66319.9902 %

Figure 3.28 Notched Beam FEM Model Results – Data

Figure 3.28 is all of the data obtained from the simulations. This data was used to create Figure 3.29.

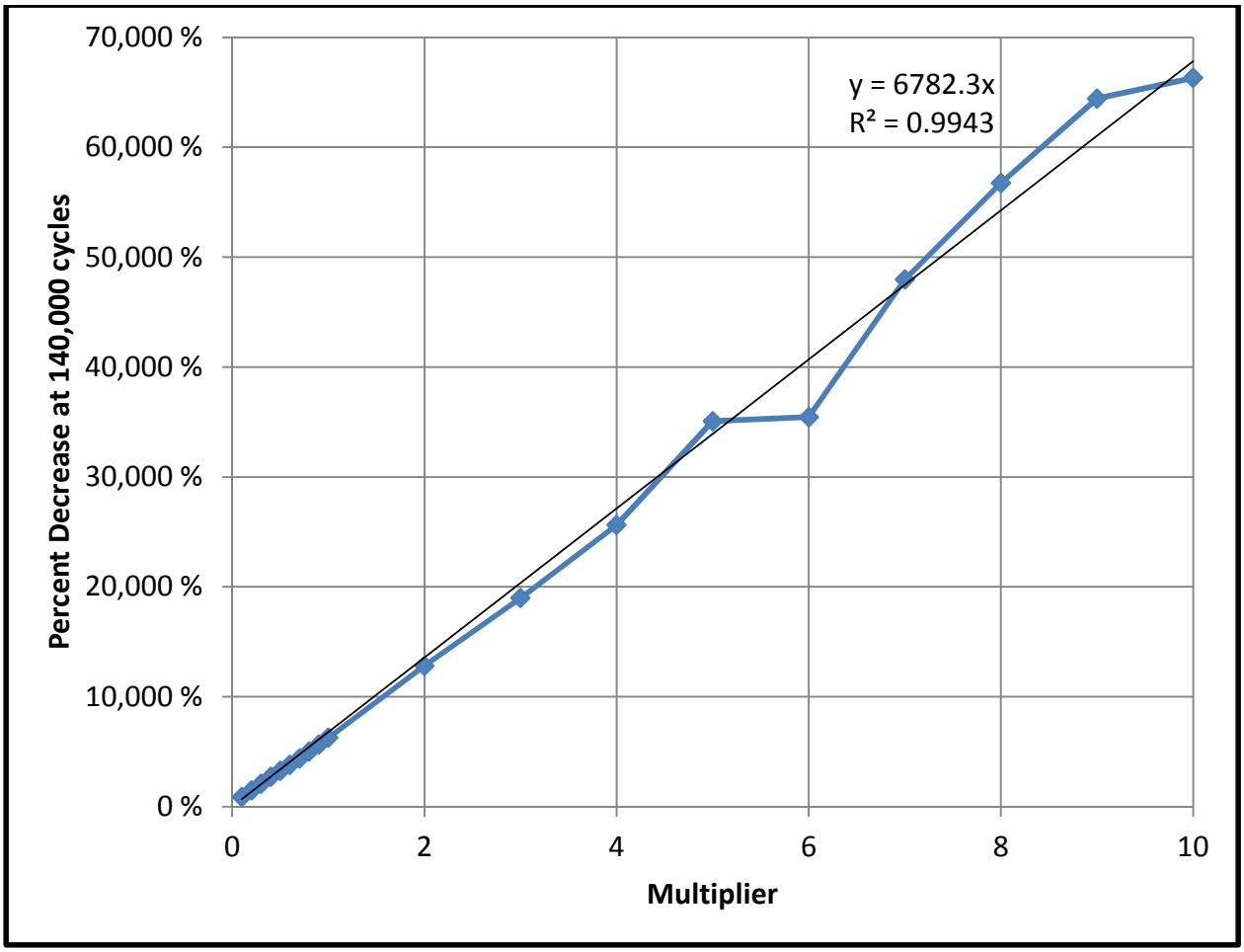

Figure 3.29 Notched Beam FEM Model Results – Plot

The data appears to follow a linear trend. Fitting a line to the data and forcing an intercept of zero an equation of the line is obtained. Using this equation and solving for y it is possible to see what value of a multiplier would be needed. Recall from Section 3.1.2.2 the target value for the percent stiffness decrease is 17.7%. To obtain 17.7% stiffness degradation a multiplier of 0.00261 would be needed. This value will be applied to the finite element model of the bike frame in the following sections.

3.2 Bike FEM

3.2.1 Overview

A finite element model of the bike that was used in the experimental section of this thesis is developed in this section. The material model that was developed in the previous section is implemented into this FEM model. This combination is used to investigate if the damage multiplier that is expected from the previous section is accurate and can predict the results of the experiment performed on the bike frame. It is shown that this multiplier is not predictive. The bike frame finite element model is then used to determine what the damage multiplier would need to be to match the experimental results.

3.2.2 FEM Model

Figure 3.30 shows a meshed visual representation of the bike frame model used.

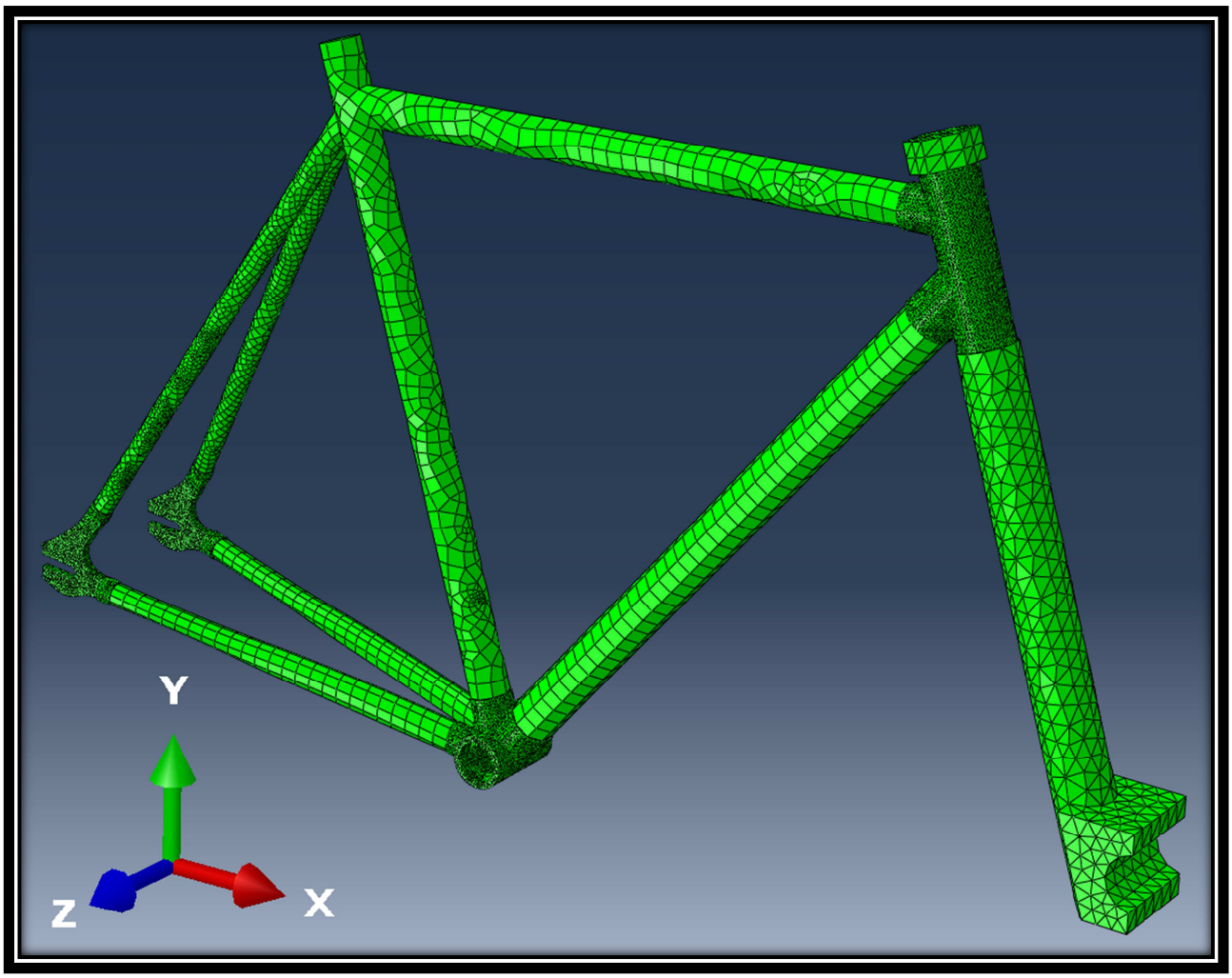

Figure 3.30 Finite Element Model of Bike Frame

The model uses both shell and continuum elements. The shell elements are used on structural members that have one dimension much longer than the other; these shells are used to simulate a tube. The continuum elements are used on shorter members that don't necessarily have a dimension that is much longer than the others. These elements are connected through an Abaqus built in function called shell-to-solid coupling which is discussed in Section 3.2.2.4. The shell elements are mostly S4R but also contain some S3R, which are all assigned by the Abaqus built-in meshing function. The continuum elements are C3D10 and C3D4.

The geometry was modeled in AutoCAD and brought over to Abaqus using an AutoCAD export function and an Abaqus import function. The file extension on the parts were .sat.

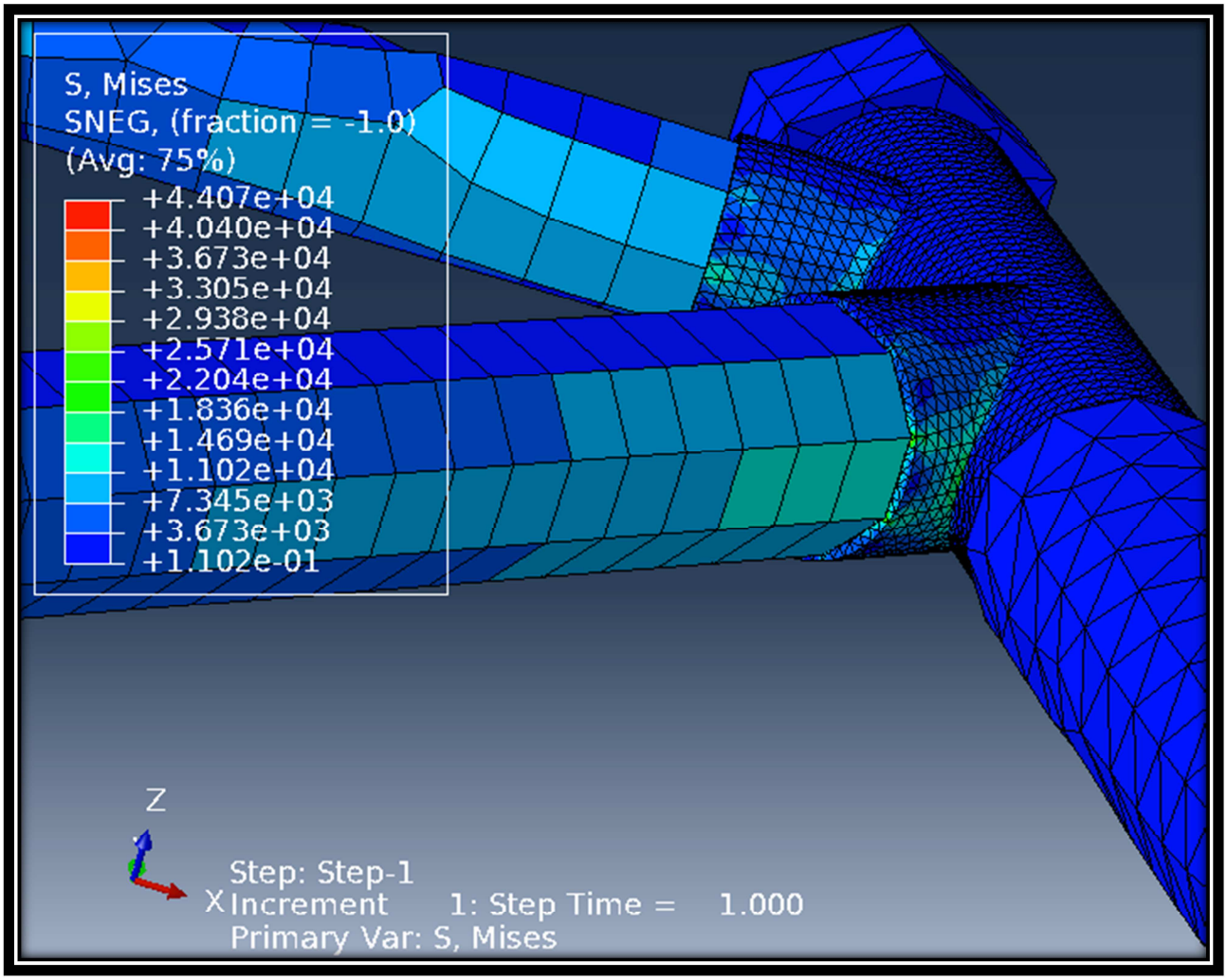

Figure 3.31 Von Mises Stress – Looking at Underside of the Head Tube

The Von Mises stress is highest around the head tube. As seen in Figure 3.31 the underside of the head tube has values of around 30,000 Pa.

3.2.2.1 Implicit Solver

Abaqus/Standard was used to solve the finite element model of the bike frame. This was done because the Abaqus/Explicit model was not able to run in a reasonable amount of time and efforts to improve its speed were not successful.

Abaqus/Standard uses an implicit solver which generally utilizes Newton's method.[21] From the literature supplied with the Abaqus program it seems that the equilibrium equation is solved through a series of increments. Abaqus/Standard generally uses Newton's method as a numerical technique for solving the equilibrium equations.[21] This solver seems to be faster, but uses a larger amount of memory, than Abaqus/Explicit. The damage model was applied outside of Abaqus through an iterative process using a Python script. This script degraded Young's modulus based on the amount of accumulated elastic strain , since an upper bound was place on the damage parameter a lower bound on Young's modulus was created, which prevented problems with elements becoming too soft and causing solver issues.

3.2.2.2 Boundary Conditions

The boundary conditions for this model were meant to mimic the experiment. Recall that the experiment was based on the ASTM Standard F2711, described in Section 2.2.1.1, which called for free rotation at both the front and rear axis, just as an end user would experience. These axles were also meant to prevent translation, keeping the bike stationary during the experiment.

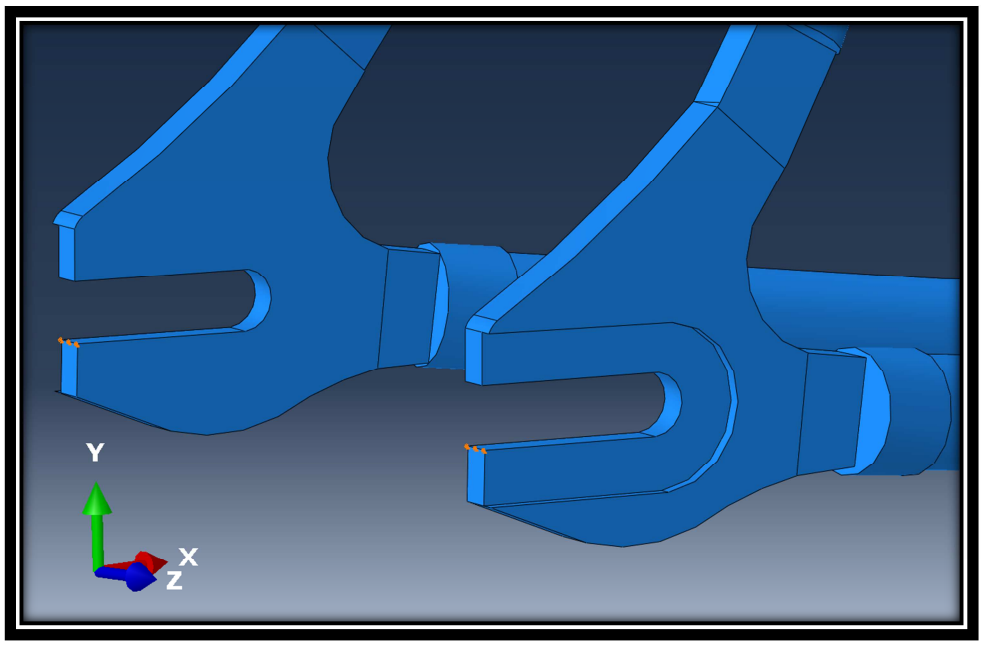

Figure 3.32 Rear Axle Boundary Condition – Rear Dropouts

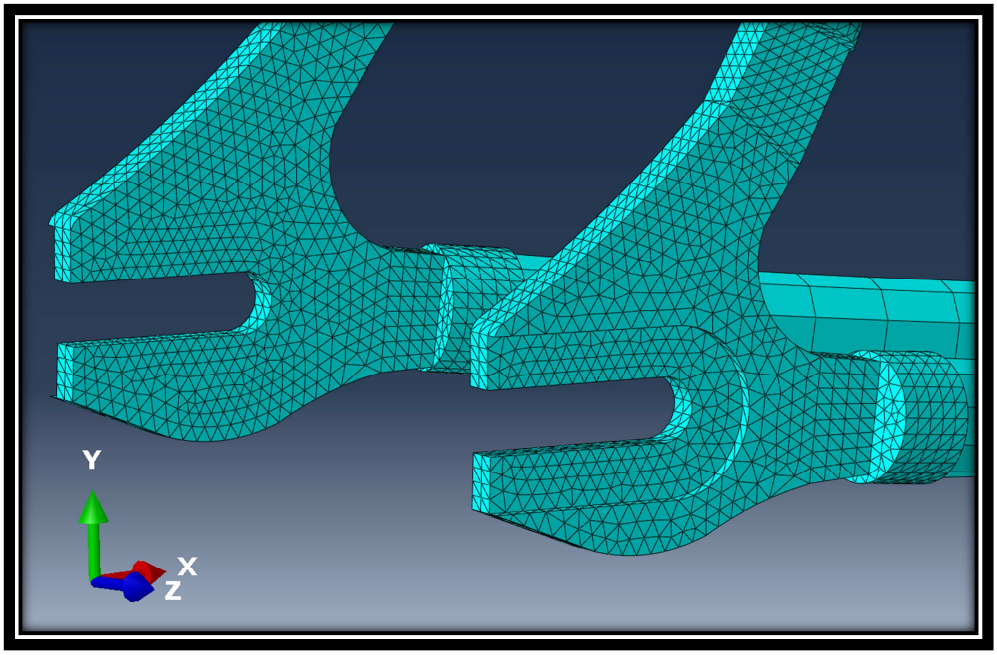

Figure 3.33 Rear Axle Boundary Conditions – Rear Dropouts Mesh

The boundary conditions simulating the rear axle were placed on the rear dropouts, as seen in Figure 3.32. As seen in Figure 3.33 a geometrical line, consisting of 3 nodes in the mesh had translation fixed in all three directions, x, y, and z, but each is free to rotate. This is not quite accurate to the experiment because of the rear dropouts bearing on an actual axle. The axle is a cylindrical shape, which would provide much more bearing area. This assumption is made to avoid the use of creating contacts between different parts. Contact problems are usually more computationally expensive and more difficult to implement. The assumption worked well as will be discussed in the results. Also, most of the interesting damage accumulation aspects will be in the head tube.

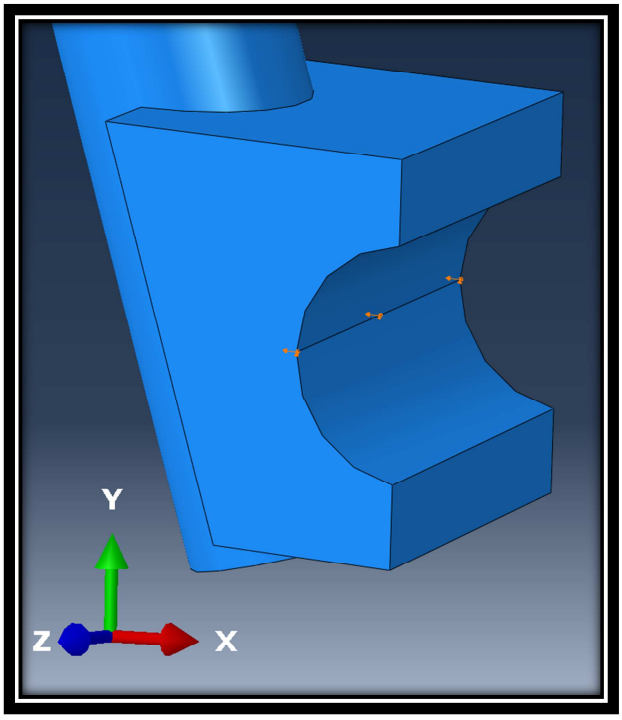

Figure 3.34 Front Axle Boundary Conditions – Front Fork

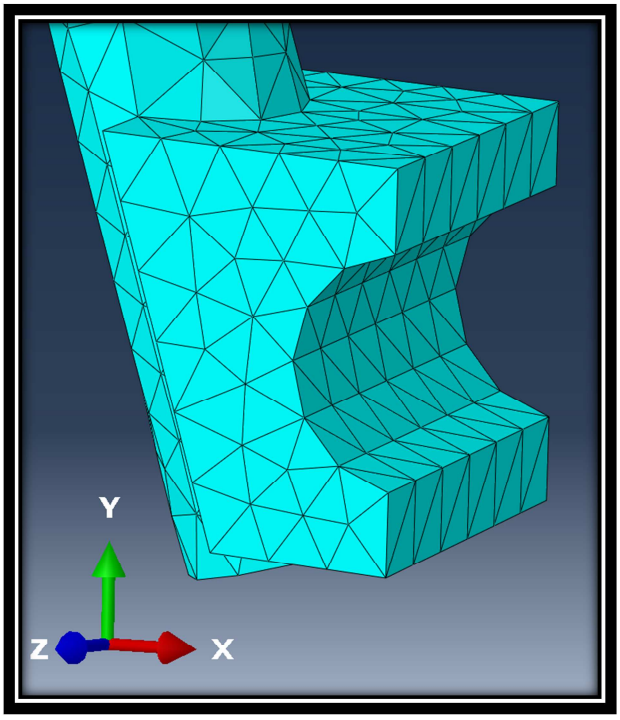

Figure 3.35 Front Axle Boundary Conditions – Front Fork Mesh

Pertaining to the Front Fork, the displacement was applied to a geometrical line, seen in Figure 3.34, associated with 7 nodes in the mesh, seen in Figure 3.35. Each node along this line had translation fixed in the y and z direction, and displacement was applied in the x direction. Fixing translation in the y and z directions is in line with the standard and mimics the experiment well because the Instron is such a rigid machine all translation was in the vertical direction on the experiment, in the x direction in the model, and horizontal translation in the experiment and y and z in the model, was restricted by the sturdiness of the Instron frame. Rotation was allowed at each node.

3.2.2.3 Element Type

Abaqus has a built in meshing function that was used to mesh the bike frame. The program user assigns a specific element type to each part and a seed size, indicating the approximate size of each element. Abaqus then fits a mesh to the geometry of the part. If the shape is uniform throughout and the seed size is a multiple of the length of the part then the elements will have side lengths that are exactly the same as the seed dimension. For example, if a cube is 4 in x 4 in x 4 in, and a seed size of half inch is specified, then Abaqus will assign a mesh such that the sizes of the element are each a half inch and looking along a given edge one will see 8 different elements. If the user assigns a brick or rectangular box element, each element will come out to be a cube with a side length of half inch. If the user specifies a tetrahedral element then each element will have 3 sides with the length of a half inch, essentially a cube halved along the diagonal However, if the geometry is complex, Abaqus will still fit the geometry exactly but it will have to vary the size of the elements to fit it.

The tubes of the bike frame are composed of shell elements using Abaqus S4R and S3R shell elements with a rough dimension of half inch. Though there are spots where the elements get considerably smaller, this is because of the method Abaqus uses to mesh. Abaqus has a meshing function and fits a mesh to the exact geometry, as described above, and the geometry of where the seat stays connected seems to be the most complex geometry on the bike frame and therefore element sizes are reduced to fit this complex geometry. The front fork is composed of Abaqus C3D4 elements with an approximate dimension of half inch, stresses and damage arising in the front fork is thought to be negligible because of it being made out of steel, thereby forcing the aluminum bike frame to take on the majority of the stress, strain, and damage being caused by the cyclic loading. Therefore, the front fork is of less interest and the element sizes are much larger than the other solids of the bike frame. The head tube, crankcase, and both rear dropouts are composed of Abaqus elements C3D10 with a seed size of 0.1 in. Damage will most likely accumulate in the head tube quicker than other parts and therefore will be the site of failure. This is based on a thesis done at WPI, that investigates proper design of an aluminum bike frame by subjecting a bike frame to cyclic loading until failure.[17] Their work shows that the bike frame failed at the head tube.[17] And for this reason the head tube is probably of the most interest, but to be safe and capture all critical areas the solids of the bike frame used a smaller seed size and a quadratic element.

The solid elements were connected to the shell elements using a shell to solid coupling function in Abaqus, which is discussed later.

3.2.2.3.1 Shells

Shell element types used are S4R and S3R and assigned by the Abaqus auto meshing function. S4R elements are conventional stress/displacement elements, using 4 nodes, quadrilateral in shape, with reduced integration, and use first-order interpolation.[22] S3R elements are conventional stress/displacement elements, using 3 nodes, triangular in shape, with reduced integration, and use first-order interpolation.[22] Both of these element types are considered finite-strain shell elements and are general-purpose conventional shell elements.[22]

3.2.2.3.2 Solids

Solid element types used are C3D10 and C3D4. Element type C3D4 is used on to make up the Front Fork and C3D10 are used to make up the solid sections in the bike frame which include the head tube, crankcase, and the rear dropouts. C3D10 elements are continuum stress/displacement, three-dimensional, 10 node elements.[10] They are tetrahedral in shape and are second-order elements. C3D4 elements are continuum stress/displacement, three-dimensional, 4 node elements. They are tetrahedral in shape and are first-order elements. First-order elements are used on the Front Fork because they require less computation and are therefore faster, this is acceptable because the Front Fork is not of interest to this model.

3.2.2.4 Shell-to-Solid Coupling Verification

Abaqus has a built in function called Shell-to-Solid Coupling that allows for a transition from shell element modeling to solid element modeling.[22] This function is a surface-based technique for coupling shell elements to solid elements.[22] This function works such that the user selects a shell edge, of the shell to be joined, and the surface of the solid to which the shell is to be joined. A region of influence is specified by the user. This region of influence can be thought of as a cylinder whose center, longitudinal axis, is the shell edge that has been specified.[22] The user enters a value for the radius of this cylinder when assigning the shell-to-solid coupling constraint. All of the nodes within this cylinder, for both the shell and solid, are coupled by coupling both displacements and rotations. In a very basic way this connection can be thought of as a weld, two pieces of material are put next to each other and then a connection is made such that material from both pieces join together and to make this connection material is taken from both pieces of material a specific distance into each piece.

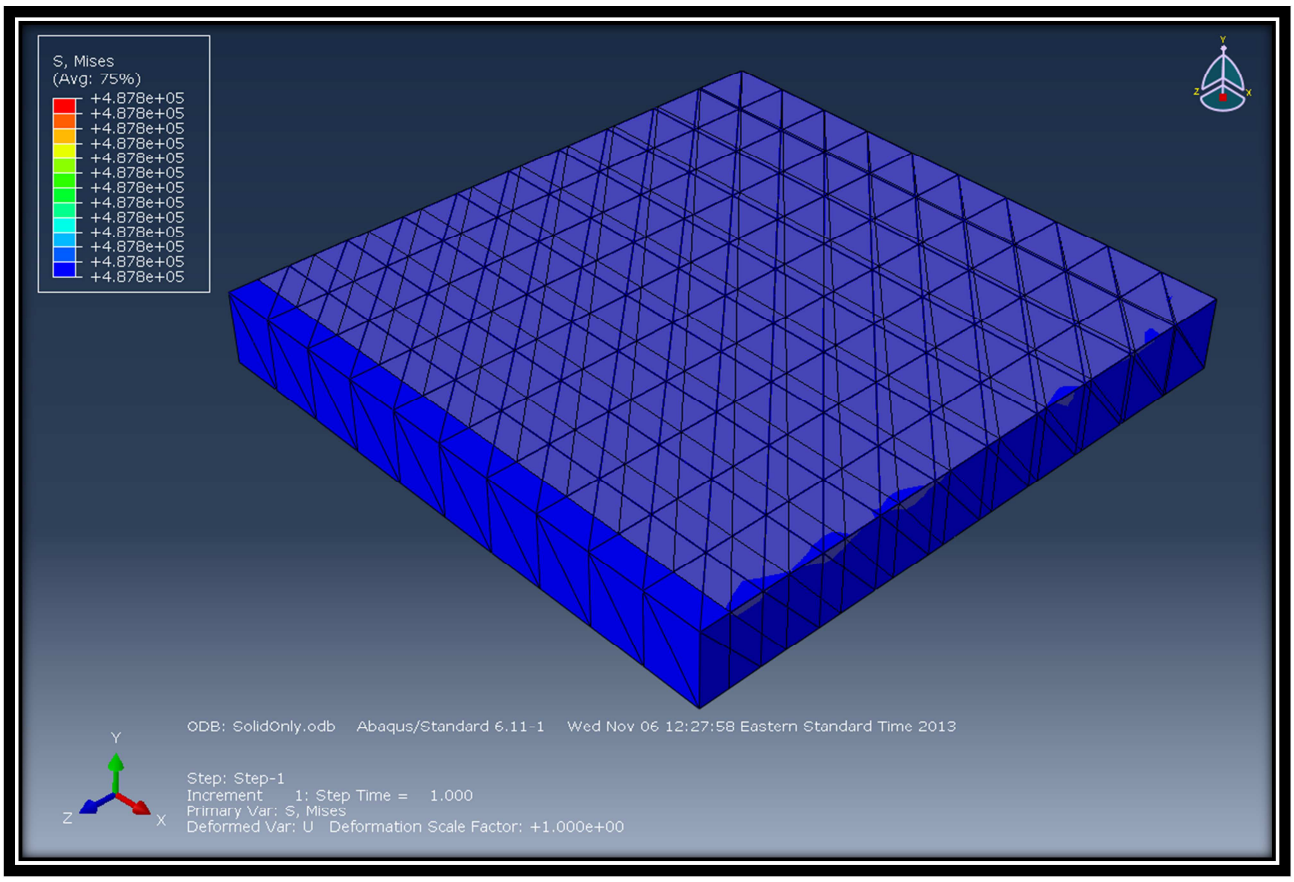

Figure 3.36 Shell-to-Solid Coupling Verification – Solid Only

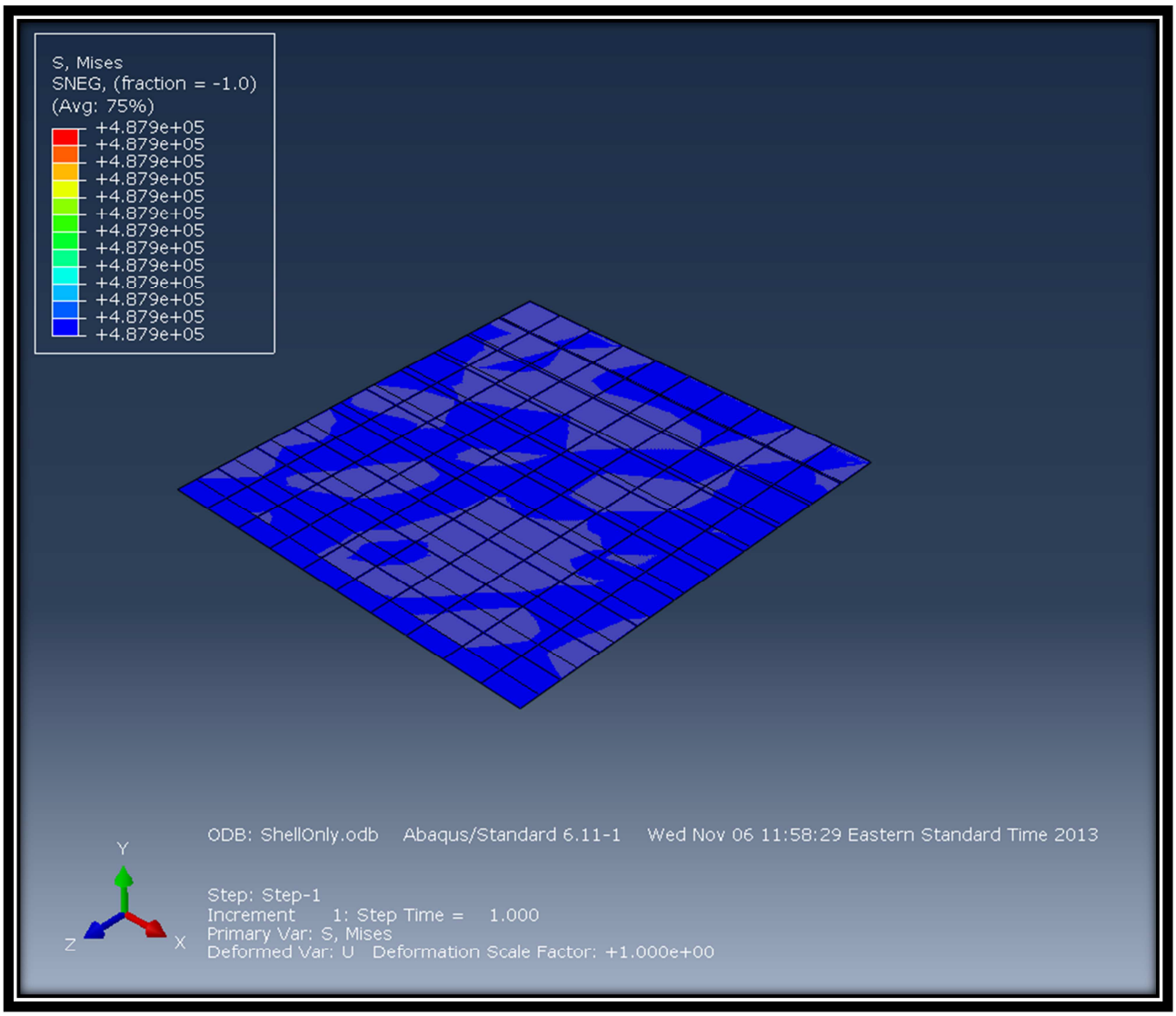

Figure 3.37 Shell-to-Solid Coupling Verification – Shell Only

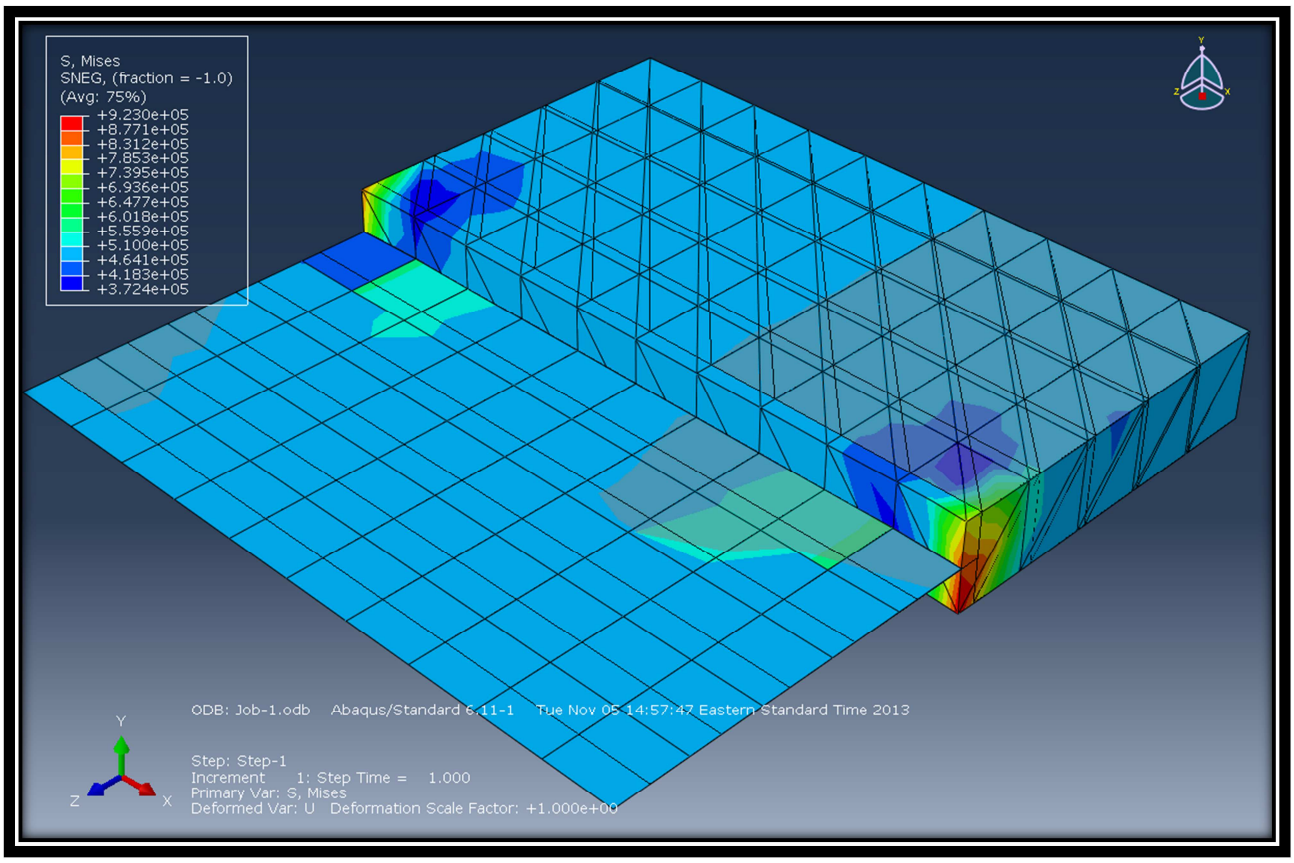

Figure 3.38 Shell-to-Solid Coupling Verification – Shell Coupled to Solid

Summary of Reaction Forces: For Displacement of 0.1 → 5% strain	
Shell-to-Solid Coupling	236,745
Shell Only	232,334
Solid Only	243,902
Analytical (true strain)	243,951

Summary of Reaction Forces: For Displacement of 0.0001 → 0.005% strain	
Shell-to-Solid Coupling	248.699
Shell Only	249.981
Solid Only	249.994
Analytical (true strain)	249.994

Figure 3.39 Shell-to-Solid Coupling Verification – Results

This built in function was used to connect the shells, or tubes, of the bike to the solids of the bike. This connection was verified as working correctly on sample pieces of material as seen in Figures 3.36 through 3.39. The verification was performed by modeling a piece of material three different ways and comparing the results. The material was first modeled using just a single solid block meshed with solid elements, Figure 3.36. It was then modeled using just shell elements, Figure 3.37. And finally it was modeled using half solid elements and half shell elements, Figure 3.38. Each simulation had displacement boundary conditions of rollers, applied to either an edge or surface, preventing translation in the z direction on one end. The opposite end of the plate, either the edge or surface, was displaced in the z direction. This created a uniaxial tension test on the specimens. The results are shown in Figure 3.39 and compared to an analytic hand calculation; as can be seen from this figure the shell-to-solid coupling is

performing as expected. The values shown in Figure 3.39 are noted as reaction forces, these are found by summing all reaction forces along the displaced edge or surface.

3.2.3 Shell Thickness Determination

To determine the correct thickness of the material the bike was fabricated from it was measured using a set of calipers. The solids were easy to measure because they were readily accesable. The shells were more of a challenge. To determine the thickness of the shells, the top tube, down tube, seat tube, chain stays, and seat stays, the tubes needed to be sectioned. A portion of the tube was cut from the bike, these sections are depicted in Figure 3.40.

Figure 3.40 Bike Frame Tube Sections – Locations Sections Were Taken From

The thickness of each tube was measured in eight places; four measurements were taken on one end, End A, and four measurements were taken on the opposite end, End B. End A and End B are arbitrary and are only used for data organization. These measurements were all averaged together and this average value was considered the tube thickness. The measurements, along with the average values can be seen in Figure 3.41.

Chain Stays		Seat Stays		Top Tube	
Measurements		Measurements		Measurements	
End A	End B	End A	End B	End A	End B
0.065 in	0.073 in	0.067 in	0.073 in	0.053 in	0.053 in
0.067 in	0.074 in	0.064 in	0.073 in	0.052 in	0.052 in
0.068 in	0.070 in	0.072 in	0.069 in	0.053 in	0.051 in
0.070 in	0.073 in	0.065 in	0.075 in	0.052 in	0.052 in
End Averages		End Averages		End Averages	
End A	End B	End A	End B	End A	End B
0.068 in	0.073 in	0.067 in	0.073 in	0.053 in	0.052 in
Tube Avg = 0.070 in		Tube Avg = 0.070 in		Tube Avg = 0.052 in	
Seat Tube		**Down Tube**			
Measurements		Measurements			
End A	End B	End A	End B		
0.070 in	0.066 in	0.049 in	0.055 in		
0.063 in	0.053 in	0.048 in	0.061 in		
0.064 in	0.063 in	0.050 in	0.058 in		
0.067 in	0.063 in	0.046 in	0.058 in		
End Averages		End Averages			
End A	End B	End A	End B		
0.066 in	0.061 in	0.048 in	0.058 in		
Tube Avg = 0.064 in		Tube Avg = 0.053 in			

Figure 3.41 Bike Frame Tube Sections – Measurements of Sections

The thickness of each tube is relatively similar. Assigning these different tube thicknesses to their respective shell sections was not possible. When the bike frame was modeled all of the tubes were merged into a single part in Abaqus, this was done to reduce the number of connections that were needed. By merging all shell sections, or tubes, into a single part Abaqus treated it as one piece of material. Therefore, a single tube thickness would be needed to apply to all of the shell sections, though averaging over all of the measurements in Figure 3.41 was a reasonable solution, it was thought that there could be a more accurate way because the different

tubes probably provide different amounts of stiffness to the frame which would be desired to be captured.

To accomplish this, different shell thicknesses were applied to the finite element model of the bike frame and the simulation was run using the same maximum displacement used in the experiment. By utilizing the data from the experiment a target reaction force of 122.19 lbs was desired. The results are shown in Figure 3.42.

Shell Thickness [in]	Reaction Force [lbs]
0.0600 in	-130.664 lbs
0.0590 in	-128.986 lbs
0.0580 in	-127.295 lbs
0.0570 in	-125.590 lbs
0.0560 in	-123.870 lbs
0.0550 in	-122.137 lbs
0.0540 in	-120.390 lbs
0.0530 in	-118.627 lbs
0.0520 in	-116.851 lbs
0.0510 in	-115.062 lbs
0.0500 in	-113.260 lbs

Figure 3.42 Bike Frame Tube Sections – Single Tube Thickness Simulation Results

A tube thickness of 0.055 in was used and applied to all of the tubes. This value was assigned to the shell sections that were applied to these different parts in the bike frame.

3.2.4 Python Wrapping Script

Abaqus is used only to solve the FEM simulation constitutive equations. A Python script assembles the job by writing the input file, running the job, and telling Abaqus what information to output. This Python script then sifts through the output data and determines a new modulus of elasticity for each element, using the same material model described in Section 3.1.5.

3.2.4.1 Write Initial File

The initial model was developed in Abaqus/Cae, which is Abaqus' graphical user interface. The geometry was created in AutoCAD and that geometry was exported from AutoCAD and subsequently imported into Abaqus. An input file was created from this model and run to ensure the input file worked as expected.

The Write Initial File script used the original input file as a template and created a new input file that is run as the first part of the loading cycle. A load cycle is defined as starting at a zero displacement moving to a fully loaded position and then unloading again to a zero displacement, this is a full load cycle. However, in this simulation only the first half of this loading cycle was run, that is from zero displacement up to the max displacement of 0.1671 in, the strain that was accumulated in this first half is then doubled, which accounts for the entire loading cycle. This is done because all of the strain in that is produced in the loading cycle is elastic and therefore will be recovered. Therefore, the strain is equal in magnitude for the loading half-cycle to that of the unloading half of the cycle.

The Write Initial File script takes this original input file and expands it to create the first half of the cycle, the loading half-cycle. The expansion consists of assigning every element a unique element number and section properties. This allowed for assigning every single element in the model with a unique Young's modulus and Poission's ratio, though Poission's ratio is never changed. As the model progresses damage is accumulated and Young's Modulus is degraded. Every element will have a different amount of strain and therefore a different amount of damage, therefore each element needed to be able to have a unique Young's Modulus.

3.2.4.2 Run Job

After the Write Initial File script finished with its described task an input file that is ready to be run is created. This input file is then run by Abaqus and an output file is created. This output file contains all of the stress, strains, forces, and displacements needed to create a new model by updating Young's modulus based on the amount of elastic strain experienced.

3.2.4.3 Apply Strains

The Apply Strains script goes through the strain output data of the run, and calculates the equivalent strain parameter and the new damage value. This new damage value is used to decrease the initial modulus value, where the initial modulus is the modulus of the undamaged bike. A new modulus is found by multiplying the initial, undamaged modulus, by the degradation factor obtained from the total accumulated equivalent strain. This new modulus

value is then written into a new input file, for each element, in preparation for the next simulation run.

3.2.5 Material Model Implementation

There are three main parts to this project: Material Model, Bike Experiment, and Bike FEM. The Material Model uses experimental data from a published paper. This data was obtained by performing an experiment on a single piece of Aluminum Alloy 2024 material, no connections of any kind. This experimental data shows that stiffness degrades with increasing cycles. The Bike Experiment uses a fabricated bike frame made of Aluminum Alloy 6061, utilizing welded connections. Being that the aluminum bike is made of aluminum material it would be expected that when the bike is subjected to a cyclic loading the stiffness of the bike would degrade at least as much as the individual specimens would. Perhaps more stiffness degradation would be observed because of the contribution of the welded connections and the material.

The Bike FEM was used to determine if this is, indeed, the case. A material model was developed to attempt to explain the stiffness degradation in the aluminum material. This material model was then applied to the Bike FEM. The Bike FEM results were then to be confirmed with the Bike Experiment.

In Section 3.1.6 a multiplier value was found. This value is repeated in Figure 3.43.

Notched Beam Values	
Stiffness Degradation	**Multiplier**
17.7%	0.00261

Figure 3.43 Multiplier Values Repeated from Section 3.1.6

The multiplier value obtained from developing the material model on the notched beam need to be extrapolated. While the bike frame underwent 1.2 million cycles the bike frame simulation was only run for 12 cycles, hence:

$$\frac{1{,}200{,}000\ Experiment\ Cycles}{12\ FEM\ Cycles} \times 0.00261 = 261$$

Therefore, using a multiplier value of 261, and running the Bike FEM simulation only 12 cycles, it would be expected to match the data from the bike experiment.

Recall that the material model was developed for a two dimensional simulation. The bike frame is a three dimensional simulation and the material model was expanded accordingly. This three dimensional material model is applied as follows:

$$\begin{bmatrix}\sigma_{11}\\ \sigma_{22}\\ \sigma_{33}\\ \sigma_{12}\\ \sigma_{23}\\ \sigma_{31}\end{bmatrix} = (1 - D_{total}) \begin{bmatrix} 2\mu+\lambda & \lambda & \lambda & 0 & 0 & 0\\ \lambda & 2\mu+\lambda & \lambda & 0 & 0 & 0\\ \lambda & \lambda & 2\mu+\lambda & 0 & 0 & 0\\ 0 & 0 & 0 & 2\mu & 0 & 0\\ 0 & 0 & 0 & 0 & 2\mu & 0\\ 0 & 0 & 0 & 0 & 0 & 2\mu \end{bmatrix} \begin{bmatrix}\varepsilon_{11}\\ \varepsilon_{22}\\ \varepsilon_{33}\\ \varepsilon_{12}\\ \varepsilon_{23}\\ \varepsilon_{31}\end{bmatrix}$$

3.2.6 Results

Simulations were run utilizing a wide range of multipliers, spanning many orders of magnitude. While the desired multiplier needed to match the experimental results is expected to be around 261 this multiplier was utilized to investigate how the multiplier affected the stiffness of the bike frame over the given number of cycles. Figures 3.44 through 3.49 show all of the acquired data in various forms, which will be explained in more detail below.

In Figures 3.44 through 3.47 the axis denoting the number of cycles is in the actual number of cycles, not the number of simulation cycles. Recall that each simulation was run for 12 loading cycles, and that each of these 12 cycles represents 100,000 real world cycles, for a total of 1,200,000 cycles that the bike frame experienced in the experiment.

Figure 3.44 shows stiffness as a function of the number of cycles for most of the multipliers for which a simulation was run. When the multiplier is much lower than 0.01 noticing the difference between the data curve and when the multiplier is set to zero is difficult to discern. Notice that Figure 3.44 is crowded with all the different multiplier data curves on it; it is included because it gives a good representation as to what is happening overall. Notice that as the multiplier is increased the bike fails earlier, which is expected. If the amount of damage accumulating in a bike frame is increased, then that bike will not have as long of a life span.

Figures 3.45 through 3.47 breaks the data represented in Figure 3.44 into different sections. In these curves it is easier to see the details of the different simulation results. Notice the phrase

“BS,HT,CC” in the legend of Figures 3.44 through 3.47. This phrase means that all of the components, with the exception of the Front Fork and rear dropouts, were allowed to degrade. That is, the material model was applied to all other components. This was done to prevent stress concentrations of the loading and support members from degrading at an artificially accelerated pace.

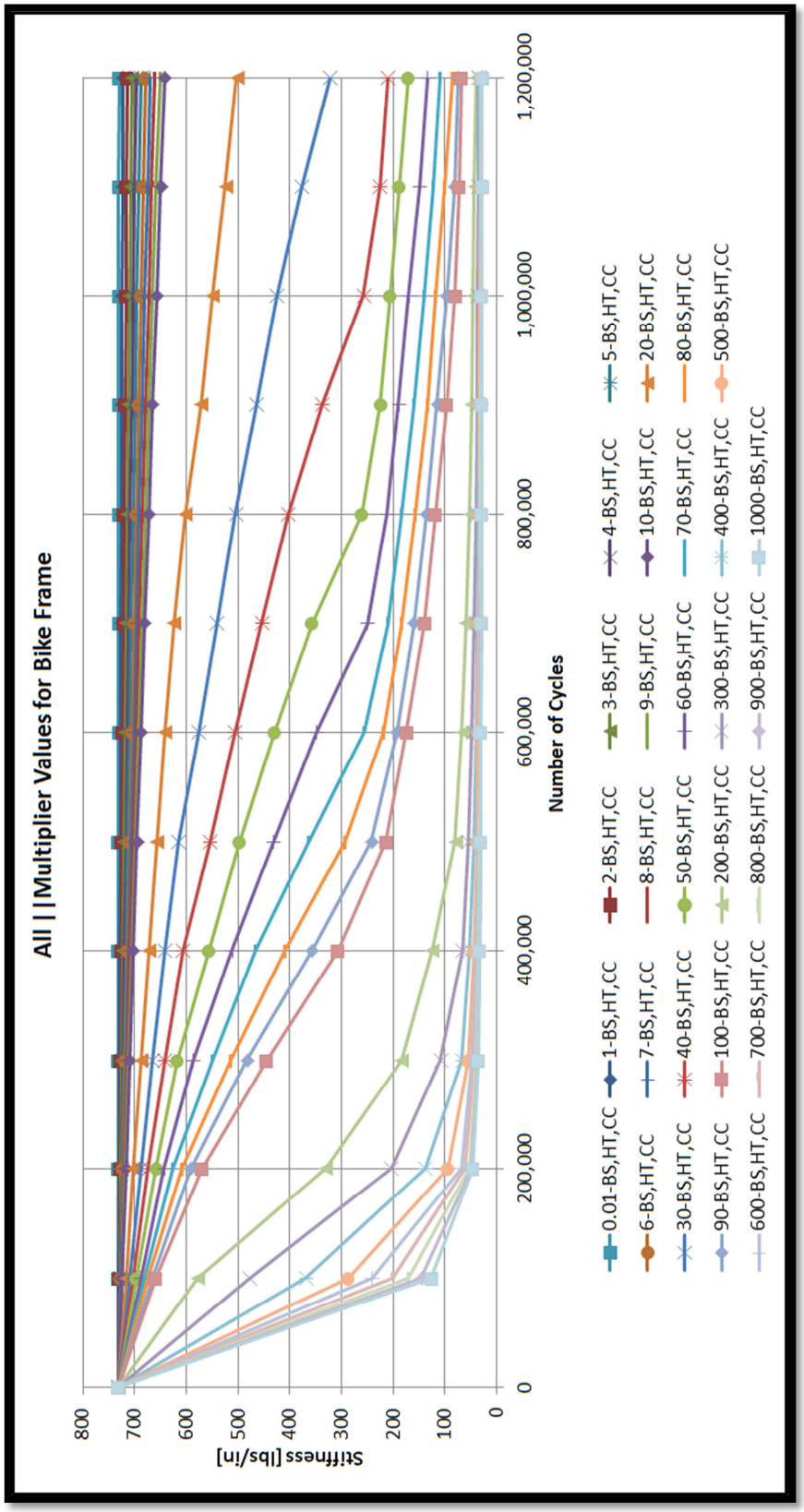

Figure 3.44 Bike FEM Results – Multiplier Values from 0.01 to 1000

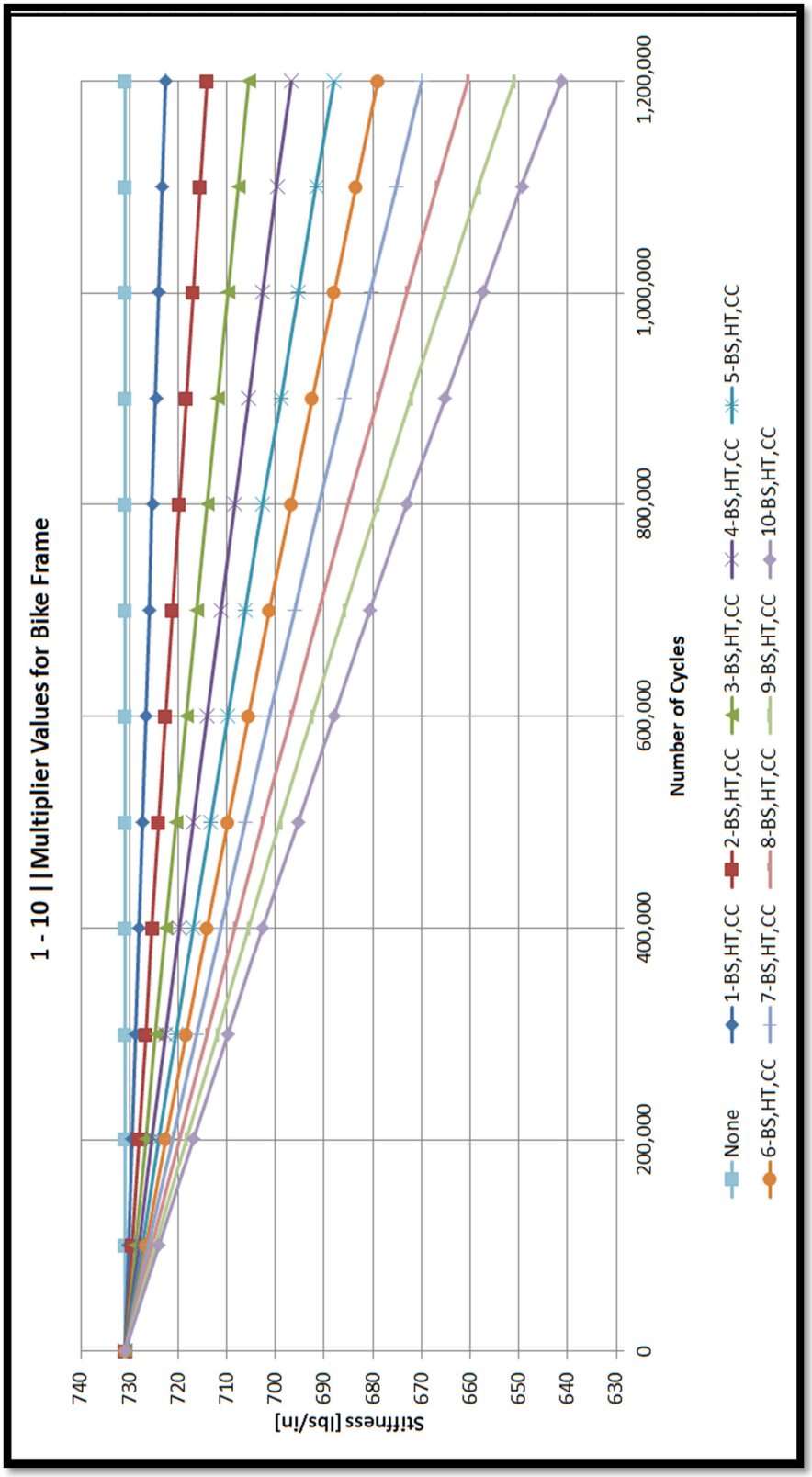

Figure 3.45 Bike FEM Results – Multiplier Values from 1 to 10

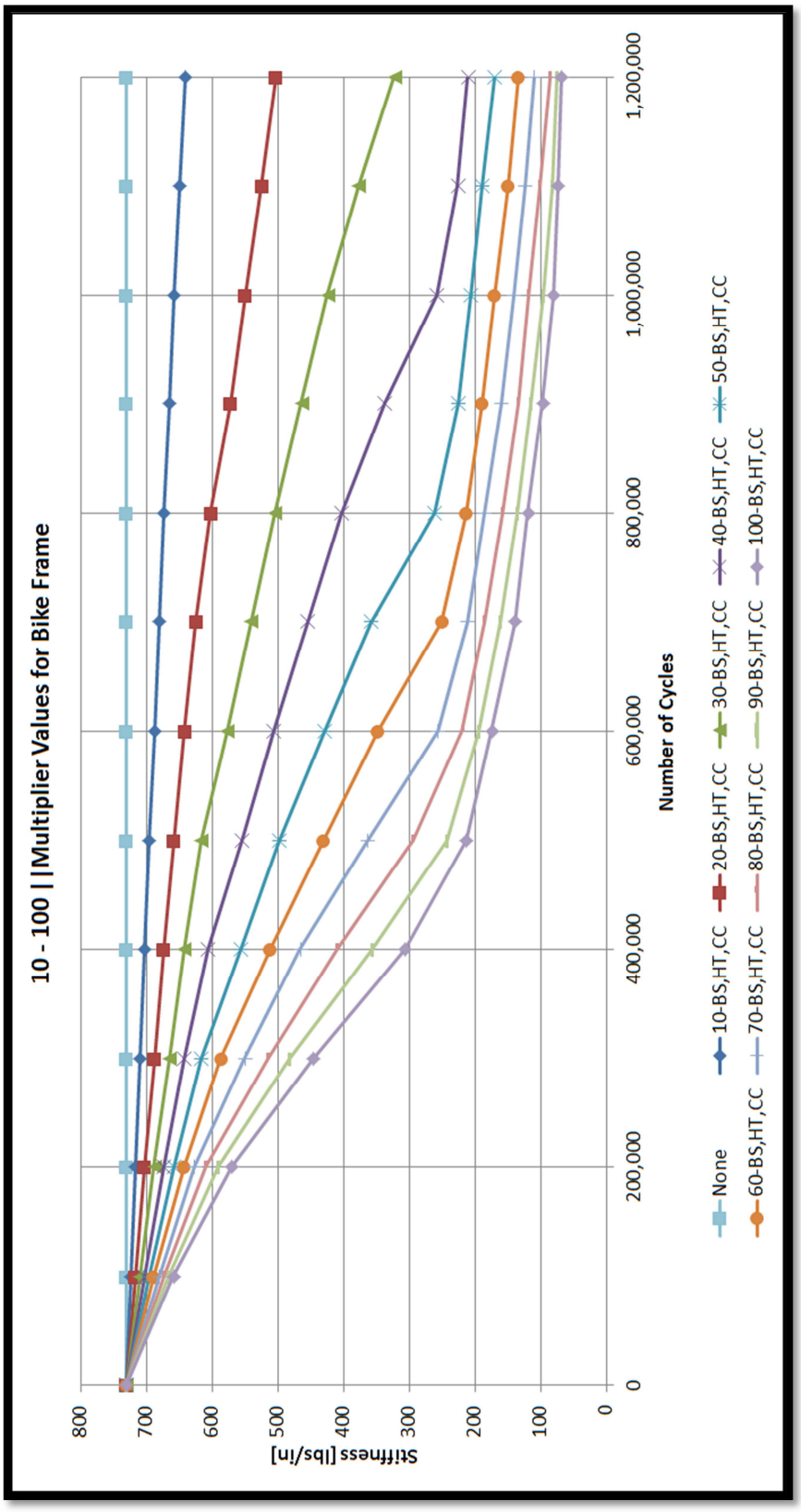

Figure 3.46 Bike FEM Results – Multiplier Values from 10 to 100

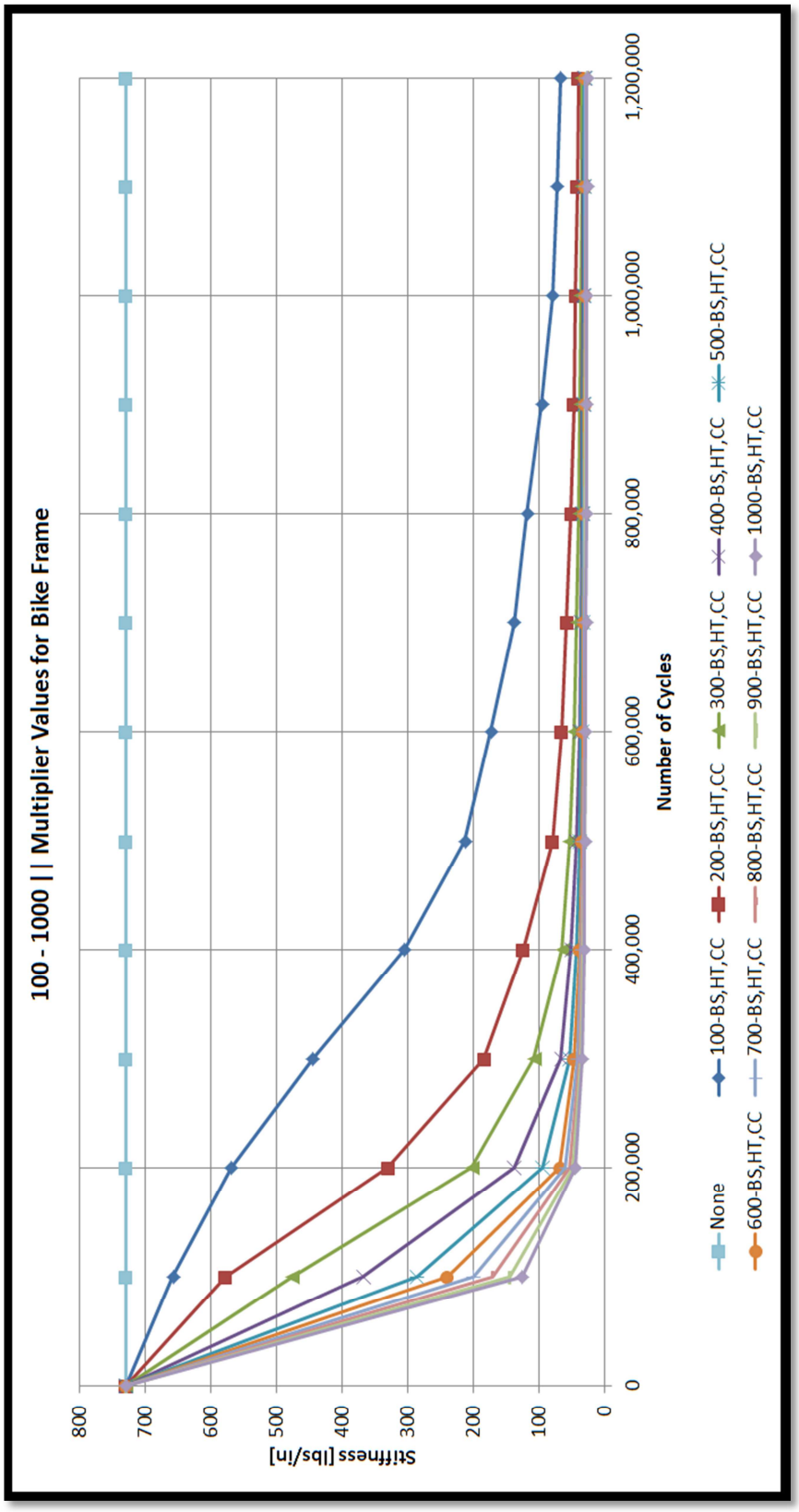

Figure 3.47 Bike FEM Results – Multiplier Values from 100 to 1000

Figure 3.48 shows the percent stiffness degradation as a function of the multiplier value. The percent stiffness degradation was obtained by performing a percentage decrease calculation using the first and last point in the set of data for that given multiplier. It is clear from Figures 3.44 through 3.48 that the multiplier value of 261 does not match the experimental data, when the multiplier gets around 100 and above the stiffness of the bike frame falls off much too dramatically. Recall from the experimental data a target percentage stiffness degradation of 0.0662% for a 90% confidence interval is desired. From Figure 3.48 it is difficult to tell what the multiplier would need to be to achieve the target 0.0662% stiffness degradation.

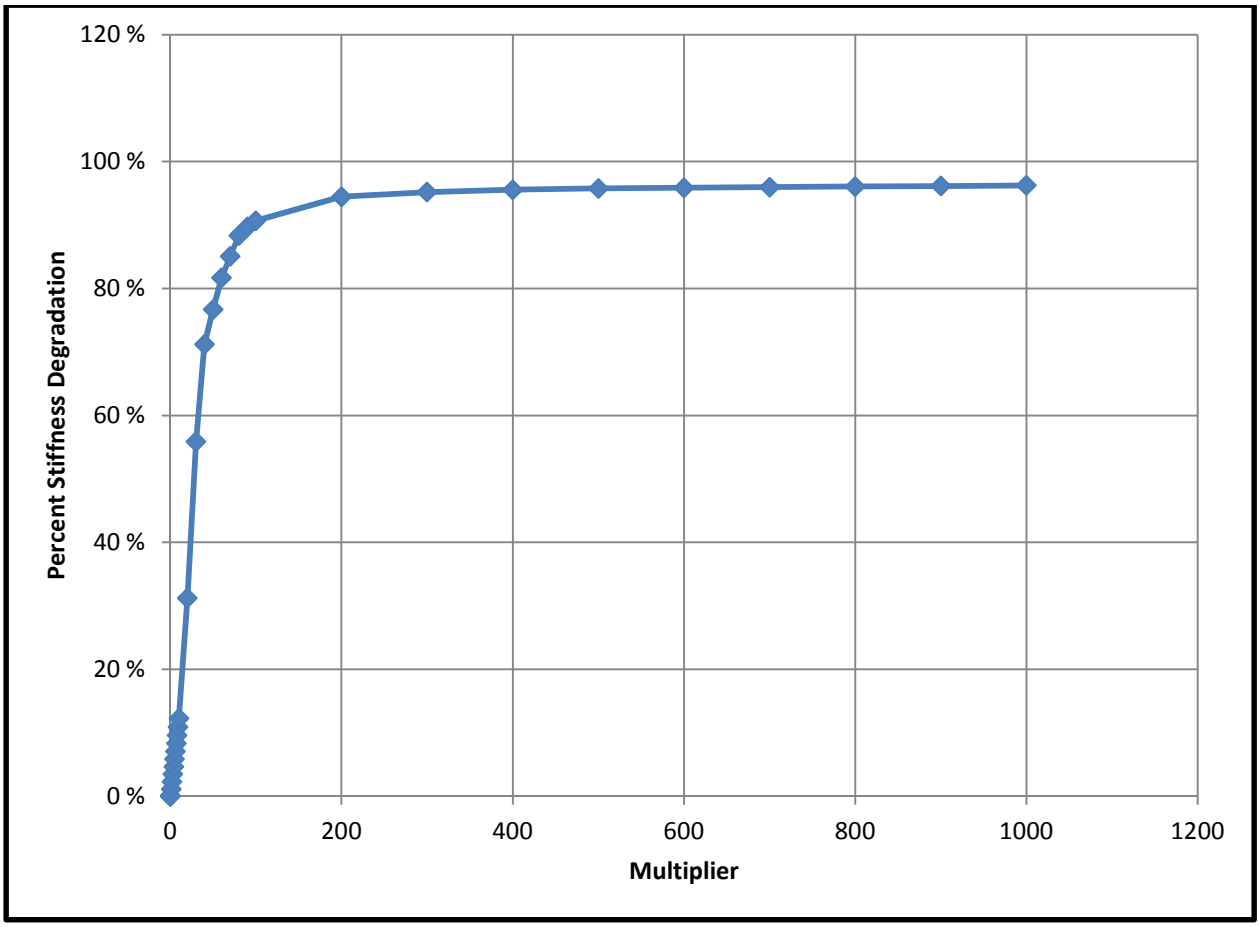

Figure 3.48 Stiffness as a Function of Multiplier Values – from 0.0001 to 1000

Figure 3.49 zooms in on the area of interest from Figure 3.48 and fits a linear regression line to the data to allow for finding the needed multiplier to achieve the 0.0662% stiffness degradation needed to match the experiment.

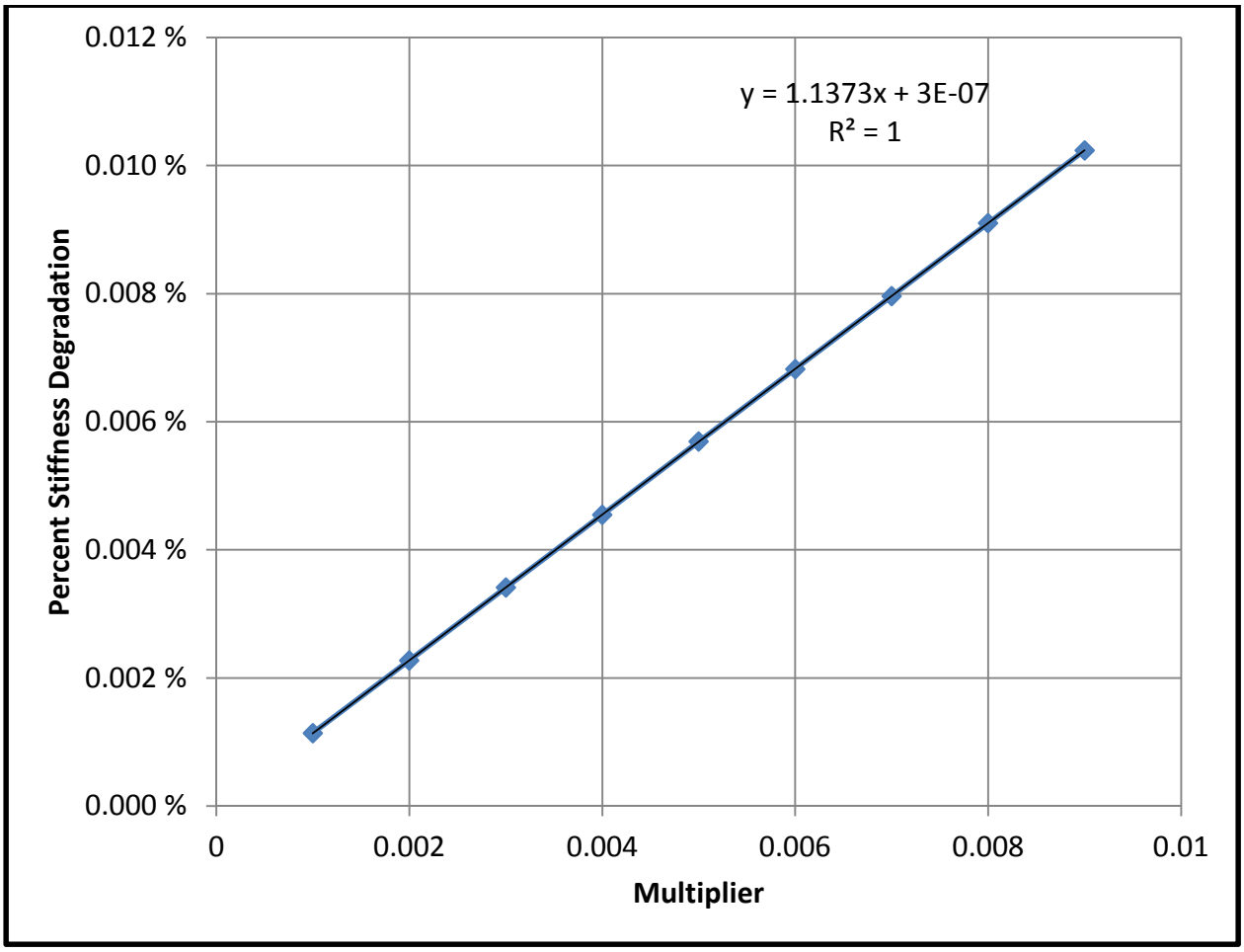

Figure 3.49 Stiffness as a Function of Multiplier Values – from 0.001 to 0.009

The following equations solve for the needed multiplier to match the experimental data:

$y = 1.1373x + 3 \times 10^{-7}$

$Percent\ Stiffness\ Degradation = 1.1373(multiplier) + 3 \times 10^{-7}$

$0.0662\% = 1.1373(multiplier) + 3 \times 10^{-7}$

$$\frac{0.0662\% - 3 \times 10^{-7}}{1.1373} = multiplier$$

$0.0582 = multiplier$

Therefore, a multiplier of 0.0582 would be needed to match the experimental data. This value is far from the 261 that the material model from Section 3.1.6 expected would be needed. The needed multiplier to match the experimental results is around 5000 times smaller than would be predicted from the notched beam results.

4.0 Summary and Conclusions

The stiffness of a structure is determined by its constituent materials and the geometry of its members. While the geometry of a structure will not change drastically over the course of its life, due to maintenance operations, several different mechanisms are actively changing the properties of the materials.

The overarching goal of this thesis is to characterize stiffness degradation of high performance, welded, aluminum structures. While structures such as airplanes and naval ships are the applications of interest they are large, complex, difficult to model, and expensive to experiment on. An aluminum bike frame was used as a feasible and economical substitute.

In this thesis a material model was developed using a single adjustment parameter, or damage multiplier. This material model was developed to match experimental data obtained from a published experiment. The material model utilized accumulated elastic strain and a multiplier to reduce the elastic modulus of the aluminum material. This material model was implemented using a two dimensional finite element model of a notched beam.

Once the multiplier that allowed for matching the published experimental results was obtained the material model was implemented in a three dimensional finite element model of a bike frame that was developed from a bike frame that had been purchased.

An experiment was designed to specifically investigate stiffness degradation using the purchased bike frame. This experiment was designed using an ASTM standard as a starting point, but deviated to fit the available equipment and to address the specific objectives of this thesis The results of this experiment were used to determine if stiffness degradation does indeed occur, and to what degree, in a high performance, welded, aluminum structure. These results were also used to verify or refute the modeling results obtained when the material model was implemented into the three dimensional, bike frame, finite element model.

The experimental results obtained from the bike frame show that stiffness degradation does occur in a high performance, welded, aluminum structure. Using a simple linear regression model and a 90% confidence interval there is a lower bound of 0.0662% and an upper bound of 0.6414% reduction in stiffness over 1.2 million loading cycles on the bike frame.

When the material model was developed using the notched beam, matching the published experimental results, a multiplier of 0.00261 was found to be needed to obtain the 17.7% stiffness degradation, over 140,000 loading cycles of the notched beam.

When these multipliers were used in the finite element model of the bike frame they did not provide the expected results that were obtained from the bike experiment. The needed multiplier to match the experimental results is around 5000 times smaller than would be predicted from the notched beam results. This is a fairly large discrepancy and only possible future research can be postulated at this time as the exact reason for the discrepancy is unknown.

Performing the three point bend experiment done in the literature would be an ideal next step. The experimental procedure in this paper is suspect. The data collection method does not recalibrate the displacement measurement. This proved to be problematic in the bike frame experiment leading to the Multiple Points data collection method. Another aspect of data collection done in the published experiment, that proved problematic in the bike frame experiment, is that the measurements are taken while the cycling is being performed. An alternative to this would be to stop the experiment at specific intervals and perform static tests, which would produce more stable and accurate results, hence the method used on the bike frame experiment. Without verifying the published experiment by performing the experiment independently this is merely speculation while laying out a trajectory for future work.

It can be concluded that stiffness does degrade in a high performance, welded, aluminum structure due to changes in material properties in the absence of geometry changes. An elastic strain based damage model has possible predictive qualities, with further investigation being required.

REFERENCES

[1] Zagrai, Andrei, et al, (2008) Micro- and Macroscale Damage Detection Using the Nonlinear Acoustic Vibro-Modulation Technique. *American Society for Nondestructive Testing*, 19:104-128. http://dx.doi.org/10.1080/09349840801931817

[2] ASTM Standard F2711, 2008 (2012), "Standard Test Methods for Bicycle Frames," ASTM International, West Conshohocken, PA, 2012, DOI: 10.1520/F2711-08R12, www.astm.org.

[3] ASTM Standard F2043, 2009, "Standard Classification for Bicycle Usage," ASTM International, West Conshohocken, PA, 2009, DOI: 10.1520/F2043-09, www.astm.org.

[4] ASTM Standard F2802, 2009"Standard Specification for Condition 1 Bicycle Frames," ASTM International, West Conshohocken, PA, 2012, DOI: 10.1520/F2802-09, www.astm.org.

[5] "Ascent Single-Speed Road Bike Frame – Road Bike Frames." *Ascent Single-Speed Road Bike*, <http://www.performancebike.com/bikes/Product_10052_10551_1106345_-1_400332__400332> (Feb. 4, 2014).

[6] "ASM Material Data Sheet." *Aluminum 6061-T6; 6061-T651*, <http://asm.matweb.com/search/SpecificMaterial.asp?bassnum=MA6061t6> (Feb. 4, 2014).

[7] "ASM Material Data Sheet." *Aluminum 2024-T4; 2024-T351*, <http://asm.matweb.com/search/SpecificMaterial.asp?bassnum=MA2024T4> (Feb. 4, 2014).

[8] Andrei Zagrai ; Dimitri Donskoy ; Alexander Chudnovsky ; Edward Golovin ; Vinod S. Agarwala; Micro/meso scale fatigue damage accumulation monitoring using nonlinear acoustic vibro-modulation measurements. Proc. SPIE 6175, Testing, Reliability, and Application of Micro- and Nano-Material Systems IV, 617506 (April 04, 2006); doi:10.1117/12.658558.

[9] "Abaqus 6.11 Help Documents." *27.1.3 Two-dimensional solid element library*, (CD-ROM), Dassault Systèmes, 2011.

[10] "Abaqus 6.11 Help Documents." *27.1.1 Solid (continuum) elements*, (CD-ROM), Dassault Systèmes, 2011.

[11] "Abaqus 6.11 Help Documents." *2.4.5 Explicit dynamic analysis*, (CD-ROM), Dassault Systèmes, 2011.

[12] Kohnen, Robert. Tour Magazine. *Pedaled Soft*. (Translated by Niko Weber)

[13] "Boldt.us." *rusted cargo ship beached*, <http://boldt.us/humor/rusted_cargo_ship_beached.html> (Feb. 4, 2014).

[14] Benito, J. A., J. M. Manero, et al. (2005). "Change of Young's modulus of cold-deformed pure iron in a tensile test." Metallurgical and Materials Transactions A (Physical Metallurgy and Materials Science) 36A(12): 3317-3324.

[15] Zagrai, A. 2012. *Relative Compliance Questions*. (Email to Kevin Muich)

[16] "ASTM A36 Mild/Low Carbon Steel." *ASTM A36 Mild/Low Carbon Steel*, <http://www.azom.com/article.aspx?ArticleID=6117> (Feb. 4, 2014).

[17] Dwyer, Forrest., Shaw, Adrian., and Tombarelli, Richard. 2012. Material and Design Optimization for an Aluminum Bike Frame.

[18] "Decision 411 Forecasting." *Testing the assumptions of linear regression*, <http://people.duke.edu/~rnau/testing.htm> (Feb. 4, 2014).

[19] ASTM A36 Mild/Low Carbon Steel." *ASTM A36 Mild/Low Carbon Steel*, <http://www.azom.com/article.aspx?ArticleID=6117> (Feb. 4, 2014).

[20] "Abaqus 6.11 Help Documents." *3.2.6 Triangular, tetrahedral, and wedge elements*, (CD-ROM), Dassault Systèmes, 2011.

[21] "Abaqus 6.11 Help Documents." *2.1.1 Nonlinear Solution Methods in Abaqus/Standard*, (CD-ROM), Dassault Systèmes, 2011.

[22] "Abaqus 6.11 Help Documents." *33.3.3 Shell-to-Solid Coupling*, (CD-ROM), Dassault Systèmes, 2011.

APPENDIX A

This appendix contains the following graphs showing the complete set of data used to obtain the information in Figure 3.29.

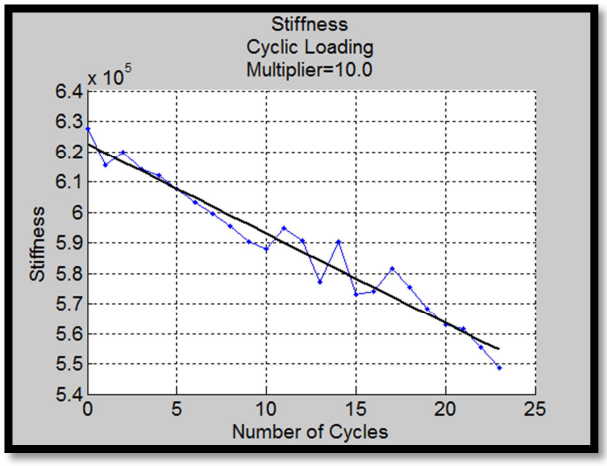

Figure A.1 Multiplier Value of 10.0 – Stiffness as a Function of number of Cycles

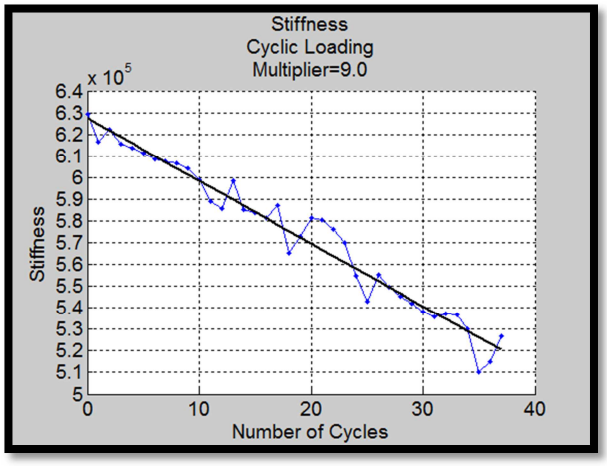

Figure A.2 Multiplier Value of 9.0 – Stiffness as a Function of number of Cycles

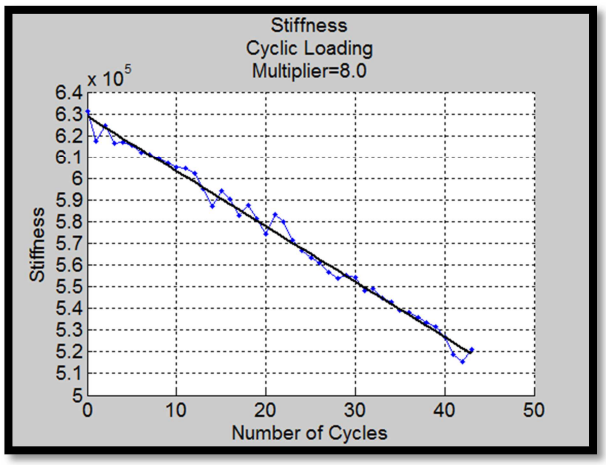

Figure A.3 Multiplier Value of 8.0 – Stiffness as a Function of number of Cycles

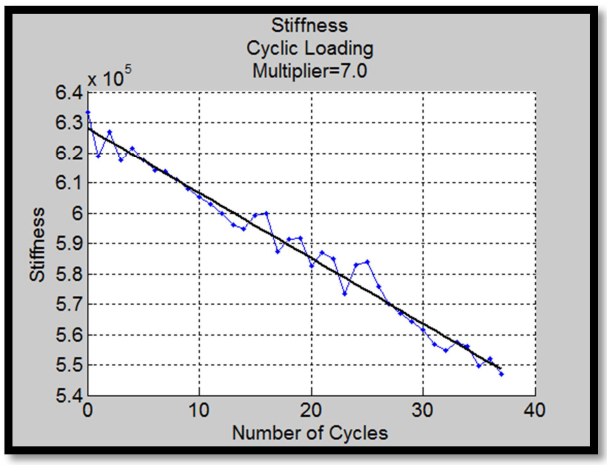

Figure A.4 Multiplier Value of 7.0 – Stiffness as a Function of number of Cycles

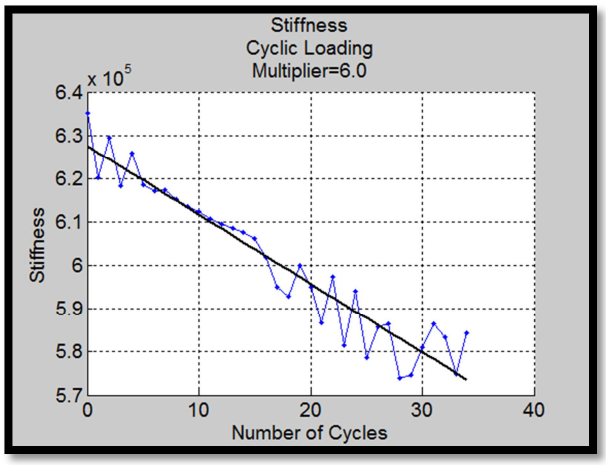

Figure A.5 Multiplier Value of 6.0 – Stiffness as a Function of number of Cycles

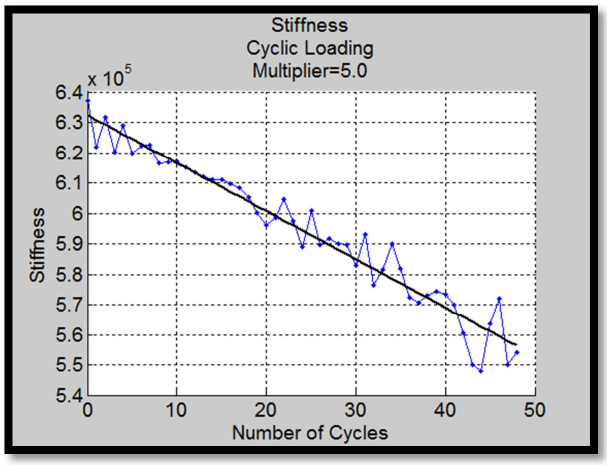

Figure A.6 Multiplier Value of 5.0 – Stiffness as a Function of number of Cycles

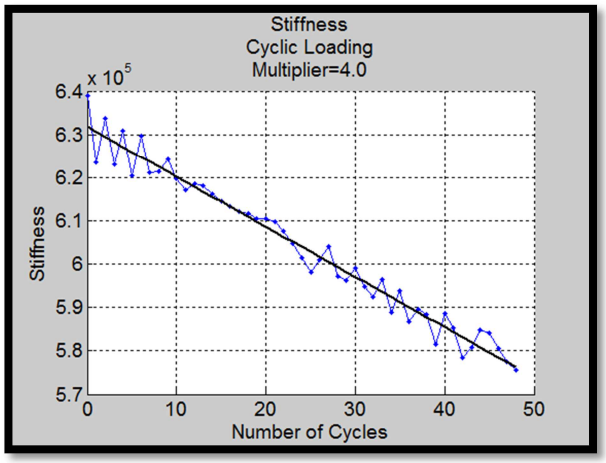

Figure A.7 Multiplier Value of 4.0 – Stiffness as a Function of number of Cycles

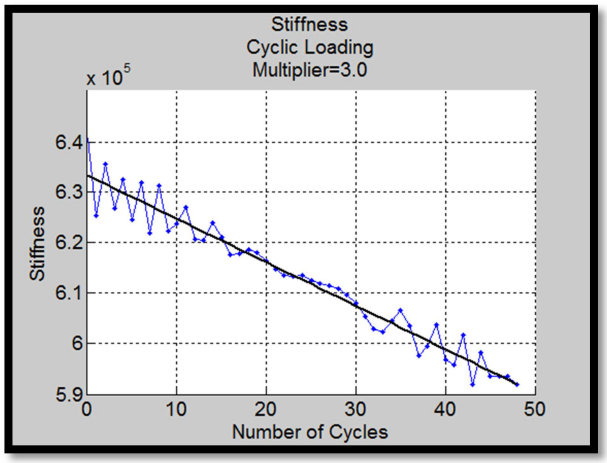

Figure A.8 Multiplier Value of 3.0– Stiffness as a Function of number of Cycles

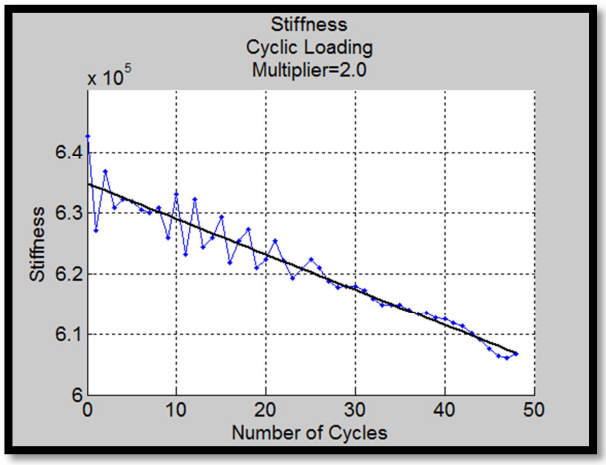

Figure A.9 Multiplier Value of 2.0 – Stiffness as a Function of number of Cycles

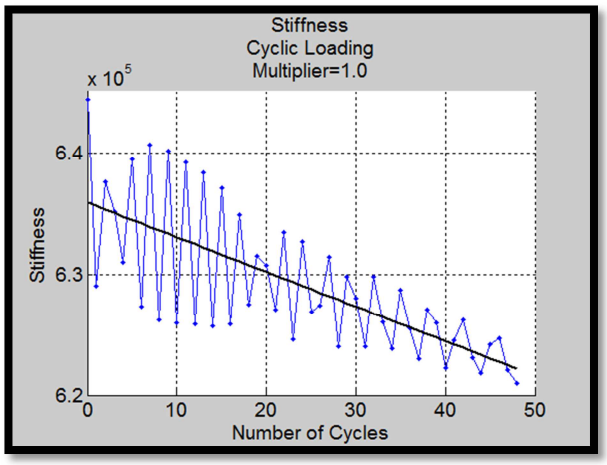

Figure A.10 Multiplier Value of 1.0 – Stiffness as a Function of number of Cycles

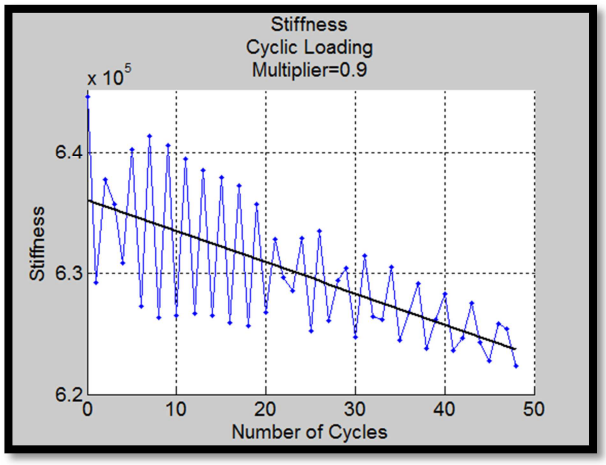

Figure A.11 Multiplier Value of 0.9 – Stiffness as a Function of number of Cycles

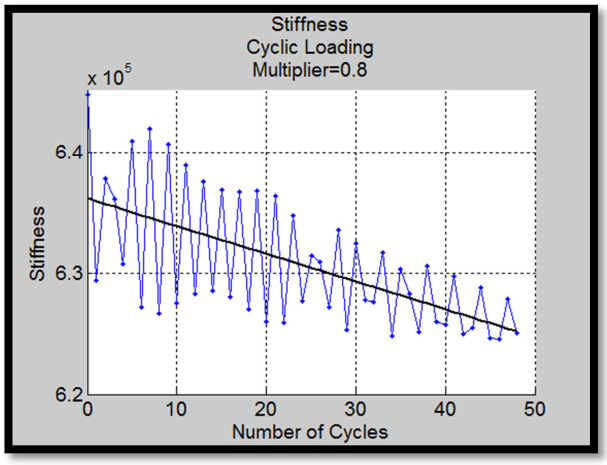

Figure A.12 Multiplier Value of 0.8 – Stiffness as a Function of number of Cycles

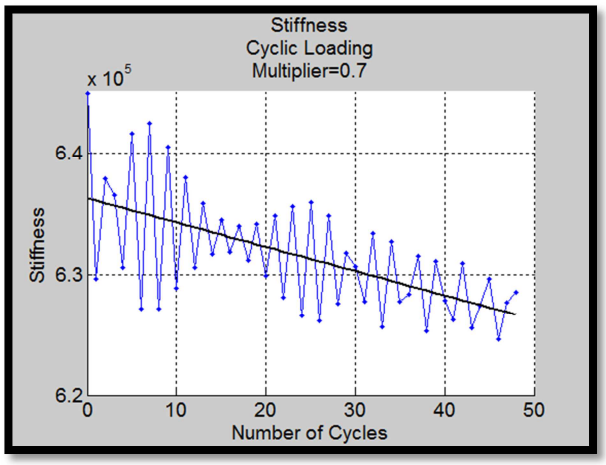

Figure A.13 Multiplier Value of 0.7 – Stiffness as a Function of number of Cycles

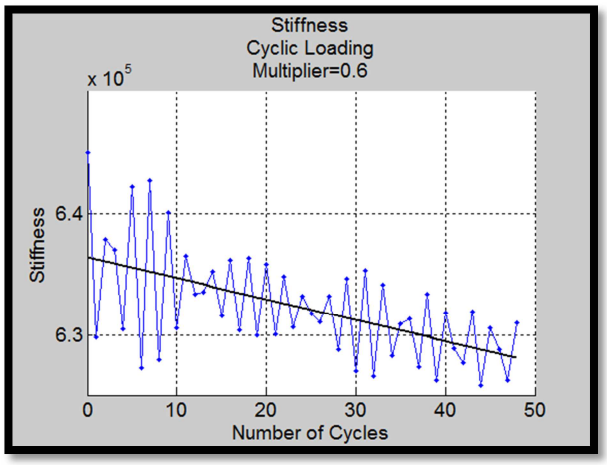

Figure A.14 Multiplier Value of 0.6 – Stiffness as a Function of number of Cycles

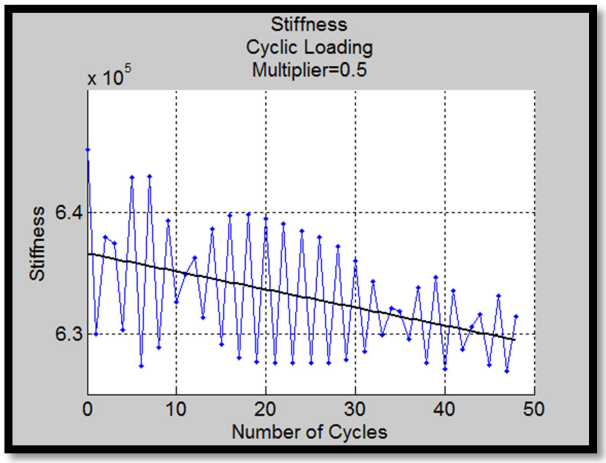

Figure A.15 Multiplier Value of 0.5 – Stiffness as a Function of number of Cycles

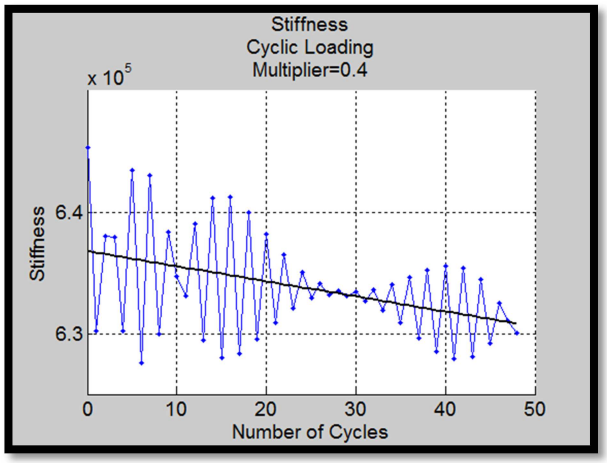

Figure A.16 Multiplier Value of 0.4 – Stiffness as a Function of number of Cycles

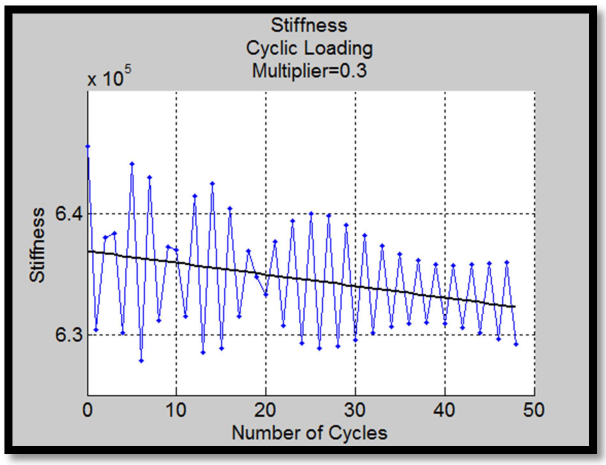

Figure A.17 Multiplier Value of 0.3 – Stiffness as a Function of number of Cycles

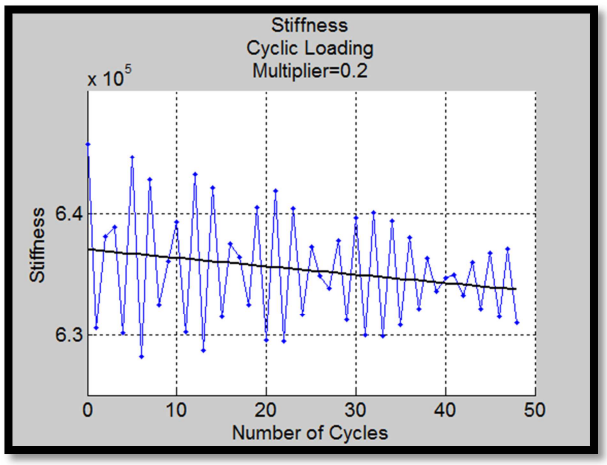

Figure A.18 Multiplier Value of 0.2 – Stiffness as a Function of number of Cycles

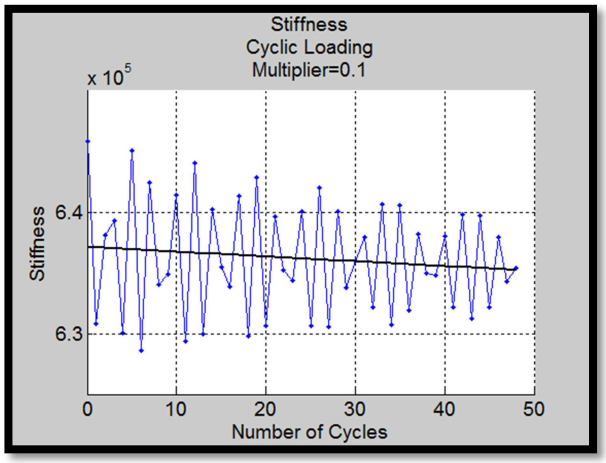

Figure A.19 Multiplier Value of 0.1 – Stiffness as a Function of number of Cycles